

# A geometric characterization of unstable blow-up solutions with computer-assisted proof

Jean-Philippe Lessard <sup>\*</sup>   Kaname Matsue <sup>†, ‡</sup>   Akitoshi Takayasu <sup>§</sup>

March 24, 2021

## Abstract

In this paper, blow-up solutions of autonomous ordinary differential equations (ODEs) which are unstable under perturbations of initial conditions are studied. Combining dynamical systems machinery (e.g. phase space compactifications, time-scale desingularizations of vector fields) with tools from computer-assisted proofs (e.g. rigorous integrators, parameterization method for invariant manifolds), these *unstable* blow-up solutions are obtained as trajectories on stable manifolds of hyperbolic (saddle) equilibria at infinity. In this process, important features are obtained: smooth dependence of blow-up times on initial points near blow-up, level set distribution of blow-up times, singular behavior of blow-up times on unstable blow-up solutions, organization of the phase space via separatrices (stable manifolds). In particular, we show that unstable blow-up solutions themselves, and solutions defined globally in time connected by those blow-up solutions can separate initial conditions into two regions where solution trajectories are either globally bounded or blow-up, no matter how the large initial points are.

**Keywords:** unstable blow-up solutions, rigorous numerics, compactifications, desingularization, parameterization method, separatrix

## 1 Introduction

Our concern in the present paper is blow-up solutions of the following initial value problem of an autonomous system of ordinary differential equations (ODEs) in  $\mathbb{R}^n$ :

$$\frac{dy(t)}{dt} = f(y(t)), \quad y(0) = y_0, \quad (1.1)$$

---

<sup>\*</sup>McGill University, Department of Mathematics and Statistics, 805 Sherbrooke Street West, Montreal, QC, H3A 0B9, Canada ([jp.lessard@mcgill.ca](mailto:jp.lessard@mcgill.ca))

<sup>†</sup>Institute of Mathematics for Industry, Kyushu University, Fukuoka 819-0395, Japan ([kmatsue@imi.kyushu-u.ac.jp](mailto:kmatsue@imi.kyushu-u.ac.jp))

<sup>‡</sup>International Institute for Carbon-Neutral Energy Research (WPI-I<sup>2</sup>CNER), Kyushu University, Fukuoka 819-0395, Japan

<sup>§</sup>Faculty of Engineering, Information and Systems, University of Tsukuba, 1-1-1 Tennodai, Tsukuba, Ibaraki 305-8573, Japan ([takitoshi@risk.tsukuba.ac.jp](mailto:takitoshi@risk.tsukuba.ac.jp))

where  $t \in [0, T)$  with  $0 < T \leq \infty$ ,  $f : \mathbb{R}^n \rightarrow \mathbb{R}^n$  is a  $C^1$  function and  $y_0 \in \mathbb{R}^n$ . We call a solution  $\{y(t)\}$  of the initial value problem (1.1) a *blow-up solution* if

$$t_{\max} \stackrel{\text{def}}{=} \sup \{ \bar{t} \mid \text{a solution } y \in C^1([0, \bar{t})) \text{ of (1.1) exists} \} < \infty.$$

The maximal existence time  $t_{\max}$  is then called the *blow-up time* of (1.1). Blow-up solutions can be seen in many dynamical systems generated by ODEs, or partial differential equations (PDEs) like nonlinear heat equations or Keller-Segel systems. These dynamical systems are categorized as exhibiting finite-time singularities, and have been the center of attention of many researchers, who have studied these phenomena from mathematical, physical, numerical viewpoints and so on (e.g. [23, 32, 51, 60] from theoretical viewpoints and e.g. [1, 5, 14, 15, 63] from numerical viewpoints). Fundamental questions for blow-up problem are *whether or not a solution blows up* and, if it does, *when, where, and how* it blows up. In general, blow-up phenomena depend on initial data (conditions), and rigorously characterizing them as functions of initial data remains nontrivial.

A typical approach for studying and proving existence of blow-up solutions is via *energy estimates* (see e.g. [23]), namely inequalities (involving energy functionals associated with the systems) giving sufficient conditions for existence of blow-up. In such cases, relatively large initial data induce finite-time blow-up. However, in general, these criteria do not provide an answer on how large initial points should be to exhibit blow-up and how solutions behave when these criteria are violated. There are several cases where initial points are divided such that solutions through them either exist globally in time or blow-up by means of (bounded) stationary solutions (e.g. [24]). A stationary solution with the above property is referred to as *the separatrix*, which plays a key role in describing asymptotic behavior of solutions. Despite their importance, results about the existence and explicit description of separatrices are limited. On the other hand, there are also results about blow-ups in which the magnitude of initial points does not matter. Alternative approaches to the energy estimates have been introduced to prove such blow-ups, but their dependence on initial points remain unknown in many cases, while arguments based on energy estimates easily yield the continuous dependence of blow-up behavior on initial points by continuity of energy functionals. Furthermore, there are also blow-up solutions whose asymptotic behavior is described not only by divergence, but also by complex behavior like oscillations, some of which are mentioned in Section 1.2. Mathematical and physical importance for studying blow-up behavior follow from such rich nature, but their comprehensive understanding are limited to well-known systems like PDEs mentioned above at present. See e.g. [23, 25] for more detailed summaries of blow-up problems including another well-known characterization of blow-up solutions by means of (backward) *self-similarity*.

Meanwhile, the second author has recently proposed a description of blow-up solutions from the viewpoint of dynamical systems. More precisely, *compactifications* of the phase space  $\mathbb{R}^n$  is applied to mapping the infinity onto points on the boundary  $\mathcal{E}$  of a compact manifold or their tangent spaces denoted by  $\overline{\mathcal{D}}$  with  $\partial\mathcal{D} = \mathcal{E}$ . Accordingly the vector field (1.1) is transformed to one on the corresponding manifolds, but the behavior of solutions near the boundary is still singular reflecting the behavior of the original vector field at infinity. The time-scale transformation, which shall be called the *time-scale desingularization*, is then introduced to desingularize the singularity of the vector field around  $\mathcal{E}$ . Consequently, *dynamics at infinity* can be characterized through the time-transformed vector field, called *the desingularized vector field*, on  $\overline{\mathcal{D}}$ . Standard arguments in the theory of dynamical systems through compactifications show that divergent solutions of (1.1) correspond to time-global solutions of the desingularized vector field converging to invariant sets

on  $\mathcal{E}^1$ . A significant consequence of the preceding studies is that, a solution of (1.1) with bounded initial point is a blow-up solution, namely  $t_{\max} < \infty$ , if the image of the solution through a compactification mentioned above is on the stable manifold of a *hyperbolic* equilibrium on  $\mathcal{E}$  for the desingularized vector field<sup>2</sup>. Simultaneously, the second and the third authors have developed a *computer-assisted* methodology for proving the existence of blow-up solutions for concretely given dynamical systems with rigorous bound of their blow-up times [48, 49, 57]. The basic idea is the combination of compactifications as well as time-scale desingularizations mentioned above with rigorous integrator of ODEs based on interval (and affine) arithmetic and topological characterizations of asymptotic behavior such as locally defined Lyapunov functions. The methodology works successfully for validating profiles and blow-up times of blow-up solutions generated by hyperbolic *stable* equilibria at infinity, while blow-up generated by unstable equilibria at infinity is not reported yet due to several technical difficulties. Note that there is another work for characterizing blow-up solutions with computer assistance by the first author and his collaborators based on analytic approach [16] whose detail is briefly mentioned in Section 1.2.

On the other hand, from the viewpoint of dynamics at infinity itself, namely when the viewpoint of blow-up characterizations is not considered, asymptotic behavior of unstable invariant sets at infinity is quite natural to study towards description of global bounded dynamics (e.g. [19, 20, 21, 29, 39]). We then believe that blow-up solutions generated by unstable invariant sets at infinity contribute towards the comprehensive understanding of global dynamics, including characteristics such as criteria for the existence, dependence on initial points and analytic information of blow-up times. Despite many mathematical and numerical studies of blow-ups, characterizations and computations of blow-up solutions which are unstable under perturbations of initial points in a standard way are not realistic because we have to treat two numerical difficulties simultaneously:

- instability of profiles under perturbations of initial points, and
- treatment of infinity.

We shall call such blow-up solutions *unstable blow-up solutions* in the present paper, or *saddle-type blow-up solutions* respecting the structure of equilibria at infinity in successive sections. This fuzzy nature is difficult to characterize clearly in general, while such behavior can be partially observed in several practical problems as mentioned in Section 1.2.

The main aim of the present paper is to reveal the nature of unstable blow-up solutions through *computer-assisted proofs*, equivalently *rigorous numerics*, of blow-up characterizations with the dynamical systems machineries mentioned above. Computer-assisted proofs are one way to both characterize and visualize mathematical objects. Keeping the success of computer-assisted proofs for various applications to dynamical systems (e.g. [13, 16, 48, 49, 57]) in mind, we believe that studying blow-up solutions with computer-assisted proofs provides rich insights into asymptotic behavior of solutions to differential equations as well as new research directions of global dynamics and finite-time singularities.

Our first target here is the validation of unstable blow-up solutions. As for treatments of dynamics at infinity, compactifications and time-scale desingularizations are suitable. In the present study, invariant sets at infinity are restricted to equilibria. In order to extract asymptotic behavior

---

<sup>1</sup>The above ideas themselves are applied to describe dynamics around bounded invariant sets in several preceding works (e.g. [20]).

<sup>2</sup>The same conclusion holds for hyperbolic periodic orbits on  $\mathcal{E}$ . A brief comment about the statement is mentioned in Remark 1.1. Several theoretical generalizations are discussed in [46].

solutions around unstable equilibria, we apply *the parameterization method* (e.g. see [10, 11, 12]) to validating local stable manifolds of equilibria, which is the main difference from the preceding works. Once local stable manifolds of equilibria through the parameterization are validated, extension of these manifolds through flow trajectories can be also validated through the standard ODE integrations, as in preceding works [48, 49, 57]. There are two main contributions of applications of the parameterization method for validating blow-up solutions which have not been obtained in previous studies. The first point is that blow-up solutions can be validated *no matter what the stability of the equilibria at infinity is*. We see that the parameterization method overcomes the sensitivity problem for computing blow-up solutions which break under generic perturbations of initial points. The second point is *the explicit and exact description of blow-up times* near blow-up. Since our parameterizations of local stable manifolds are expressed as real-analytic functions and the conjugate dynamical systems (on stable manifolds) are linear, we can directly compute the blow-up time as a function of points on stable manifolds by standard calculus. The parameterization method as well as dynamical treatment of blow-up solutions not only enables us to study global nature of dynamical systems around infinity but also unravel an analytic and computable nature of blow-up times.

Computer-assisted proofs applied here provide both qualitatively and quantitatively important and interesting features of blow-up nature. The main features of blow-up solutions we shall extract in the present paper are summarized as follows, which are collected as our second target in the present work;

- The blow-up time is locally real-analytic as a function of initial points near blow-up.
- Level sets of blow-up times locally constructs a foliation, independent of dynamics at infinity, near blow-up.
- Unstable blow-up solutions or time-global solutions connecting those blow-up solutions can separate initial points into two regions, either globally bounded or blow-up, no matter how large initial points are.
- The above feature induces discontinuity of blow-up times.

All these features rely on computer-assisted proofs, implying that all results are mathematically rigorous and the methodology towards these results are available to a large class of ordinary differential equations *without any knowledge of blow-up behavior*.

## 1.1 Organization of the paper

The rest of the present paper is organized as follows. In Section 2, we review a methodology for characterizing blow-up solutions from the viewpoint of dynamical systems, which is based on compactifications and time-scale desingularizations studied in e.g. [45]. Three types of compactifications are shown there: *directional*, *Poincaré-type* and *parabolic-type* ones. While advantages and disadvantages of each compactification depending the situation are mentioned, we see that divergent solutions including blow-up solutions can be characterized by using any choice of the above compactifications in a systematic way. In Section 3, the parameterization method for calculating invariant manifolds is summarized. In the present paper, we restrict our attention to stable manifolds of equilibria. Under an essential assumption called the non-resonance condition

of eigenvalues, local stable manifolds can be characterized as zeros of a countable family of nonlinear equations on Banach spaces. Combining with the method of *radii polynomials*, which is one of standard functional-analytic and algebraic machineries for finding zeros of (infinite-dimensional) nonlinear maps, computer-assisted proofs of the existence and characterization of local stable manifolds are provided. Note that the non-resonance condition yields that validated stable manifolds can be given as locally *real-analytic* functions. In Section 4, we provide a methodology of computer-assisted proofs of the existence of blow-up solutions. Since the detailed implementations such as the choice of compactifications and time-scale transformations is problem dependent, only the basic idea for validating blow-up solutions are presented therein. We also show that the present methodology enables us to provide an exact and explicit formula of the maximal existence time, equivalently the blow-up time, of solutions as a smooth or real-analytic function of initial points near blow-up, provided all our implementations work successfully. The present characterization of the maximal existence time provides us with a quantitative feature of blow-up solutions such as distributions of blow-up times depending on initial data which are not provided in preceding works [48, 49, 57]. The applicability of the present methodology is shown in successive sections. All examples here focus on *saddle-type blow-up solutions*, namely blow-up solutions characterized by trajectories of hyperbolic saddle equilibria at infinity for an appropriately transformed dynamical systems. Note that generic perturbations of bounded initial points violate computing such blow-up behavior in general. Nevertheless, the present methodology successfully validate these solutions.

In Section 5, a two-dimensional ODE possessing saddle-type blow-up solutions is considered. A locally defined (i.e. directional) compactification is applied, and a saddle-type blow-up solutions as well as the blow-up time as a function of initial points is validated to check the applicability of our methodology to locally distributed blow-up solutions. In particular, the blow-up profile as well as its blow-up time as a function of initial points are successfully validated and visualized. In Section 6, we consider a three-dimensional system. The Poincaré-type compactification is applied, and one- and two-dimensional stable manifolds of saddle equilibria at infinity are validated. The aim is to show the applicability of our methodology to saddle-type blow-up solutions distributed on multi-dimensional stable manifolds of unstable invariant sets at infinity. Furthermore, distribution of blow-up times as a function of initial points on two-dimensional stable manifolds are validated, which shows a relationship of blow-up times and the structure of stable manifolds at infinity. In Section 7, a two-dimensional ODE which is quasi-homogeneous in an asymptotic sense is considered. The system possesses both stable and unstable equilibria at infinity. The parabolic-type compactification is applied and a saddle-type blow-up solution is firstly validated, while validations of blow-up solutions asymptotic to stable equilibria at infinity are already demonstrated in a preceding work [48]. The main aim of this section is to study a global nature of solution families in a neighborhood of saddle-type blow-up solutions. In particular, the role of the *separatrix* decomposing initial points into collections of blow-up solutions and time-global solutions is observed. This property can induce a *singular behavior of blow-up times*, which cannot be seen in families of blow-up solutions asymptotic to stable equilibria at infinity. Moreover, it is also shown that the separatrix nature of blow-up solutions can divide the sets of initial points into those with globally-bounded nature and blow-up nature, *no matter how large magnitudes of initial points are*. Note again that this separation cannot be seen in blow-up solutions asymptotic to stable equilibria at infinity. All the codes for generating results with computer-assisted proofs in Sections 5, 6 and 7 are available at [42].

## 1.2 Remarks on unstable blow-up solutions in science and engineering

Unstable blow-up solutions can arise in scientific and engineering studies. We review several preceding studies to assert the importance of unstable blow-up solutions.

### 1.2.1 Singular shock waves

In the Riemann problem of the systems of *conservation laws*

$$U_t + f(U)_x = 0 \quad (1.2)$$

for some smooth  $f : \mathbb{R}^n \rightarrow \mathbb{R}^n$ , namely the initial value problem of (1.2) with

$$U(0, x) = \begin{cases} U_L & x < 0, \\ U_R & x > 0, \end{cases} \quad \text{for } U_L, U_R \in \mathbb{R}^n,$$

*shock waves* are characterized by locally integrable (weak) solutions with discontinuities with the constraints called *jump conditions* or the *Rankine-Hugoniot conditions*. With the assumption of *viscous shock criterion*, the Riemann problem is reduced to find connecting orbits of the traveling wave ODE associated with (1.2) connecting  $U_L$  and  $U_R$ . In the 1980s and 1990s, shock waves with a singular nature on the front were observed for a simple system of conservation laws, which are referred to as *delta-shocks* or *singular shocks*. Roughly speaking, singular shocks are characterized by shocks with Dirac's delta singularity on the shock front (see e.g. [38, 40, 56] for precise discussions of delta-shocks and singular shocks). A typical feature of singular shocks with the presence of the delta-like singularity is that several constraints in jump conditions are violated<sup>3</sup>, which is referred to as the presence of the *Rankine-Hugoniot deficit* of a shock measuring the magnitude of singularity on the shock front. From the viewpoint of dynamical systems, there is a characterization of singular shocks (e.g. [54]), showing that *singular shocks can consist of a collection of blow-up solutions and "invariant sets at infinity"*. In several concrete problems such as the Keyfitz-Kranser model [40] and the two-phase model [38], the geometric singular perturbation theory plays a key role in characterizing singular shocks as a singular perturbation of blow-up connections for the traveling wave problems associated with the original conservation laws with the regularization keeping the self-similarity of waves (well-known as *Dafermos regularization*). Preceding studies with blowing-up (desingularization) of singularities and the geometric singular perturbation theory indicate that singular shocks are characterized by trajectories approaching to *normally hyperbolic invariant manifolds*, corresponding to the infinity for appropriately transformed dynamical systems [33, 55]<sup>4</sup>. Blow-up solutions associated with unstable equilibria at infinity as well as quantities involving dynamics at infinity can thus play key roles in characterizing such singular nature.

### 1.2.2 Suspension bridge

The equation of the following form is well studied as a model expressing scientific and engineering phenomena:

$$w''''(t) + kw''(t) + f(w(t)) = 0 \quad (t \in \mathbb{R}), \quad (1.3)$$

<sup>3</sup>In  $n$ -dimensional systems of conservation laws, jump conditions are characterized by  $n$  (non)linear equations.

<sup>4</sup>It is also indicated that the Rankine-Hugoniot deficit is measured by trajectories at infinity connecting blow-up solutions [38]. When the Rankine-Hugoniot deficit is absent, the corresponding shock wave is characterized in the ordinary sense.

where  $k \in \mathbb{R}$  is a parameter and  $f$  is a locally Lipschitzian. This equation arises in the dynamical phase-space analogy of a nonlinearly supported elastic structure [34] and a model characterizing pattern formations in physical, chemical and biological systems [7]. See also e.g. [52]. In [4], a possible finite-time blow-up for the solution of (1.3) is discussed with a mild assumption

$$f \in \text{Lip}_{loc}(\mathbb{R}), \quad f(t)t > 0 \quad \text{for every } t \in \mathbb{R} \setminus \{0\}.$$

A fundamental result involving blow-up is that the existence of a blow-up solution  $w(t)$  for (1.3) as  $t \rightarrow t_{\max} < \infty$  implies that

$$\liminf_{t \rightarrow t_{\max}} w(t) = -\infty \quad \text{and} \quad \limsup_{t \rightarrow t_{\max}} w(t) = +\infty, \quad (1.4)$$

namely a blow-up with oscillation. Moreover, the existence of the above oscillatory blow-up for (1.3) with a specific nonlinearity  $f$  is proved. There are several reports about the relationship between the system (1.3) to traveling waves for the the model equation of a *suspension bridge*

$$u_{tt} + u_{xxxx} + \gamma u^+ = W(t, x),$$

proposed by Lazer-McKenna [41]. According to many preceding works and historical sources, one of the most interesting behaviors for suspension bridges (including the Tacoma Narrow Bridge where was collapsed in November 1940) is the following:

Large vertical oscillations can rapidly change, almost instantaneously, to a *torsional oscillation* (quotation from [26]).

Preceding works involving this catastrophic phenomenon discuss the mechanism of torsional oscillations in detail<sup>5</sup>, one of which is considered to be the oscillatory blow-up behavior mentioned above. It should be noted that there is another direction to the origin of such torsional oscillations. In [2], it is explained that *internal resonances* can trigger the torsional instability.

Later successive works (e.g. [27]) have reported the qualitative nature of the above blow-up such as infinitely many change of signs before blow-up, vanishing intervals of oscillations several quantitative estimates. In order to obtain the nature, several growth conditions of  $f$  (but generalized under these conditions unlike [26]), restrictions to  $k$  and an inequality for derivatives of solution  $w$  at an initial time are assumed. It should be noted that *norms of initial points are not essential to characterize the above behavior*. See [27] for details. Recently, the first author and collaborators [16] have characterized the above blow-up nature for particular nonlinearity  $f$  in (1.3) by constructing a concrete asymptotic form of blow-up profiles and validating a periodic solution with rigorous numerics. In [16], it is also validated that the periodic solution for an auxiliary equation is unstable, which indicates that *the corresponding blow-up solution is unstable under perturbations of initial points*. It is thus expected that the blow-up nature which is unstable under perturbations of initial points plays a key role in describing rich and interesting, sometimes catastrophic, scientific and engineering nature.

**Remark 1.1.** *In [45], it is proved that blow-up behavior with wide oscillations like (1.4) can be characterized by periodic orbits at infinity, which is referred to as a periodic blow-up. More*

<sup>5</sup>In [27], there are several additional comments about the case of London's Millennium Bridge (April 2007) and the Assago metro Bridge in Milan (February 2011). See the reference papers therein for details about these engineering topics.

precisely, global trajectories on the stable manifold of a hyperbolic periodic orbit at infinity for an appropriately transformed vector field correspond to blow-up solutions with oscillations whose asymptotic behavior, such as the blow-up rate and the oscillatory nature, are uniquely determined by the order of the original vector field and the periodic orbit at infinity. The fundamental machinery for this characterization is the same as that shown in Section 2. Arguments in the present paper can thus contribute to reveal a universal mechanism of unstable blow-up solutions and validations of their quantitative nature.

## 2 Preliminary 1: Characterization of blow-up solutions

In this section we briefly review a characterization of blow-up solutions for autonomous, finite dimensional ODEs from the viewpoint of dynamical systems. Details of the present methodology are already provided in [45, 49]. At the end of this section, we mention our central interests in this paper.

Consider the initial value problem of an autonomous system of ODEs

$$y' = \frac{dy(t)}{dt} = f(y(t)), \quad y(0) = y_0, \quad (2.1)$$

where  $t \in [0, T)$  with  $0 < T \leq \infty$ ,  $f : \mathbb{R}^n \rightarrow \mathbb{R}^n$  is a  $C^1$  function and  $y_0 \in \mathbb{R}^n$ .

### 2.1 Asymptotically quasi-homogeneous vector fields

First of all, we review a class of vector fields in our present discussions.

**Definition 2.1** (Asymptotically quasi-homogeneous vector fields, cf. [18, 45]). Let  $f : \mathbb{R}^n \rightarrow \mathbb{R}^n$  be a smooth function. Let  $\alpha_1, \dots, \alpha_n, k \geq 1$  be natural numbers. We say that  $f$  is a *quasi-homogeneous function of type  $(\alpha_1, \dots, \alpha_n)$  and order  $k$*  if

$$f(s^{\alpha_1} x_1, \dots, s^{\alpha_n} x_n) = s^k f(x_1, \dots, x_n), \quad \forall x \in \mathbb{R}^n, \quad s \in \mathbb{R}.$$

Next, let  $X = \sum_{j=1}^n f_j(x) \frac{\partial}{\partial x_j}$  be a smooth vector field on  $\mathbb{R}^n$ . We say that  $X$ , or simply  $f = (f_1, \dots, f_n)$  is a *quasi-homogeneous vector field of type  $(\alpha_1, \dots, \alpha_n)$  and order  $k + 1$*  if each component  $f_j$  is a quasi-homogeneous function of type  $(\alpha_1, \dots, \alpha_n)$  and order  $k + \alpha_j$ .

Finally, we say that  $X = \sum_{j=1}^n f_j(x) \frac{\partial}{\partial x_j}$ , or simply  $f$  is an *asymptotically quasi-homogeneous vector field of type  $(\alpha_1, \dots, \alpha_n)$  and order  $k + 1$  at infinity* if

$$\lim_{s \rightarrow +\infty} s^{-(k+\alpha_j)} \{f_j(s^{\alpha_1} x_1, \dots, s^{\alpha_n} x_n) - s^{k+\alpha_j} (f_{\alpha,k})_j(x_1, \dots, x_n)\} = 0$$

holds uniformly for  $(x_1, \dots, x_n) \in S^{n-1}$  for some quasi-homogeneous vector field  $f_{\alpha,k} = ((f_{\alpha,k})_j)_{j=1}^n$  of type  $(\alpha_1, \dots, \alpha_n)$  and order  $k + 1$ .

Throughout successive sections, consider the (autonomous) vector field (2.1), where  $f : \mathbb{R}^n \rightarrow \mathbb{R}^n$  is an asymptotically quasi-homogeneous smooth vector field of type  $\alpha = (\alpha_1, \dots, \alpha_n)$  and order  $k + 1$  at infinity.



## 2.2 Directional compactifications

There are several compactifications reflecting (asymptotic) quasi-homogeneity of vector fields at infinity. For example, the transform  $y = (y_1, \dots, y_n) \mapsto T_d(y) = (s, \hat{x}) \equiv (s, \hat{x}_1, \dots, \hat{x}_{i-1}, \hat{x}_{i+1}, \dots, \hat{x}_n)$  given by

$$y_j = \frac{\hat{x}_j}{s^{\alpha_j}} \quad (j \neq i), \quad y_i = \pm \frac{1}{s^{\alpha_i}} \quad (2.2)$$

is a kind of compactification<sup>6</sup>, for which the infinity corresponds to the subspace  $\mathcal{E} \stackrel{\text{def}}{=} \{s = 0\}$ . The domain of definition for this compactification is  $\mathbb{R}^{i-1} \times \{y_i > 0\} \times \mathbb{R}^{n-i}$  and the image is

$$\mathcal{D} = \{(s, \hat{x}_1, \dots, \hat{x}_{i-1}, \hat{x}_{i+1}, \dots, \hat{x}_n) \mid s > 0, \hat{x}_j \in \mathbb{R} \quad (j \neq i)\}. \quad (2.3)$$

The horizon  $\mathcal{E}$  is identified with  $\partial\mathcal{D}$  in the space  $\{(s, \hat{x}_1, \dots, \hat{x}_{i-1}, \hat{x}_{i+1}, \dots, \hat{x}_n) \in \mathbb{R}^n\}$ . We shall call such a compactification a *directional compactification with the type*  $\alpha = (\alpha_1, \dots, \alpha_n)$ , according to [45]. The set  $\mathcal{E} = \{s = 0\}$  representing the infinity is called *the horizon*. This compactification is geometrically characterized as a local coordinate of quasi-Poincaré hemisphere of type  $\alpha$ :

$$\mathcal{H}_\alpha \stackrel{\text{def}}{=} \left\{ (y_1, \dots, y_n, s) \in \mathbb{R}^{n+1} \mid \frac{1}{(1 + p(y)^{2c})} \sum_{i=1}^n y_i^{2\beta_i} + s^{2c} = 1 \right\},$$

at  $(x_1, \dots, x_n, s) = (0, \dots, 0, x_i = \pm 1, 0, \dots, 0, 0)$ . See [45] for details. Note that the coordinate representation (2.2) only makes sense in  $\{\pm y_i > 0\}$ , in which sense directional compactifications are *local* ones. In particular, whenever we consider trajectories whose  $y_i$ -component can change sign, we have to take care of transformations among coordinate neighborhoods, which is quite tough for numerical integration of differential equations. Nevertheless, this compactification is a very simple and powerful tool *if we consider solutions near infinity whose  $y_i$ -component is known a priori to have identical sign*. A homogeneous compactification of this kind is shown in Figure 1-(a).

## 2.3 Admissible global quasi-homogeneous compactifications

Here we define a class of globally defined compactifications.

**Definition 2.2** (Admissible global quasi-homogeneous compactification). Fix natural numbers  $\alpha_1, \dots, \alpha_n$ . Let  $\beta_1, \dots, \beta_n$  be natural numbers<sup>7</sup> such that

$$\alpha_1\beta_1 = \alpha_2\beta_2 = \dots = \alpha_n\beta_n \equiv c \in \mathbb{N}. \quad (2.4)$$

Define a functional  $p(y)$  as

$$p(y) \stackrel{\text{def}}{=} \left( y_1^{2\beta_1} + y_2^{2\beta_2} + \dots + y_n^{2\beta_n} \right)^{1/2c}.$$

<sup>6</sup>Although  $T_d$  is not a compactification in the topological sense, we shall use this terminology for  $T_d$  from its geometric interpretation shown below.

<sup>7</sup>The simplest choice of the natural number  $c$  is the least common multiple of  $\alpha_1, \dots, \alpha_n$ . Once we choose such  $c$ , we can determine the  $n$ -tuples of natural numbers  $\beta_1, \dots, \beta_n$  uniquely. The choice of natural numbers in (2.4) is essential to desingularize vector fields at infinity, as shown below.

Define the mapping  $T : \mathbb{R}^n \rightarrow \mathbb{R}^n$  as

$$T(y) = x, \quad x_i \stackrel{\text{def}}{=} \frac{y_i}{\kappa(y)^{\alpha_i}}, \quad (2.5)$$

where  $\kappa = \kappa(y)$  is a  $C^1$  positive function. We say that  $T$  is an *admissible global (quasi-homogeneous) compactification (of type  $\alpha$ )* if all the following conditions hold:

- (A0)  $\kappa(y) = q \circ p(y)$  for some positive, smooth function  $q = q(R)$  defined on  $R \geq 0$  which is strictly increasing in  $R > 0$ , and  $\kappa(y) > p(y)$  holds for all  $y \in \mathbb{R}^n$ ,
- (A1) For any sequence  $\{y_n\}_{n \geq 1} \subset \mathbb{R}^n$  with  $p(y_n) \rightarrow \infty$  as  $n \rightarrow \infty$ ,  $\lim_{n \rightarrow \infty} \{p(y_n)/\kappa(y_n)\} = 1$  holds,
- (A2)  $\nabla \kappa(y) = ((\nabla \kappa(y))_1, \dots, (\nabla \kappa(y))_n)$  satisfies

$$(\nabla \kappa(y))_i \sim \frac{1}{\alpha_i} \frac{y_i^{2\beta_i-1}}{p(y)^{2c-1}} \quad \text{as } p(y) \rightarrow \infty.$$

- (A3) Letting  $y_\alpha = (\alpha_1 y_1, \dots, \alpha_n y_n)^T$  for  $y \in \mathbb{R}^n$ , we have  $\langle y_\alpha, \nabla \kappa \rangle < \kappa(y)$  holds for any  $y \in \mathbb{R}^n$ .

In the present argument, the notation  $f(x) \sim g(x)$  means that there exists a constant  $K > 1$  such that  $K^{-1}g(x) < f(x) < Kg(x)$  for large  $x$ . As proved in [49],  $T$  maps  $\mathbb{R}^n$  into

$$\mathcal{D} \stackrel{\text{def}}{=} \{x \in \mathbb{R}^n \mid p(x) < 1\}. \quad (2.6)$$

The infinity in the original coordinate then corresponds to a point on the boundary

$$\mathcal{E} = \{x \in \mathbb{R}^n \mid p(x) = 1\}.$$

We call the boundary  $\mathcal{E}$  the *horizon*, according to [45, 49]<sup>8</sup>. The horizon determines directions where solution trajectories diverge.

**Definition 2.3.** We say that a solution orbit  $y(t)$  of (2.1) with the maximal existence time  $(a, b)$ , possibly  $a = -\infty$  and  $b = +\infty$ , *tends to infinity in the direction  $x_* \in \mathcal{E}$  (associated with  $T$ )* (as  $t \rightarrow a^+$  or  $t \rightarrow b^-$ ) if

$$p(y(t)) \rightarrow \infty, \quad \left( \frac{y_1}{\kappa(y)^{\alpha_1}}, \dots, \frac{y_n}{\kappa(y)^{\alpha_n}} \right) \rightarrow x_* \quad \text{as } t \rightarrow a^+ \text{ or } t \rightarrow b^-.$$

Let the type  $\alpha = (\alpha_1, \dots, \alpha_n) \in \mathbb{Z}_{>0}^n$  fixed. Also, let  $\{\beta_i\}_{i=1}^n$  and  $c$  be a collection of natural numbers satisfying (2.4).

### 2.3.1 Poincaré-type compactifications

The prototype of our admissible global compactifications is the *Poincaré's type*.

**Definition 2.4.** The *Poincaré-type compactification* is defined as the mapping  $T = T_{para}$  given in (2.5) with  $\kappa(y) = \kappa_{qP}(y) \stackrel{\text{def}}{=} (1 + p(y)^{2c})^{1/2c}$ .

<sup>8</sup>In preceding works with the *homogeneous* setting, the boundary  $\mathcal{E}$  is often called *the equator*.

The homogeneous case  $\alpha = (1, \dots, 1)$  is geometrically simple. Indeed,  $p(y) = \|y\|$  and we can choose  $\beta = (1, \dots, 1)$  and  $c = 1$ . Hence  $\kappa(y) = \kappa_{qP}(y) = (1 + \|y\|^2)^{1/2}$ , which is a well-known (global, but homogeneous) compactification<sup>9</sup>, and the resulting mapping  $T$  is the embedding of  $\mathbb{R}^n$  into the Poincaré hemisphere

$$\mathcal{H} = \{(x_1, \dots, x_n, \lambda) \in \mathbb{R}^{n+1} \mid \|x\|^2 + \lambda^2 = 1, \lambda > 0\}.$$

A homogeneous compactification of this kind is shown in Figure 1-(b).

### 2.3.2 Parabolic-type compactifications

The Poincaré-type compactifications include radicals in the definition, which cause the loss of smoothness at infinity, as discussed in [45]. Therefore an alternative type of compactification, which shall be called *parabolic-type* compactification, is also applied for expressing unbounded solutions in a global chart. Compactifications of the present type were originally introduced in [28] and generalized in [49].

For any  $x \in \mathcal{D}$ , define  $y \in \mathbb{R}^n$  by

$$S(x) = y, \quad y_j = \frac{x_j}{(1 - p(x)^{2c})^{\alpha_j}}, \quad j = 1, \dots, n.$$

Let  $\tilde{\kappa}_\alpha(x) \stackrel{\text{def}}{=} (1 - p(x)^{2c})^{-1}$ , which satisfies  $\tilde{\kappa}_\alpha(x) \geq 1$  for all  $x \in \mathcal{D}$ . Moreover,  $y \neq 0$  implies  $\tilde{\kappa}_\alpha(x) > 1$ . We also have

$$p(y)^{2c} = \tilde{\kappa}_\alpha(x)^{2c} p(x)^{2c} = \tilde{\kappa}_\alpha(x)^{2c} \left(1 - \frac{1}{\tilde{\kappa}_\alpha(x)}\right). \quad (2.7)$$

This equality indicates that  $p(y) = p(S(x)) < \tilde{\kappa}_\alpha(x)$  holds for all  $x \in \mathcal{D}$ .

**Lemma 2.5** ([49]). *Let  $F(\kappa; R) \stackrel{\text{def}}{=} \kappa^{2c} - \kappa^{2c-1} - R^{2c}$  for  $R \geq 0$ . Then, for any  $R \geq 0$ , there is a unique  $\kappa = q(R)$  satisfying  $q(0) = 1$  such that  $F(q(R); R) \equiv 0$ . Moreover,  $q(R) > 1$  holds for all  $R > 0$  and  $q(R)$  is smooth with respect to  $R \geq 0$ .*

Now we have  $\tilde{\kappa}_\alpha(x)$  satisfies  $F(\tilde{\kappa}_\alpha(x); p(y)) = 0$ . By the uniqueness of  $\kappa(y) = q(R)$  with respect to  $R = p(y)$ , for any  $y \in \mathbb{R}^n \setminus \{\mathbf{0}\}$ ,  $\kappa(y) = \kappa_{para}(y) \equiv \kappa(S(x)) \stackrel{\text{def}}{=} \tilde{\kappa}_\alpha(x)$  is well defined.

**Definition 2.6** (Quasi-parabolic compactification, [49]). Let the type  $\alpha = (\alpha_1, \dots, \alpha_n) \in \mathbb{Z}_{>0}^n$  fixed. Let  $\{\beta_i\}_{i=1}^n$  and  $c$  be a collection of natural numbers satisfying (2.4). Define  $T_{para} : \mathbb{R}^n \rightarrow \mathcal{D}$  as

$$T_{para}(y) \stackrel{\text{def}}{=} x, \quad x_i = \frac{y_i}{\kappa_{para}(y)^{\alpha_i}},$$

where  $\kappa = \kappa_{para}(y) = \tilde{\kappa}_\alpha(x)$  is the unique zero of  $F(\kappa; p(y)) = 0$  given in Lemma 2.5. We say that  $T_{para}$  is the *quasi-parabolic compactification (with type  $\alpha$ )*.

It is proved in [49] that  $T_{para}$  is an admissible global quasi-homogeneous compactification. It is easy to understand the geometric nature of the present compactification when  $\alpha = (1, \dots, 1)$ , in which case  $T_{para}$  is defined as

$$x_j = \frac{2y_j}{1 + \sqrt{1 + 4\|y\|^2}} \quad \Leftrightarrow \quad y_j = \frac{x_j}{1 - \|x\|^2}, \quad j = 1, \dots, n.$$

<sup>9</sup>In many references, this compactification is called the *Poincaré compactification*. The quasi-homogeneous counterpart is introduced in [45] where the corresponding mapping  $T$  is called the *quasi-Poincaré compactification*.

See [22, 28] for the homogeneous case, which is called the *parabolic compactification*. A homogeneous compactification of this kind is shown in Figure 1-(c).

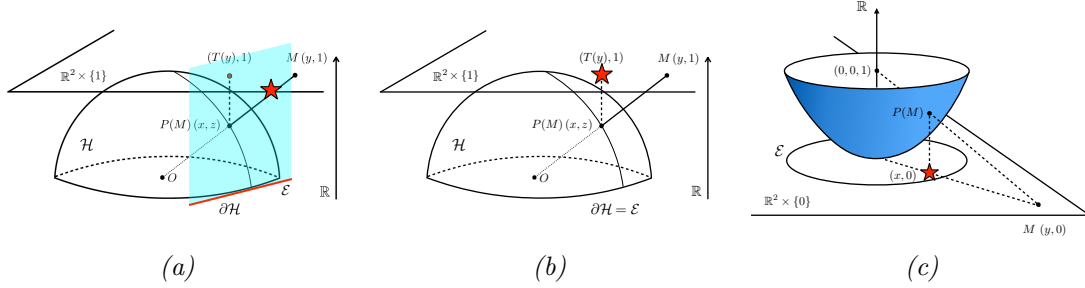


Figure 1: Homogeneous compactifications of  $\mathbb{R}^2$

(a): Directional compactification with type  $\alpha = (1, 1)$ . The original point  $M = (y, 1) \in \mathbb{R}^2 \times \{1\}$  is mapped into the point (drawn as the red star) on the upper-half tangent space (colored by skyblue) of a point on  $\partial\mathcal{H}$ , where  $\mathcal{H}$  is the Poincaré's hemisphere determining the Poincaré compactification. The boundary  $\mathcal{E}$  of the upper-half tangent space (the red line) is the horizon.

(b): Poincaré compactification with type  $\alpha = (1, 1)$ . The image  $T(y)$  of the original point  $y \in \mathbb{R}^2$  is defined as the projection of the intersection point  $P(M) \in \mathcal{H}$ , given by the line segment connecting  $M = (y, 1) \in \mathbb{R}^3$  and the origin  $O \in \mathbb{R}^3$ , onto the original phase space  $\mathbb{R}^2$ . The horizon is identified with  $\partial\mathcal{H}$ . The precise definition is its projection onto  $\mathbb{R}^2 \times \{1\}$ .

(c): Parabolic compactification with type  $\alpha = (1, 1)$ . The image  $x$  of the original point  $y \in \mathbb{R}^2$  is defined as the projection of the intersection point  $P(M) \in \mathcal{H}$  determined by the paraboloid  $x_1^2 + x_2^2 = x_3$  in  $\mathbb{R}^3$  and the line segment connecting  $M = (y, 0) \in \mathbb{R}^3$  and the focus point  $(0, 0, 1) \in \mathbb{R}^3$ , onto the original phase space  $\mathbb{R}^2$ . The horizon is identified with the circle  $\{x_1^2 + x_2^2 = 1\}$  on the paraboloid. The precise definition is its projection onto  $\mathbb{R}^2 \times \{0\}$ .

**Remark 2.7.** For any compactifications we have introduced, the compactification  $T$  is analytic at any point in the domain of definition by using the binomial theorem in the standard calculus and the inverse function theorem for analytic mappings (e.g. [17]).

## 2.4 Dynamics at infinity, blow-up criterion and the present targeting objects

Once we fix a compactification associated with the type  $\alpha = (\alpha_1, \dots, \alpha_n)$  of the vector field  $f$  with order  $k + 1$ , we can derive the vector field which makes sense including the horizon. Then the *dynamics at infinity* makes sense through the appropriately transformed vector field called the *desingularized vector field*, which we will denote by  $g$  throughout this paper. The common approach is twofold. First, we rewrite the vector field (2.1) with respect to the new variable used in compactifications. Second, we introduce the time-scale transformation  $d\tau = s(t)^{-k} dt$  for directional compactifications and  $d\tau = \kappa(y(t))^k dt$  for admissible global quasi-homogeneous compactifications, respectively. We then obtain the vector field with respect to the new time variable  $\tau$ , which is continuous, including at the horizon.

**Remark 2.8.** *Continuity for the desingularized vector field  $g$  including the horizon is guaranteed by the smoothness of  $f$  and asymptotic quasi-homogeneity ([45]). However, smoothness of  $g$  is not guaranteed on the horizon in general. More precisely,  $g$  inherits the smoothness of  $f$  through directional (of the form (2.2)) and parabolic-type compactifications. However, it is not always the case through Poincaré-type compactifications due to the presence of radicals. Details are discussed in [45]. The validity for the introduction of the time-scale desingularizations  $d\tau = s(t)^{-k}dt$  and  $d\tau = \kappa(y(t))^k dt$  is also discussed in [45].*

#### 2.4.1 Directional compactifications

For simplicity, set  $i = 1$  in (2.2). Let

$$\hat{f}_j(s, x_2, \dots, x_n) \stackrel{\text{def}}{=} s^{k+\alpha_j} f_j(s^{-\alpha_1}, s^{-\alpha_2} x_2, \dots, s^{-\alpha_n} x_n), \quad j = 1, \dots, n. \quad (2.8)$$

We obtain the desingularized vector field for directional compactifications whose details are shown in [45].

**Definition 2.9** (Time-variable desingularization: directional compactification version). Define the new time variable  $\tau_d$  by

$$d\tau_d = s(t)^{-k} dt \quad (2.9)$$

equivalently,

$$t - t_0 = \int_{\tau_0}^{\tau} s(\tau_d)^k d\tau_d,$$

where  $\tau_0$  and  $t_0$  denote the correspondence of initial times, and  $s(\tau_d)$  is the solution trajectory  $s(t)$  under the parameter  $\tau_d$ . We shall call (2.9) *the time-variable desingularization of order  $k + 1$* .

The desingularized vector field  $g = g_d$  in  $\tau_d$ -time scale is

$$\begin{pmatrix} \frac{ds}{d\tau_d} \\ \frac{dx_2}{d\tau_d} \\ \vdots \\ \frac{dx_n}{d\tau_d} \end{pmatrix} = g_d(s, x_1, \dots, x_{n-1}) \stackrel{\text{def}}{=} \begin{pmatrix} -s & 0 & \cdots & 0 \\ 0 & 1 & \cdots & 0 \\ \vdots & \vdots & \ddots & \vdots \\ 0 & 0 & \cdots & 1 \end{pmatrix} B \begin{pmatrix} \hat{f}_1 \\ \hat{f}_2 \\ \vdots \\ \hat{f}_n \end{pmatrix} \quad (2.10)$$

where  $B$  is the inverse<sup>10</sup> of the matrix

$$\begin{pmatrix} \alpha_1 & 0 & \cdots & 0 & 0 \\ \alpha_2 x_2 & 1 & \cdots & 0 & 0 \\ \vdots & \vdots & \ddots & \vdots & \vdots \\ \alpha_{n-1} x_{n-1} & 0 & \cdots & 1 & 0 \\ \alpha_n x_n & 0 & \cdots & 0 & 1 \end{pmatrix}.$$

---

<sup>10</sup>The existence of  $B$  immediately follows by cyclic permutations and the fact that  $\alpha_n > 0$ .

## 2.4.2 Poincaré-type compactifications

Let  $\kappa_{qP}(y) \stackrel{\text{def}}{=} (1 + p(y)^{2c})^{1/2c}$  and consider the compactification (2.5).

**Definition 2.10** (Time-variable desingularization: Poincaré-type compactification version). Define the new time variable  $\tau_d$  by

$$d\tau_{qP} = \kappa_{qP}(y(t))^k dt \quad (2.11)$$

equivalently,

$$t - t_0 = \int_{\tau_0}^{\tau} \kappa_{qP}(y(\tau_{qP}))^{-k} d\tau_{qP},$$

where  $\tau_0$  and  $t_0$  denote the correspondence of initial times, and  $y(\tau_{qP})$  is the solution trajectory  $y(t)$  under the parameter  $\tau_{qP}$ . We shall call (2.11) *the time-variable desingularization of order  $k + 1$* .

The change of coordinate and the above desingularization yield the following vector field  $g$ , which is continuous on  $\bar{D} = \{p(x) \leq 1\}$ :

$$\dot{x}_i = \frac{dx_i}{d\tau} = g_i(x) \stackrel{\text{def}}{=} \tilde{f}_i(x) - \alpha_i x_i \sum_{j=1}^n (\nabla \kappa)_j \kappa^{\alpha_j - 1} \tilde{f}_j(x), \quad (2.12)$$

where

$$\tilde{f}_j(x_1, \dots, x_n) := \kappa^{-(k+\alpha_j)} f_j(\kappa^{\alpha_1} x_1, \dots, \kappa^{\alpha_n} x_n), \quad j = 1, \dots, n, \quad (2.13)$$

which is the alternate object of  $\hat{f}_j$ 's in (2.8),  $\kappa = \kappa_{qP}(y)$  and

$$(\nabla \kappa)_j \equiv (\nabla_y \kappa(y))_j = \frac{\beta_j y_j^{2\beta_j - 1}}{c \kappa^{2c-1}} = \frac{\beta_j \kappa^{2c - \alpha_j} x_j^{2\beta_j - 1}}{c \kappa^{2c-1}} = \frac{x_j^{2\beta_j - 1}}{\alpha_j \kappa^{\alpha_j - 1}}. \quad (2.14)$$

In the above equality we have used (2.5) and the identity  $\alpha_j \beta_j \equiv c$  for all  $j = 1, \dots, n$ . Note from [45] that  $\kappa = \kappa_{qP}(y)$  has an equivalent expression by means of  $x$ :

$$\kappa = \kappa_{qP}(T^{-1}(x)) = \left( 1 - \sum_{j=1}^n x_j^{2\beta_j} \right)^{-1/2c}.$$

## 2.4.3 Parabolic-type compactifications

Let  $\kappa_{para}(y)$  be a functional given in Definition 2.6.

**Definition 2.11** (Time-variable desingularization: parabolic-type compactification version). Define the new time variable  $\tau_d$  by

$$d\tau_{para} = (1 - p(x)^{2c})^{-k} \left\{ 1 - \frac{2c-1}{2c} (1 - p(x)^{2c}) \right\}^{-1} dt \quad (2.15)$$

equivalently,

$$t - t_0 = \int_{\tau_0}^{\tau} \left\{ 1 - \frac{2c-1}{2c} (1 - p(x(\tau_{para}))^{2c}) \right\} (1 - p(x(\tau_{para}))^{2c})^k d\tau_{para},$$

where  $\tau_0$  and  $t_0$  denote the correspondence of initial times, and  $y(\tau_{qP})$  is the solution trajectory  $y(t)$  under the parameter  $\tau_{qP}$ . We shall call (2.11) *the time-variable desingularization of order  $k + 1$* .

The change of coordinate and the above desingularization yield the following vector field  $g$ , which is continuous on  $\overline{D} = \{p(x) \leq 1\}$ :

$$\dot{x}_i = g_i(x) \stackrel{\text{def}}{=} \left(1 - \frac{2c-1}{2c}(1 - p(x)^{2c})\right) \left\{ \tilde{f}_i(x) - \alpha_i x_i \sum_{j=1}^n (\nabla \kappa)_j \kappa^{\alpha_j - 1} \tilde{f}_j(x) \right\}, \quad (2.16)$$

where  $\nabla_y \kappa(y)$  has the form similar to (2.14), more precisely,

$$(\nabla_y \kappa(y))_j = \frac{y_j^{2\beta_j - 1}}{\alpha_j \kappa(y)^{2c-1} \left(1 - \frac{2c-1}{2c} \kappa(y)^{-1}\right)}$$

derived in [48]. Moreover, the smoothness of  $f$  and the asymptotic quasi-homogeneity guarantee the smoothness of the right-hand side  $g$  of (2.16) including the horizon  $\{p(x) = 1\}$ . See [49] for details.

#### 2.4.4 Blow-up criterion

For any compactifications we have introduced, *dynamics at infinity* can be analyzed through the associated desingularized vector field. In particular, dynamics around the horizon characterize dynamics at infinity, including blow-up behavior.

For an equilibrium  $p$  for a desingularized vector field  $g$ , let  $W^s(p) = W^s(p; g)$  be the stable manifold of  $p$  for the dynamical system generated by  $g$ . We state the result for characterizing blow-up solutions in the case of directional compactifications. The corresponding results for other compactifications are stated in [45, 49].

**Theorem 2.12** (Stationary blow-up, [45]). *Assume that (2.1) has an equilibrium at infinity in the direction  $\mathbf{x}_* = (0, x_*) \in \mathcal{E}$ . Suppose that  $\mathbf{x}_*$  is hyperbolic with  $n_s > 0$  (resp.  $n_u = n - n_s$ ) eigenvalues of  $Jg_d(\mathbf{x}_*)$  with negative (resp. positive) real parts for desingularized vector field  $g = g_d$  defined in (2.10). If there is a solution  $y(t)$  of (2.1) with a bounded initial data  $y(0)$  whose image  $\mathbf{x} = T_d(y)$  is on the stable manifold  $W^s(\mathbf{x}_*; g_d)$ , then  $t_{\max} < \infty$  holds; namely,  $y(t)$  is a blow-up solution. Moreover,*

$$s(t)^{-1} \sim c(t_{\max} - t)^{-1/k} \quad \text{as } t \rightarrow t_{\max}$$

where  $c > 0$  is a constant and  $k + 1$  is the order of asymptotically quasi-homogeneous vector field  $f$ . Finally, if the  $j$ -th component  $\mathbf{x}_*$  is not zero, then we also have

$$y_j(t) \sim c(t_{\max} - t)^{-\alpha_j/k} \quad \text{as } t \rightarrow t_{\max},$$

where  $c$  is a constant with the same sign as  $y_j(t)$  as  $t \rightarrow t_{\max}$ .

The key point of the theorem is that *blow-up solutions for (2.1) are characterized as trajectories on stable manifolds of invariant sets<sup>11</sup> for the desingularized vector field located at the horizon  $\mathcal{E}$* . Computations of blow-up solutions are therefore reduced to stable manifolds of invariant sets, such as (hyperbolic) equilibria, for the associated vector field.

<sup>11</sup>Hyperbolicity ensures not only blow-up behavior of solutions but their asymptotic behavior with the specific form. Several case studies of blow-up solutions beyond hyperbolicity are shown in [46].

### 2.4.5 Saddle-type blow-up solutions

A remarkable feature obtained from the above theorem is that stability of equilibria on the horizon does not matter for characterizing blow-up solutions. Therefore we can also characterize blow-up solutions whose blow-up direction is characterized by *unstable* equilibria<sup>12</sup>. We shall call blow-up solutions of such kinds *unstable blow-up solutions*. If we emphasize structure of equilibria on the horizon, we shall call them the following.

**Definition 2.13.** We say that a blow-up solution is *sink-type* (resp. *saddle-type*) if it is transformed into a trajectory on  $W^s(x_*)$  with a sink (resp. saddle) equilibrium  $x_*$  on the horizon for the associated desingularized vector field in the sense of arguments in the present subsection.

There are many studies of blow-up solutions through analytic arguments (e.g. [23, 32, 60]) or numerical simulations (e.g. [1, 14, 15, 63]), many of which would be sink-type through related numerical simulations and computer-assisted proofs (e.g. [45, 48, 49]). On the other hand, saddle-type blow-up solutions are quite difficult to calculate and to understand the role in global dynamics, since generic small perturbation of initial state (for (2.1)) breaks the structure. Except special cases such as *planar* dynamical systems (e.g. [20, 21]), there are few studies for characterizing saddle-type blow-up solutions themselves and their global nature, such as behavior of solutions near such blow-up solutions. The following sections unravel validations and characterizations of saddle-type blow-up solutions.

## 2.5 Remark on appropriate choice of compactifications

We have introduced three compactifications in this section. Each compactification has its own set of advantages and disadvantages, which depend on our requirements. Here we remark the choice of compactifications in case that the original vector field  $f$  is polynomial<sup>13</sup>. In our examples (Sections 5, 6 and 7), all these compactifications are applied. It is worth mentioning several features of each compactification towards effective choice and applications of our machineries to practical and advanced problems.

### 2.5.1 Directional compactifications

A typical way to study dynamics at infinity is the application of directional compactifications introduced in Section 2.2, which is simple in the sense that the magnitude of points in the original coordinate can be measured by an independent variable  $s$ . Heuristically, associated desingularized vector fields are as complex as the original vector fields since the new variable  $\hat{x}_j$  in (2.2) depends only on the original variable  $y_j$  and the scaling variable  $s$ . Moreover,  $\hat{x}_j$  is proportional to  $y_j$ . Characterization of blow-up times is also simple, since they are characterized only by the asymptotic behavior of  $s = s(\tau)$ . On the other hand, directional compactifications are defined only *locally*. If our interested blow-up solutions have sign-changing structure, multiple charts of compactifications can be necessary for complete descriptions of blow-up solutions. From the numerical viewpoint, change of coordinates may cause additional computation costs and errors. *If one already*

---

<sup>12</sup>Potentially the similar characterization of blow-up solutions can be achieved with general invariant sets on the horizon. But we pay attention only to equilibria on the horizon in the present study.

<sup>13</sup>This assumption is not essential but just for simplifications to show advantages and disadvantages of each compactification.



knows from preceding mathematical or numerical arguments that targeting blow-up solutions have identical signs during time evolutions for a certain component, directional compactifications with appropriate choice of the constant-sign components are efficient.

### 2.5.2 Global compactifications

If we study blow-up solutions with sign-changing structure, or one does not have sufficient knowledge of solution trajectories near infinity, globally defined compactifications like Poincaré-type and parabolic type are more appropriate than directional ones, since one does not suffer from violation of integrations of differential equations due to the change of signs, or change of local charts. Since the horizon, topologically sphere-shaped boundary of the compactified space, is invariant under associated desingularized vector fields, *we do not worry about the ejection of trajectories to outside their domain of definition even computing trajectories corresponding to blow-up solutions*, unless unrealistic or mathematically inappropriate choice of numerical parameters. On the other hand, application of such global compactifications generally increases the order of associated desingularized vector fields as polynomial ones, which cause complication of arguments. For example, in the case of the vector field shown in Section 7, we have to study (desingularized) polynomial vector fields with order over 10, while the original one before compactification is order at most 2 or 3. Without systematic implementations of vector fields or their derivatives like automatic differentiations, applications to concrete systems require lengthy calculations.

### 2.5.3 Poincaré-type or parabolic-type?

Among globally defined compactifications, more than one compactifications are introduced here, namely the Poincaré-type and the parabolic-type. The simplest one in the class of *admissible* compactifications is the Poincaré-type, which is easy to understand from geometric viewpoints and widely applied in many fields of mathematics. However, the Poincaré-type compactification has an unavoidable defect, which is the presence of *radicals* in the definition. Radicals generally lose the smoothness of desingularized vector fields on the horizon. In other words, desingularized vector fields under the Poincaré-type compactification are  $C^0$  but not  $C^1$  in general around the horizon. Therefore typical “linear stability analysis” in the theory of dynamical systems does not always make sense on the horizon. Nevertheless, it should be noted that there is an exception where the Poincaré-type compactifications can be applied without losing the smoothness of resulting vector fields, which is the case if  $f$  is *quasi-homogeneous* (not only in the asymptotic sense). In this case, the associated desingularized vector field is also smooth and hence no obstruction of  $C^1$  smoothness on the horizon arises. Details are discussed in [45].

Although the order of polynomials significantly increases when we apply the parabolic-type compactifications, we do not worry about the lack of smoothness of desingularized vector fields. Indeed, *parabolic-type transformations of the present type originally transforms rational functions into rational ones*, unlike the Poincaré-type ones (cf. [28]). We thus do not worry about mathematical obstructions to consider dynamics at infinity when we apply parabolic-type compactifications.

**Remark 2.14.** *The geometrically simplest compactification would be the one-point compactifications such as embedding of  $\mathbb{R}^n$  into  $S^n$ , which is known as the Bendixson’s compactification. One can use the Bendixson’s compactification to map the infinity to a bounded point, where the corresponding dynamics possess the high degeneracy in general (e.g. [31]). In order to avoid the*

degeneracy at infinity, we have to apply an additional desingularization (blowing-up) of the infinity. The Poincaré-type and parabolic-type compactifications avoid such extra tasks for obtaining desingularized dynamics at infinity.

### 3 Preliminary 2: Parameterization method

In this section, we introduce the theory of the parameterization method [10, 11, 12] to compute rigorous charts of local stable and unstable manifolds of fixed points of ODEs of the form  $\dot{x} = g(x)$ , where  $g$  is a desingularized vector field. We begin by making some assumptions, which will be sufficient for the purpose of the present paper.

- A1. Assume  $g : \mathbb{R}^n \rightarrow \mathbb{R}^n$  is a polynomial vector field with a steady state  $\tilde{x} \in \mathbb{R}^n$  (i.e.  $g(\tilde{x}) = 0$ ).
- A2. Assume that the eigenvalues of the Jacobian matrix  $Dg(\tilde{x})$  are real, nonzero and distinct (hence the Jacobian matrix  $Dg(\tilde{x})$  is diagonalizable over the real and  $\tilde{x}$  is hyperbolic).

Denote by  $\lambda_1, \dots, \lambda_m < 0$  the *stable eigenvalues* of  $Dg(\tilde{x})$  with  $\xi_1, \dots, \xi_m \in \mathbb{R}^n$  some associated *stable eigenvectors*. From now on, we focus on the computation of a local stable manifold, which we denote by  $W_{\text{loc}}^s(\tilde{x})$ , and note that  $\dim W_{\text{loc}}^s(\tilde{x}) = m \leq n$ . The computation of the unstable manifold is similar (e.g. see [8]). The idea of the computational approach is to represent the chart of the local stable manifold using a Taylor series representation  $P : B^m \rightarrow \mathbb{R}^n$  of the form

$$P(\theta) = \sum_{|\alpha|=0}^{\infty} a_{\alpha} \theta^{\alpha}, \quad a_{\alpha} \in \mathbb{R}^n, \quad (3.1)$$

where  $B^m \subset \mathbb{R}^m$  is a domain (usually chosen to be a ball) on which the Taylor series converges, and where  $\alpha = (\alpha_1, \dots, \alpha_m) \in \mathbb{N}^m$ ,  $|\alpha| = \alpha_1 + \dots + \alpha_m$ ,  $\theta = (\theta_1, \dots, \theta_m) \in \mathbb{R}^m$  and  $\theta^{\alpha} = \theta_1^{\alpha_1} \dots \theta_m^{\alpha_m}$ . This requires making an extra assumption, which involves the notion of a resonance.

**Definition 3.1.** The eigenvalues  $\lambda_1, \dots, \lambda_m$  are said to have a *resonance* of order  $\alpha = (\alpha_1, \dots, \alpha_m) \in \mathbb{N}^m$  if

$$\alpha_1 \lambda_1 + \dots + \alpha_m \lambda_m - \lambda_j = 0, \quad (3.2)$$

for some  $j \in \{1, \dots, m\}$  with  $|\alpha| \geq 2$ . If there are no resonances at any order  $|\alpha| \geq 2$ , then the eigenvalues  $\lambda_1, \dots, \lambda_m$  are said to be *non-resonant*.

We are ready to state our third hypothesis.

- A3. Assume that the eigenvalues  $\lambda_1, \dots, \lambda_m$  are *non-resonant*

Construct the following real-valued matrices: an  $m \times m$  diagonal matrix with the diagonal entries made up of the stable eigenvalues

$$\Lambda = \begin{pmatrix} \lambda_1 & \dots & 0 \\ \vdots & \ddots & \vdots \\ 0 & \dots & \lambda_m \end{pmatrix} \quad (3.3)$$

and an  $n \times m$  matrix whose columns are the associated eigenvectors

$$A_0 = [\xi_1 | \dots | \xi_m].$$

Using the basis defined by the stable eigenvectors, the linearized equation for  $\dot{x} = g(x)$  restricted to the stable subspace takes the form

$$\dot{y} = \Lambda y, \quad y \in \mathbb{R}^m.$$

The associated flow is given by  $e^{\Lambda t}$ . As indicated above our goal is to construct an analytic function  $P: B^m \rightarrow \mathbb{R}^n$  such that  $P(B^m) = W_{loc}^s(\tilde{x})$ . To obtain constraints, so that we can solve for  $P$ , we begin by insisting that  $P$  be a conjugacy between the flow  $\varphi$  of  $\dot{x} = g(x)$  restricted to  $W_{loc}^s(\tilde{x})$  and the flow  $e^{\Lambda t}$  of the linear equation. The most obvious restriction is that  $P$  must map fixed points to fixed points and hence

$$P(0) = \tilde{x}.$$

To obtain the conjugacy we assume that

$$DP(0) = A_0$$

and

$$\varphi(t, P(\theta)) = P(e^{\Lambda t}\theta), \quad (3.4)$$

for all  $\theta \in B^m$ . The geometric meaning of this conjugacy is illustrated in Figure 2. To see that  $P(B^m) \subset W_{loc}^s(\tilde{x})$  observe that

$$\lim_{t \rightarrow \infty} \varphi(t, P(\theta)) = \lim_{t \rightarrow \infty} P(e^{\Lambda t}\theta) = P\left(\lim_{t \rightarrow \infty} e^{\Lambda t}\theta\right) = P(0) = \tilde{x},$$

since the entries of  $\Lambda$  are negative.

Note that any function  $P(\theta)$  satisfying Equation (3.4) is one-to-one on  $B^m$ . To see this observe that  $P$  is tangent to the stable eigenspace at the origin as  $DP(0) = A_0$ . Moreover recall that  $A_0$  is of full rank as its columns are linearly independent. By the implicit function theorem  $P$  is of rank  $m$ , and hence one-to-one, in some neighborhood  $U \subset B^m$  of 0. Now suppose that  $\theta_1, \theta_2 \in B^m$  and that  $P(\theta_1) = P(\theta_2)$ . Then for any  $t \in \mathbb{R}$ ,  $\varphi(t, P(\theta_1)) = \varphi(t, P(\theta_2))$  by the uniqueness of the initial value problem. Choose  $T > 0$  large enough so that  $e^{\Lambda T}\theta_1, e^{\Lambda T}\theta_2 \in U$ . By the conjugacy relation we have that  $P(e^{\Lambda T}\theta_1) = P(e^{\Lambda T}\theta_2)$ , and since the arguments are in  $U$ , the local immersion gives that  $e^{\Lambda T}\theta_1 = e^{\Lambda T}\theta_2$ . But  $e^{\Lambda T}$  is an isomorphism and we have  $\theta_1 = \theta_2$ .

We conclude from the discussion above that  $P(B^m) = W_{loc}^s(\tilde{x})$ .

The utility of (3.4) is limited by the appearance of the flow  $\varphi$  in the equation. In practice the flow is only known implicitly, that is it is determined by solving the differential equation. The following lemma establishes a more practical infinitesimal version of (3.4).

**Lemma 3.2.** *Let  $P: B^m \subset \mathbb{R}^m \rightarrow \mathbb{R}^n$  be a smooth function with*

$$P(0) = \tilde{x} \quad \text{and} \quad DP(0) = A_0. \quad (3.5)$$

*Then  $P(\theta)$  satisfies the conjugacy relationship (3.4) if and only if  $P$  is a solution of the partial differential equation (PDE)*

$$\lambda_1 \theta_1 \frac{\partial}{\partial \theta_1} P(\theta_1, \dots, \theta_m) + \dots + \lambda_m \theta_m \frac{\partial}{\partial \theta_m} P(\theta_1, \dots, \theta_m) = g(P(\theta_1, \dots, \theta_m)) \quad (3.6)$$

*for all  $\theta = (\theta_1, \dots, \theta_m) \in B^m$ .*

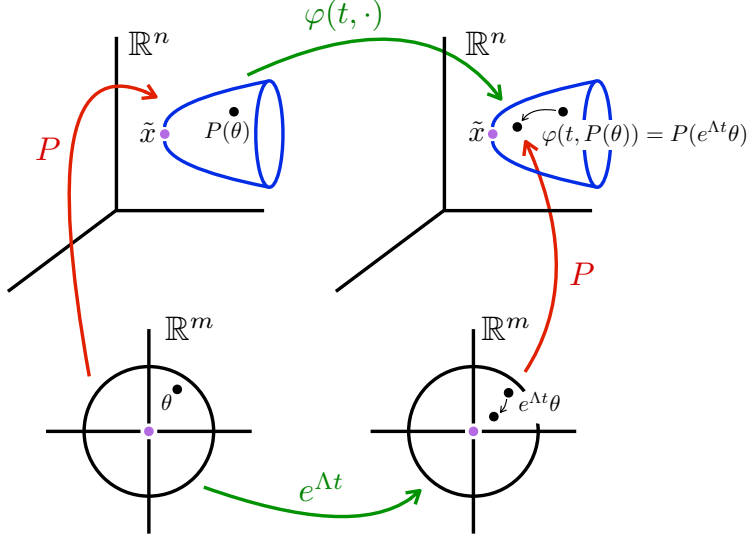


Figure 2: **Schematic of the Parameterization Method for Vector Fields in  $\mathbb{R}^n$ :** The figure illustrates the conjugacy described by Equation (3.4). The bottom half of the figure represents the parameter space in  $\mathbb{R}^m$  (the domain of the parameterization  $P$ ) while the top half of the figure represents the phase space in  $\mathbb{R}^n$ . The image of  $P$  is the local stable manifold shown in blue. The dynamics in the parameter space is generated by exponentiating the matrix of stable eigenvalues  $\Lambda$ . The dynamics in phase space is generated by the flow  $\varphi$  associated with the vector field  $g$ . The diagram *commutes* in the sense that applying first the chart map  $P$  and then nonlinear flow  $\varphi(t, \cdot)$  is required to be the same as applying the linear dynamics  $e^{\Lambda t}$  and then the chart map  $P$ . The result is that the dynamics on the local stable manifold are described by the stable linear dynamics.

*Proof.* Let  $P: B^m \rightarrow \mathbb{R}^n$  be a smooth function with  $P(0) = \tilde{x}$  and  $DP(0) = A_0$ .

( $\Leftarrow$ ) Suppose that  $P(\theta)$  solves the partial differential equation (3.6) in  $B^m$ . Choose a fixed  $\theta \in B^m$  and fix  $t > 0$ . Define the function  $\gamma: [0, t] \rightarrow \mathbb{R}^n$  by

$$\gamma(t) \stackrel{\text{def}}{=} P(e^{\Lambda t} \theta). \quad (3.7)$$

Then,  $\gamma(0) = P(\theta)$  and

$$\gamma'(t) = \frac{d}{dt} P(e^{\Lambda t} \theta) = DP(e^{\Lambda t} \theta) \Lambda e^{\Lambda t} \theta = g(P(e^{\Lambda t} \theta)) = g(\gamma(t)),$$

where we pass from the first to the second equality by the chain rule, from the second to the third equality by the invariance equation (3.6) and the fact that  $e^{\Lambda t} \theta \in B^m$  when  $t > 0$ , and from the third to the fourth equation by the definition of  $\gamma$ . Hence  $\gamma$  is the solution of the initial value problem

$$\gamma'(t) = g(\gamma(t)), \quad \text{and} \quad \gamma(0) = P(\theta). \quad (3.8)$$

Therefore by definition  $\varphi(t, \gamma(0)) = \gamma(t)$ , and it follows from (3.7) and (3.8) that

$$\varphi(t, P(\theta)) = P(e^{\Lambda t} \theta).$$

( $\implies$ ) Suppose that  $P$  satisfies the conjugacy relationship (3.4) for all  $\theta \in B^m$ . Fix  $\theta \in B^m$  and differentiate both sides with respect to  $t$  in order to obtain

$$g(\varphi(t, P(\theta))) = DP(e^{\Lambda t}\theta)\Lambda e^{\Lambda t}\theta.$$

Taking the limit as  $t \rightarrow 0$  gives that  $P(\theta)$  is a solution of (3.6).  $\square$

As a consequence of Lemma 3.2, it should now be clear that computing a local  $m$ -dimensional stable manifold is equivalent to find a solution  $P: B^m \rightarrow \mathbb{R}^n$  of the PDE (3.6). As mentioned earlier, the idea is to use a Taylor series representation of the form (3.1). Note that since  $g: \mathbb{R}^n \rightarrow \mathbb{R}^n$  is a polynomial vector field, the power series expansion of  $g(P(\theta))$  involves Cauchy products. Denote the Taylor expansion of  $g(P(\theta))$  as

$$g(P(\theta)) = \sum_{|\alpha|=0}^{\infty} (g(a))_{\alpha} \theta^{\alpha}, \quad j = 1, \dots, n,$$

where we abuse slightly the notation and used the same notation  $g(a)$  to denote the vector field  $g$  where the monomial terms in the variables  $x_1, \dots, x_n$  are replaced by Cauchy products in the variables  $a_1, \dots, a_n$ .

Formally plugging the Taylor expansion (3.1) in the PDE (3.6) results in

$$DP(\theta)\Lambda\theta = \sum_{|\alpha|=0}^{\infty} (\alpha \cdot \lambda) a_{\alpha} \theta^{\alpha} = \sum_{|\alpha|=0}^{\infty} (g(a))_{\alpha} \theta^{\alpha} = g(P(\theta)),$$

where  $\alpha \cdot \lambda \stackrel{\text{def}}{=} \alpha_1 \lambda_1 + \dots + \alpha_m \lambda_m$  and  $a_{\alpha} = ((a_1)_{\alpha}, \dots, (a_n)_{\alpha}) \in \mathbb{R}^n$ . The first order constraints (3.5) imply that

$$a_0 = ((a_1)_0, \dots, (a_n)_0) = \tilde{x} \in \mathbb{R}^n \quad \text{and} \quad a_{e_j} = \xi_j \in \mathbb{R}^n \quad (j = 1, \dots, m),$$

where  $e_j$  is the  $j^{\text{th}}$  vector of the canonical basis of  $\mathbb{R}^n$ . In other words, the Taylor coefficients  $a_{\alpha}$  for  $|\alpha| \in \{0, 1\}$  are fixed and do not need to be solved for.

Computing the higher order Taylor coefficients  $a_{\alpha} = ((a_1)_{\alpha}, \dots, (a_n)_{\alpha})$  (for  $|\alpha| \geq 2$ ) of (3.1) reduces to find the solution of the zero finding problem  $F(a) = 0$ , with  $F$  given by

$$(F(a))_{\alpha} \stackrel{\text{def}}{=} (\alpha \cdot \lambda) a_{\alpha} - (g(a))_{\alpha}, \quad |\alpha| \geq 2. \quad (3.9)$$

Also denote, for  $j = 1, \dots, n$  and  $|\alpha| \geq 2$ ,

$$(F_j(a))_{\alpha} \stackrel{\text{def}}{=} (\alpha \cdot \lambda) (a_j)_{\alpha} - (g_j(a))_{\alpha},$$

so that we may write  $F(a) = (F_1(a), F_2(a), \dots, F_n(a))$ .

**Remark 3.3.** When  $|\alpha| \in \{0, 1\}$ , the constraints  $(F(a))_{\alpha} = 0$  correspond to finding the steady state ( $|\alpha| = 0$ ) and the stable eigenvalues/eigenvectors ( $|\alpha| = 1$ ). Since this information is already assumed to be at hand, we only need to solve for  $(F(a))_{\alpha} = 0$  for  $|\alpha| \geq 2$ .

Denote the Banach space

$$\ell^1 \stackrel{\text{def}}{=} \left\{ b = (b_\alpha)_{|\alpha| \geq 2} : b_\alpha \in \mathbb{R} \text{ and } \|b\|_1 \stackrel{\text{def}}{=} \sum_{|\alpha|=2}^{\infty} |b_\alpha| < \infty \right\} \quad (3.10)$$

and the product Banach space  $X \stackrel{\text{def}}{=}} (\ell^1)^n = \ell^1 \times \ell^1 \times \cdots \times \ell^1$  with induced norm

$$\|a\|_X \stackrel{\text{def}}{=} \max_{j=1, \dots, n} \|a_j\|_1. \quad (3.11)$$

Moreover, denoting the Banach space

$$\tilde{\ell}^1 \stackrel{\text{def}}{=} \left\{ b = (b_\alpha)_{|\alpha| \geq 2} : b_\alpha \in \mathbb{R} \text{ and } \sum_{|\alpha|=2}^{\infty} |(\alpha \cdot \lambda) b_\alpha| < \infty \right\}, \quad (3.12)$$

and  $X' \stackrel{\text{def}}{=}} (\tilde{\ell}^1)^n$ , we get that  $F : X \rightarrow X'$ .

Denote by  $B_1^m \stackrel{\text{def}}{=}} \{z = (z_1, \dots, z_m) \in \mathbb{C}^m : |z_k| \leq 1, \text{ for all } k = 1, \dots, m\}$  the unit polydisc in  $\mathbb{C}^m$ . We have the following result.

**Theorem 3.4.** *Assume that Assumptions A1, A2 and A3 are satisfied. If there exists  $\tilde{a} \in X$  such that  $F(\tilde{a}) = 0$  with  $F$  given in (3.9), then the corresponding Taylor expansion  $P : B_1^m \rightarrow \mathbb{R}^n$  given by*

$$P(\theta) \stackrel{\text{def}}{=} \tilde{x} + \sum_{k=1}^m \xi_k \theta_k + \sum_{|\alpha|=2}^{\infty} \tilde{a}_\alpha \theta^\alpha \quad (3.13)$$

provides a parameterization of a local stable manifold of  $\tilde{x}$ , that is  $P(B_1^m) = W_{\text{loc}}^s(\tilde{x})$ .

*Proof.* Assume that  $\tilde{a} \in X$  solves  $F(\tilde{a}) = 0$ . Then by construction, the function  $P(\theta)$  given in (3.13) converges absolutely and uniformly on  $B_1^m$  as for each  $j \in \{1, \dots, n\}$

$$\begin{aligned} \sup_{z \in B_1^m} |P_j(z)| &\leq |\tilde{x}_j| + \sup_{z \in B_1^m} \left| \sum_{k=1}^m (\xi_k)_j z_k + \sum_{|\alpha|=2}^{\infty} (\tilde{a}_j)_\alpha z_1^{\alpha_1} \cdots z_m^{\alpha_m} \right| \\ &\leq |\tilde{x}_j| + \sup_{z \in B_1^m} \sum_{k=1}^m |(\xi_k)_j| |z_k| + \sup_{z \in B_1^m} \sum_{|\alpha|=2}^{\infty} |(\tilde{a}_j)_\alpha| |z_1|^{\alpha_1} \cdots |z_m|^{\alpha_m} \\ &\leq |\tilde{x}_j| + \sum_{k=1}^m |(\xi_k)_j| + \sum_{|\alpha|=2}^{\infty} |(\tilde{a}_j)_\alpha| \\ &= |\tilde{x}_j| + \sum_{k=1}^m |(\xi_k)_j| + \|\tilde{a}_j\|_1 < \infty, \end{aligned}$$

since  $\|\tilde{a}\|_1 < \infty$ . By construction, the function  $P : B_1^m \rightarrow \mathbb{R}^n$  given in (3.13) satisfies the first order constraints (3.5) and the PDE (3.6). By the Lemma 3.2,  $P$  satisfies the conjugacy relationship (3.4). Finally, we conclude that  $P : B_1^m \rightarrow \mathbb{R}^n$  provides a parameterization of a local stable manifold of  $\tilde{x}$ , that is  $P(B_1^m) = W_{\text{loc}}^s(\tilde{x})$ .  $\square$

The strategy to compute a parameterization of  $W_{\text{loc}}^s(\tilde{x})$  is now clear. Fix the lengths of the eigenvectors  $\xi_1, \dots, \xi_m$  such that we can compute  $\tilde{a} \in X$  such that  $F(\tilde{a}) = 0$ . This is achieved with a Newton-Kantorovich type argument, which we now state.

Denote by  $B_r(b) \stackrel{\text{def}}{=} \{x \in X : \|x - b\|_X \leq r\}$  the closed ball of radius  $r > 0$  centered at a given  $b \in X$ , and  $B(X_1, X_2)$  the space of bounded linear operators between two Banach spaces  $X_1$  and  $X_2$ .

**Theorem 3.5 (A Newton-Kantorovich type theorem).** *Let  $X$  and  $X'$  be Banach spaces,  $A^\dagger \in B(X, X')$  and  $A \in B(X', X)$  be bounded linear operators. Assume  $F: X \rightarrow X'$  is Fréchet differentiable at  $\bar{a} \in X$ ,  $A$  is injective and  $AF: X \rightarrow X$ . Let  $Y_0, Z_0$  and  $Z_1$  be nonnegative constants, and a function  $Z_2: (0, \infty) \rightarrow (0, \infty)$  satisfying*

$$\|AF(\bar{a})\|_X \leq Y_0 \quad (3.14)$$

$$\|I - AA^\dagger\|_{B(X)} \leq Z_0 \quad (3.15)$$

$$\|A[DF(\bar{a}) - A^\dagger]\|_{B(X)} \leq Z_1, \quad (3.16)$$

$$\|A[DF(c) - DF(\bar{a})]\|_{B(X)} \leq Z_2(r)r, \quad \text{for all } c \in B_r(\bar{a}), \quad (3.17)$$

where  $\|\cdot\|_{B(X)}$  denotes the operator norm. Define the radii polynomial by

$$p(r) \stackrel{\text{def}}{=} Z_2(r)r^2 - (1 - Z_1 - Z_0)r + Y_0. \quad (3.18)$$

If there exists  $r_0 > 0$  such that  $p(r_0) < 0$ , then there exists a unique  $\tilde{a} \in B_{r_0}(\bar{a})$  such that  $F(\tilde{a}) = 0$ .

The strategy of Theorem 3.5 requires obtaining  $\bar{a}$  (a numerical approximation), the operator  $A^\dagger \in B(X, X')$  (an approximation of the Fréchet derivative  $DF(\bar{a})$ ) and the operator  $A \in B(X', X)$  (an approximate inverse of  $DF(\bar{a})$ ).

To compute the numerical approximation  $\bar{a}$ , we first consider a finite dimensional projection of the map  $F: X \rightarrow X'$ . Fixing a dimensional Taylor projection number  $N$ , denote by  $X^{(N)}$  the finite dimensional space

$$X^{(N)} \stackrel{\text{def}}{=} \left\{ a = (a_1, \dots, a_n) : a_j = ((a_j)_\alpha)_{|\alpha|=2}^N, \text{ for } j = 1, \dots, n \right\}.$$

Moreover, denote by  $\kappa(N) \stackrel{\text{def}}{=} \#\{\alpha \in \mathbb{N}^m : |\alpha| \in \{2, \dots, N\}\}$  the number of multi-indices  $\alpha$  with order between 2 and  $N$ . Given a vector  $b = (b_\ell)_{|\ell| \geq 0} \in \ell^1$ , consider the projection

$$\begin{aligned} \pi^N : \ell^1 &\rightarrow \mathbb{R}^{\kappa(N)} \\ b &\mapsto \pi^N b \stackrel{\text{def}}{=} (b_\alpha)_{|\alpha|=2}^N \in \mathbb{R}^{\kappa(N)}. \end{aligned}$$

We generalize that projection to get  $\Pi^N : X = (\ell^1)^n \rightarrow X^{(N)} \cong \mathbb{R}^{n\kappa(N)}$  defined by

$$\Pi^N a \stackrel{\text{def}}{=} (\pi^N a_1, \dots, \pi^N a_n) \in X^{(N)}.$$

Given  $a \in X$ , we denote

$$a^{(N)} \stackrel{\text{def}}{=} \Pi^N a \in X^{(N)}.$$

Moreover, we define the natural inclusion  $\iota^N : \mathbb{R}^{\kappa(N)} \hookrightarrow \ell^1$  as follows. For  $b = (b_\alpha)_{|\alpha|=2}^N \in \mathbb{R}^{\kappa(N)}$  let  $\iota^N b \in \ell^1$  be defined component-wise by

$$(\iota^N b)_\alpha = \begin{cases} b_\alpha, & |\alpha| = 2, \dots, N \\ 0, & |\alpha| > N. \end{cases}$$

Similarly, let  $\iota^{(N)} : X^{(N)} \hookrightarrow X$  be the natural inclusion defined as follows. Given  $a = (a_1, \dots, a_n) \in X^{(N)} \cong \mathbb{R}^{n\kappa(N)}$ , let

$$\iota^{(N)} a \stackrel{\text{def}}{=} (\iota^N a_1, \dots, \iota^N a_n) \in X.$$

Finally, define the *finite dimensional projection*  $F^{(N)} : X^{(N)} \rightarrow X^{(N)}$  by

$$F^{(N)}(a) = \Pi^{(N)} F(\iota^{(N)} a). \quad (3.19)$$

Also denote  $F^{(N)} = (F_1^{(N)}, \dots, F_n^{(N)})$ .

Assume that a numerical approximation  $\bar{a}^{(N)} = (\bar{a}_1^{(N)}, \dots, \bar{a}_n^{(N)})$  such that  $F^{(N)}(\bar{a}^{(N)}) \approx 0$  has been computed (e.g. using Newton's method). Given  $j = 1, \dots, n$ , denote  $\bar{a}_j = \iota^N \bar{a}_j^{(N)} \in \ell^1$  and denote  $\bar{a} = (\bar{a}_1, \dots, \bar{a}_n)$ , and for the sake of simplicity of the presentation, we use the same notation  $\bar{a}$  to denote  $\bar{a} \in X$  and  $\bar{a}^{(N)} \in X^{(N)}$ . Denote by  $DF^{(N)}(\bar{a})$  the Jacobian of  $F^{(N)}$  at  $\bar{a}$ , and let us write it as

$$DF^{(N)}(\bar{a}) = \begin{pmatrix} D_{a_1} F_1^{(N)}(\bar{a}) & \cdots & D_{a_n} F_1^{(N)}(\bar{a}) \\ \vdots & \ddots & \vdots \\ D_{a_1} F_n^{(N)}(\bar{a}) & \cdots & D_{a_n} F_n^{(N)}(\bar{a}) \end{pmatrix} \in M_{n\kappa(N)}(\mathbb{R}).$$

The next step is to construct the linear operator  $A^\dagger$  (an approximate derivative of the derivative  $DF(\bar{a})$ ), and the linear operator  $A$  (an approximate inverse of  $DF(\bar{a})$ ). Let

$$A^\dagger = \begin{pmatrix} A_{1,1}^\dagger & \cdots & A_{1,n}^\dagger \\ \vdots & \ddots & \vdots \\ A_{n,1}^\dagger & \cdots & A_{n,n}^\dagger \end{pmatrix}, \quad (3.20)$$

whose action on an element  $h = (h_1, \dots, h_n) \in X$  is defined by  $(A^\dagger h)_i = \sum_{j=1}^n A_{i,j}^\dagger h_j$ , for  $i = 1, \dots, n$ . Here the action of  $A_{i,j}^\dagger$  is defined as

$$(A_{i,j}^\dagger h_j)_n = \begin{cases} (D_{a_j} F_i^{(N)}(\bar{a}) h_j^{(N)})_\alpha & \text{for } 2 \leq |\alpha| \leq N, \\ \delta_{i,j}(\alpha \cdot \lambda)(h_j)_\alpha & \text{for } |\alpha| > N, \end{cases}$$

where  $\delta_{i,j}$  is the Kronecker  $\delta$ . Consider now a matrix  $A^{(N)} \in M_{n\kappa(N)}(\mathbb{R})$  computed so that  $A^{(N)} \approx DF^{(N)}(\bar{a})^{-1}$ . We decompose it into  $n^2 \kappa(N) \times \kappa(N)$  blocks:

$$A^{(N)} = \begin{pmatrix} A_{1,1}^{(N)} & \cdots & A_{1,n}^{(N)} \\ \vdots & \ddots & \vdots \\ A_{n,1}^{(N)} & \cdots & A_{n,n}^{(N)} \end{pmatrix}.$$

This allows defining the linear operator  $A$  as

$$A = \begin{pmatrix} A_{1,1} & \cdots & A_{1,n} \\ \vdots & \ddots & \vdots \\ A_{n,1} & \cdots & A_{n,n} \end{pmatrix}, \quad (3.21)$$



whose action on an element  $h = (h_1, \dots, h_n) \in X$  is defined by  $(Ah)_i = \sum_{j=1}^n A_{i,j} h_j$ , for  $i = 1, \dots, n$ . Given  $i, j \in \{1, \dots, n\}$ , the action of  $A_{i,j}$  is defined as

$$(A_{i,j} h_j)_n = \begin{cases} \left( A_{i,j}^{(N)} h_j^{(N)} \right)_\alpha & \text{for } 2 \leq |\alpha| \leq N \\ \delta_{i,j} \frac{1}{\alpha \cdot \lambda} (h_j)_\alpha & \text{for } |\alpha| > N. \end{cases}$$

Having obtained an approximate solution  $\bar{a}$  and the linear operators  $A^\dagger$  and  $A$ , the next step is to construct the bounds  $Y_0$ ,  $Z_0$ ,  $Z_1$  and  $Z_2(r)$  satisfying (3.14), (3.15), (3.16) and (3.17), respectively.

### 3.1 The $Y_0$ bound

Denote by  $d$  the highest order nonlinear term of the vector field  $f$ . Then since  $\bar{a}$  consists of Taylor coefficients of order  $N$ , then  $(F(\bar{a}))_\alpha = 0$  for all  $|\alpha| > dN$ . For  $i = 1, \dots, n$ , we set

$$Y_0^{(i)} \stackrel{\text{def}}{=} \sum_{|\alpha|=2}^N \left| \sum_{j=1}^n \left( A_{i,j}^{(N)} F_j^{(N)}(\bar{a}) \right)_\alpha \right| + \sum_{|\alpha|=N+1}^{dN} \left| \frac{1}{\alpha \cdot \lambda} (F_i(\bar{a}))_\alpha \right|$$

which is a collection of finite sums that can be evaluated with interval arithmetic. We conclude that

$$\| [AF(\bar{a})]_i \|_1 = \left\| \sum_{j=1}^n A_{i,j} F_j(\bar{a}) \right\|_1 \leq Y_0^{(i)}, \quad \text{for } i = 1, \dots, n$$

and we set

$$Y_0 \stackrel{\text{def}}{=} \max \left( Y_0^{(1)}, \dots, Y_0^{(n)} \right). \quad (3.22)$$

### 3.2 The $Z_0$ bound

We look for a bound of the form  $\|I - AA^\dagger\|_{B(X)} \leq Z_0$ . Recalling the definitions of  $A$  and  $A^\dagger$  given in (3.21) and (3.20), let  $B \stackrel{\text{def}}{=} I - AA^\dagger$  the bounded linear operator represented as

$$B = \begin{pmatrix} B_{1,1} & \cdots & B_{1,n} \\ \vdots & \ddots & \vdots \\ B_{n,1} & \cdots & B_{n,n} \end{pmatrix}.$$

We remark that  $(B_{i,j})_{n_1, n_2} = 0$  for any  $i, j \in \{1, \dots, n\}$ , whenever  $n_1 > N$  or  $n_2 > N$ . Hence we can compute the norms  $\|B_{i,j}\|_{B(\ell^1)}$  using the following standard result.

**Lemma 3.6.** *Given  $\Gamma \in B(\ell^1)$  a bounded linear operator, acting as  $(\Gamma a)_\beta = \sum_{|\alpha| \geq 2} \Gamma_{\beta, \alpha} a_\alpha$  for  $|\beta| \geq 2$ .*

$$\|\Gamma\|_{B(\ell^1)} = \sup_{|\alpha| \geq 2} \sum_{|\beta| \geq 2} |\Gamma_{\beta, \alpha}|. \quad (3.23)$$

Given  $h = (h_1, \dots, h_n) \in X = (\ell^1)^n$  with  $\|h\|_X = \max(\|h_1\|_1, \dots, \|h_n\|_1) \leq 1$ , and for  $i = 1, \dots, n$ , we obtain

$$\|(Bh)_i\|_1 = \left\| \sum_{j=1}^n B_{i,j} h_j \right\|_1 \leq \sum_{j=1}^n \|B_{i,j}\|_{B(\ell^1)}.$$

Hence we define

$$Z_0 \stackrel{\text{def}}{=} \max_{i=1,\dots,n} \left( \sum_{j=1}^n \|B_{i,j}\|_{B(\ell^1)} \right), \quad (3.24)$$

where each norm  $\|B_{i,j}\|_{B(\ell^1)}$  can be computed using formula (3.23) with vanishing tail terms.

### 3.3 The $Z_1$ bound

Recall that we look for the bound  $\|A[DF(\bar{a}) - A^\dagger]\|_{B(X)} \leq Z_1$ . Given  $h = (h_1, \dots, h_n) \in X$  with  $\|h\|_X \leq 1$ , set

$$z \stackrel{\text{def}}{=} [DF(\bar{a}) - A^\dagger]h.$$

Then, for each  $i = 1, \dots, n$ ,  $(z_i)_\alpha = 0$  for  $|\alpha| = 2, \dots, N$  and for  $|\alpha| > N$ ,

$$(z_i)_\alpha = - (Dg_i(\bar{a})h)_\alpha = - \left( \sum_{j=1}^n \frac{\partial g_i}{\partial a_j}(\bar{a}) h_j \right)_\alpha$$

Denote

$$\lambda^*(N) \stackrel{\text{def}}{=} \min_{|\alpha| > N} |\alpha \cdot \lambda|.$$

Since the tail of  $A_{i,j}$  is zero for  $i \neq j$ , then  $Az = (A_{1,1}z_1, \dots, A_{n,n}z_n)$ . Then a straightforward calculation yields, for each  $i \in \{1, \dots, n\}$ , that

$$\|A_{i,i}z_i\|_1 \leq Z_1^{(i)} \stackrel{\text{def}}{=} \frac{1}{\lambda^*(N)} \sum_{j=1}^n \left\| \frac{\partial g_i}{\partial a_j}(\bar{a}) \right\|_1,$$

so that we set

$$Z_1 \stackrel{\text{def}}{=} \max \left( Z_1^{(1)}, \dots, Z_1^{(n)} \right). \quad (3.25)$$

### 3.4 The $Z_2$ bound

For a fixed  $r_* > 0$ , set

$$Z_2(r_*) \stackrel{\text{def}}{=} \sup_{b \in B_{r_*}(\bar{a})} \left( \max_{i=1,\dots,n} \sum_{k,m=1}^n \left\| \sum_{j=1}^n A_{ij} \frac{\partial^2 g_j}{\partial a_m \partial a_k}(b) \right\|_{B(\ell^1)} \right) \quad (3.26)$$

which satisfies (by the Mean Value Inequality in Banach spaces)

$$\|A[DF(c) - DF(\bar{a})]\|_{B(X)} \leq Z_2(r_*)r, \quad \text{for all } c \in B_r(\bar{a}), \quad \text{for all } r \leq r_*.$$

Evaluating the bound (3.26) is straightforward with interval arithmetic and the easily computed formulas of the second derivatives of each component  $f_i$  of the vector field  $f$ .

### 3.5 Rigorous enclosure of the points on $W_{\text{loc}}^s(\tilde{x})$

Assume that assumptions A1, A2 and A3 are satisfied for a fixed point  $\tilde{x}$ . Let  $\lambda_1, \dots, \lambda_m < 0$  be the corresponding non-resonant real (stable) eigenvalues and  $\xi_1, \dots, \xi_m \in \mathbb{R}^n$  be some associated *stable eigenvectors*.

Consider  $N \geq 2$  the order of the Taylor approximation, and as before, assume that a numerical approximation  $\bar{a}^{(N)} = (\bar{a}_1^{(N)}, \dots, \bar{a}_n^{(N)})$  such that  $F^{(N)}(\bar{a}^{(N)}) \approx 0$  has been computed. Denote by

$$P^{(N)}(\theta) \stackrel{\text{def}}{=} \tilde{x} + \sum_{k=1}^m \xi_k \theta_k + \sum_{|\alpha|=2}^N \bar{a}_\alpha \theta^\alpha. \quad (3.27)$$

Using a computer program in MATLAB using the interval arithmetic package INTLAB, we can compute rigorously the bounds  $Y_0$ ,  $Z_0$ ,  $Z_1$  and  $Z_2$  satisfying (3.22), (3.24), (3.25) and (3.26), respectively. Define the radii polynomial  $p(r)$  defined in (3.18), and assume the existence of  $r_0 > 0$  such that  $p(r_0) < 0$ . From Theorem 3.5, there exists a unique  $\tilde{a} \in B_{r_0}(\bar{a})$  such that  $F(\tilde{a}) = 0$ . By Theorem 3.4, the corresponding Taylor expansion  $P : B_1^m \rightarrow \mathbb{R}^n$  given by (3.13) provides a parameterization of a local stable manifold of  $\tilde{x}$ , that is  $P(B_1^m) = W_{\text{loc}}^s(\tilde{x})$ . From the computer-assisted proof, we immediately obtain a rigorous upper bound for the  $C^0$  error bound between the approximate parameterization (3.27) and the true parameterization. More explicitly, for a fixed  $j = 1, \dots, n$

$$\begin{aligned} \sup_{z \in B_1^m} |P_j(z) - P_j^{(N)}(z)| &= \sup_{z \in B_1^m} \left| \sum_{|\alpha|=2}^{\infty} ((\tilde{a}_j)_\alpha - (\bar{a}_j)_\alpha) z^\alpha \right| \\ &\leq \sup_{z \in B_1^m} \sum_{|\alpha|=2}^{\infty} |(\tilde{a}_j)_\alpha - (\bar{a}_j)_\alpha| |z_1|^{\alpha_1} \cdots |z_m|^{\alpha_m} \\ &\leq \sum_{|\alpha|=2}^{\infty} |(\tilde{a}_j)_\alpha - (\bar{a}_j)_\alpha| = \|\tilde{a}_j - \bar{a}_j\|_1 \leq \|\tilde{a} - \bar{a}\|_X < r_0. \end{aligned}$$

Using that estimate, given a point  $z \in B_1^m$  in parameter space, one may evaluate rigorously the corresponding value  $P(z) \in W_{\text{loc}}^s(\tilde{x})$  on the local stable manifold using the following enclosure

$$P_j(z) \in P_j^{(N)}(z) + [-r_0, r_0], \quad j = 1, \dots, n \quad (3.28)$$

where  $P_j^{(N)}(z)$  can be computed with interval arithmetic using the formula (3.27).

## 4 Saddle-type blow-up solutions: basic methodology for validations and characterizations

In what follows, we introduce a rigorous numerical methodology for validating blow-up solutions with practical applications. We give a direct consequence from our methodology showing that the maximal existence time  $t_{\text{max}}$  of solutions can be determined as a smooth function of initial conditions. In particular, appropriate compactifications, time-scale desingularizations, and parameterizations yield the (local) *analyticity* of  $t_{\text{max}}$  as a function of initial conditions.

## 4.1 Basic methodology

First we discuss a basic methodology for validating blow-up solutions. The fundamental steps consist of the following:

1. Validation of local stable manifolds of equilibria on the horizon for desingularized vector fields;
2. Extension of validated stable manifolds via rigorous integration of desingularized vector fields.

When an equilibrium  $p$  on the horizon is *stable*, the validation procedures reported in [48, 49, 57] allow (a) studying the local stable manifold of  $p$  by means of *locally defined Lyapunov functions*; and (b) computing rigorous enclosure of solution trajectories converging to  $p$ , hence yielding a rigorous bound of the blow-up time. On the other hand, when we validate the local stable manifold of a *saddle* equilibrium  $p$  on the horizon, the same methodology and general topological approach such as *covering relations* (e.g. [62]) are not appropriate due to the following two essential reasons:

- Typical topological methods involve dynamics of sets. In particular, objects of considerations contain *both stable and unstable* information in dynamical systems in general.
- When we apply global (namely, Poincaré-, or parabolic-type) compactifications, arbitrarily *small* neighborhood of a point on the horizon includes information of *unbounded* regions in the original phase space.

For these two reasons, we observe the difficulty of applying topological methods for calculating saddle-type blow-up solutions. For example, assuming that a desingularized vector field through global compactifications is considered, perturbations of initial conditions near the horizon lead to significant changes of dynamical behavior, even if the perturbations are small. In particular, dynamical sensitivity around unstable invariant sets on the horizon is huge. Although such a difficulty can be avoided by using directional compactifications (2.2), a couple of studies on different local charts and gluing process are necessary if we aim at understanding the global dynamics including divergent behavior of solutions.

Instead, we apply the parameterization method to validating local stable manifolds of equilibria on the horizon for desingularized vector fields. An important merit of the parameterization method is that only the stable information of equilibria can be treated through the whole computations. In other words, if we can compute stable eigenvectors at the equilibria and a topological conjugacy  $P$  with high accuracy, we obtain the local stable manifold without containing intrinsic unstable information of equilibria. The potential of this feature is shown in many preceding works (e.g. [3, 8, 30, 50, 59]) for obtaining global feature of dynamical systems. We then extend the locally validated stable manifolds through the time integration of the time-reversal desingularized vector fields. Applying the time-integration to any points on the stable manifolds, we *globalize* the local stable manifold whose preimage under compactifications is a (candidate of) family of saddle-type blow-up solutions<sup>14</sup>. The second process is standard and essentially identical with the methodology used in preceding works (e.g. [48, 49, 57]).

**Remark 4.1** (Rigorous integrators of ODEs). *Many methods for rigorously integrating solution trajectories of vector fields have been proposed over the last thirty years. The most famous achievement is the resolution of Smale's 14th problem by W. Tucker [58]. We refer to*

---

<sup>14</sup>Needless to say, the proposing methodology can be applied to sink-type blow-up solutions.

[6, 9, 35, 37, 43, 44, 61] for different methods for rigorous integration of ODEs. These methods are based on fixed-point arguments, which is equivalent to show the existence of solution trajectories, and several techniques of interval arithmetic. For the sake of forward time integration, we use a C++ Library for rigorous integration of ODEs, which is named the kv library [36]. This integrator is based on an interval representation of the solutions' Taylor series and the Affine arithmetic [53], which is a technique for preventing the so-called wrapping effect in interval analysis.

**Remark 4.2** (Validating local Lyapunov functions). *As mentioned above, for stable equilibria on the horizon, earlier validation procedures studied the local stable manifold by means of locally defined Lyapunov functions. More explicitly, after integrating solution in forward/backward time, we validate solution trajectories which converge to the equilibrium on the horizon. We use a method of constructing the local Lyapunov function attached to the equilibrium, which is originally provided in [47] and is used for validation of blow-up solutions in [48, 49, 57]. Constructing the local Lyapunov function by a quadratic form over vectors, we provide the explicit domain of the Lyapunov function. By checking that the solution is inside the domain at some time, we prove that the solution converges to the equilibrium. Furthermore, by rescaling the time variables, we obtain rigorous bounds of blow-up time in the original time scale.*

One of the key information in studying blow-up solutions is the *blow-up time*, which depends on initial conditions. We now introduce an explicit estimate methodology for obtaining blow-up times. Apply the directional compactification<sup>15</sup> of type  $\alpha$  and consider the desingularized vector field (2.10) associated with an asymptotically quasi-homogeneous vector field of type  $\alpha$  and of order  $k+1$ . For simplicity,  $\tau_d$  in (2.10) is replaced by  $\tau$ . Assume that a solution trajectory  $\{(s(\tau), \hat{x}(\tau))\}_{\tau \geq 0}$  on the stable manifold of an equilibrium  $p_* = (0, \hat{x}_*) \in \mathcal{E}$  with  $s(0) > 0$  is obtained. Then the maximal existence time of the solution for the original system and the original  $t$ -time scale is calculated as follows:

$$t_{\max} = \int_0^{\infty} s(\tau)^k d\tau, \quad (4.1)$$

where  $\tau = 0$  corresponds to the initial time for the desingularized vector field. If  $t_{\max} < \infty$ , the solution  $\{s(\tau), \hat{x}(\tau)\}$  is the image of a blow-up solution under the compactification, which is always guaranteed under hyperbolicity of  $p_*$ , according to Theorem 2.12. In preceding studies [48, 49, 57] for sink-type blow-up solutions, blow-up times are enclosed through the decomposition

$$t_{\max} = \int_0^{\bar{\tau}} s(\tau)^k d\tau + \int_{\bar{\tau}}^{\infty} s(\tau)^k d\tau, \quad (4.2)$$

where  $\bar{\tau}_d > 0$  is sufficiently large so that the point  $(s(\bar{\tau}), \hat{x}(\bar{\tau}))$  after the  $\tau = \bar{\tau}$ -time evolution through the trajectory is located at the local stable manifold of  $p_*$ . The first term in the r.h.s. of (4.2) is directly estimated by the ODE integration and typical enclosing formula of integrals. The second term is bounded by using the dynamical property of  $p_*$ . In [48, 49, 57], the *Lyapunov functions* locally defined around equilibria are applied (see Remark 4.2). There the integral with respect to  $\tau$  over an infinite interval is transformed into that with respect to the value of a (local) Lyapunov function  $L$  over a finite interval, which achieves a computable and rigorous enclosure of the integral. See the above references for details. As a consequence, combination of two rigorous enclosures of the r.h.s. of (4.2) yields a rigorous enclosure of blow-up times.

---

<sup>15</sup>The essential idea in the present argument is identical among various compactifications.

The basic idea for validating blow-up times in the present study is almost the same as the preceding works [48, 49, 57]. Namely, we validate enclosures of two integrals in (4.2) in an appropriate way. The main difference from preceding works is that we apply the parameterization method to validate the integral  $\int_{\tilde{\tau}}^{\infty} s(\tau)^k d\tau$  in (4.2), instead of Lyapunov functions. As shown later in Section 4.2, the integral can be calculated in an exact way, yielding the analytic property of  $t_{\max}$ . As for the direct integration part, namely the computation of  $\int_0^{\tilde{\tau}} s(\tau)^k d\tau$  in (4.2), an enclosure of the solution trajectory

$$\{(s(\tilde{\tau}), \hat{x}(\tilde{\tau})) \mid \tilde{\tau} \in [-\bar{\tau}, 0]\}$$

can be used to compute the enclosure of the integral

$$\int_0^{\tilde{\tau}} s(\tau)^k d\tau = \int_{-\tilde{\tau}}^0 s(\tilde{\tau})^k d\tilde{\tau}, \quad (4.3)$$

which is straightforward.

**Remark 4.3** ( $t_{\max}$  for other compactifications). *The expression (4.1) for  $t_{\max}$  is used when we apply directional compactifications and the time-scale desingularization (2.9). Other choices of compactifications yield other expressions of  $t_{\max}$ . For example, when we apply the Poincaré-type compactification and (2.11),  $t_{\max}$  can be expressed as*

$$t_{\max} = \int_0^{\infty} \kappa_{qP}(y(\tau))^{-k} d\tau = \int_0^{\infty} (1 - p(x(\tau))^{2c})^{k/2c} d\tau, \quad (4.4)$$

while the corresponding expression of  $t_{\max}$  to the parabolic-type compactification and (2.15) is

$$\begin{aligned} t_{\max} &= \int_0^{\infty} \left(1 - \frac{2c-1}{2c} \kappa_{para}(y)^{-1}\right) \frac{d\tau}{\kappa_{para}(T^{-1}(x(\tau)))^k} \\ &= \int_0^{\infty} \left(1 - \frac{2c-1}{2c} (1 - p(x(\tau))^{2c})\right) (1 - p(x(\tau))^{2c})^k d\tau. \end{aligned} \quad (4.5)$$

As in the case of directional compactifications, an equilibrium on the horizon  $x_*$  satisfies  $p(x_*) = 1$  in the case of Poincaré-type and parabolic-type compactifications. This property is applied to guaranteeing the convergence of the integral (4.5) in view of the parameterization  $P$  of  $W_{\text{loc}}^s(x_*)$ . More precisely, let  $X(\tau)$  be the integrand in (4.4) or (4.5) which is defined in a domain where the parameterization

$$P(\theta) = \sum_{|\alpha| \geq 0} a_{\alpha} \theta^{\alpha}, \quad P(0) = x_* \quad (4.6)$$

is defined. For simplicity, we assume that  $k/2c$  in (4.4) is a positive integer, in which case  $X(\tau)$  is polynomial. Then  $X(\tau)$  has the following expression:

$$X(\tau) = \sum_{|\alpha| > 0} b_{\alpha} (e^{\Lambda \tau} \theta)^{\alpha},$$

for some Taylor coefficients  $\{b_{\alpha}\}_{|\alpha| \geq 1}$  depending on  $\{a_{\alpha}\}_{|\alpha| \geq 0}$ . More importantly, the constant term of  $X(\tau)$  vanishes while the lowest order terms consist of exponentially decaying function of  $\tau$ . Combined with the uniform convergence of (4.6), we can explicitly calculate  $\int_0^{\infty} X(\tau) d\tau$ .

Detailed calculations with concrete choice of types and orders of compactifications and vector fields are provided in the examples of Sections 6 and 7.

**Remark 4.4.** *The absence of constant terms in the integrand of  $t_{\max}$  is the most essential property to show that  $t_{\max} < \infty$  in the preceding work [45] when  $p_* \in \mathcal{E}$  is hyperbolic, where the Hartman-Grobman-type argument is applied to extracting the exponentially decaying property of the integrand. This property is essentially independent of the choice of compactifications associated with appropriately chosen time-scale desingularizations. The present argument explicitly extracts this property to show  $t_{\max} < \infty$  by means of the parameterization method.*

Summarizing the above argument, our methodology for validating (saddle-type) blow-up solutions consists of the following.

1. Validate the local stable manifold of an equilibrium on the horizon for desingularized vector fields via the parameterization method.
2. Extend the validated stable manifold via (backward) integration, that is done by considering the time-reversed desingularized vector fields.
3. Compute a rigorous enclosure of the blow-up time through the decomposition of the form (4.2) as well as direct integrations through solution trajectories and parameterizations shown in Section 4.2.

In the subsequent sections, applicability of the present methodology is shown. In particular, we aim at showing the following features, respectively:

- **Section 5** shows an application of *directional compactifications* for validating saddle-type blow-up profiles and computing the validated curve  $t_{\max}$  as a function of initial points.
- **Section 6** shows an *application to higher-dimensional systems*. In the present study we consider an artificial 3-dimensional system. The Poincaré-type compactification is applied to an asymptotically homogeneous vector field. This example shows the global phase portrait involving multiple saddle-type blow-up solutions.
- **Section 7** shows a characteristic nature of saddle-type blow-up solutions with bounded global solutions which separate the whole phase space into two sets, one of which is the set of points such that solutions through them determine time-global solutions for both time directions and another is the set of points such that solutions through them are blow-up solutions. Dependence of  $t_{\max}$  as a function of initial data including saddle-type blow-up solutions is also addressed. The parabolic-type compactification is applied to an asymptotically quasi-homogeneous vector field.

## 4.2 Smooth dependence of $t_{\max}$ on initial points

Explicit expressions of  $t_{\max}$  shown in Section 4.1 indicate that  $t_{\max}$  depends continuously, possibly smoothly, on initial points within stable manifolds of hyperbolic equilibria (for desingularized vector fields) on the horizon, which is just a consequence of standard calculus. One of the benefits of applying the parameterization method discussed in Section 3 is that  $t_{\max}$  can be treated as a *locally analytic* function on initial points of solutions. Here we discuss the dependence of  $t_{\max}$  on initial points in more details.

Consider the desingularized vector field  $g$  associated with the directional (resp. Poincaré-type and parabolic type) compactification with the standard time-scale desingularization. Let  $p_* \in \mathcal{E}$

be a hyperbolic equilibrium for  $g$ . First note that typical choices of time-scale desingularizations  $S$ , namely the integrand of  $t_{\max}$ , satisfy the following properties (so that trajectories for  $g$  is orbitally equivalent to the original dynamical system (cf. [46])):

- It vanishes at  $p_*$ . See (4.1) (resp. (4.4) and (4.5)).
- It is positive along  $W^s(p_*; g)$ .
- It is smooth, in particular analytic, except  $k/2c \notin \mathbb{N}$  in the case of the Poincaré-type compactifications.

Assume that all assumptions in Theorem 3.5 for  $F$  given in (3.9) as well as (A1), (A2) and (A3) associated with the hyperbolic equilibrium  $p_*$  for  $g$  are satisfied, in which case the local stable manifold  $W_{\text{loc}}^s(p_*; g)$  is parameterized by an *analytic* function  $P$  defined on the unit polydisc  $B_1^m$  so that  $W_{\text{loc}}^s(p_*; g) = P(B_1^m)$ . For typical asymptotically quasi-homogeneous fields, the function  $S$  can be chosen as a polynomial or a rational function whose denominator is polynomial and positive on  $W_{\text{loc}}^s(p_*; g)$ . From these observations, we obtain the following proposition.

**Proposition 4.5** (Analytic function through parameterization). *Let  $p_*$  be an hyperbolic equilibrium for a dynamical system satisfying (A1), (A2) and (A3). Assume that a parameterization  $P$  of  $W_{\text{loc}}^s(p_*)$  satisfying  $P(0) = p_*$  is defined on the unit polydisc  $B_1^m$ , in particular  $W_{\text{loc}}^s(p_*) = P(B_1^m)$ . Let  $S$  be an analytic function defined in a neighborhood of  $W_{\text{loc}}^s(p_*)$  satisfying  $S(p_*) = 0$ . Then the integral*

$$U(\theta) \stackrel{\text{def}}{=} \int_0^\infty S \circ P(e^{\Lambda\tau}\theta) d\tau, \quad \theta \in B_1^m$$

is an analytic function on  $B_1^m$  satisfying  $U(0) = 0$ .

*Proof.* Since  $S$  and  $P$  are analytic, then so is  $S \circ P$  and hence the integrand of  $U$  is written by the convergent series

$$S \circ P(e^{\Lambda\tau}\theta) = \sum_{|\alpha| \geq 0} c_\alpha (e^{\Lambda\tau}\theta)^\alpha.$$

Denoting  $\alpha \cdot \lambda = \sum_{i=1}^m \alpha_i \lambda_i$ , the assumption  $S \circ P(0) = 0$  implies that  $c_0 = 0$  and

$$\begin{aligned} U(\theta) &= \int_0^\infty \sum_{|\alpha| > 0} c_\alpha (e^{\Lambda\tau}\theta)^\alpha d\tau = \int_0^\infty \sum_{|\alpha| > 0} c_\alpha \theta^\alpha e^{(\alpha \cdot \lambda)\tau} d\tau \\ &= \sum_{|\alpha| > 0} c_\alpha \theta^\alpha \left( \int_0^\infty e^{(\alpha \cdot \lambda)\tau} d\tau \right) \\ &= - \sum_{|\alpha| > 0} \frac{c_\alpha \theta^\alpha}{\alpha \cdot \lambda}, \end{aligned}$$

which converges uniformly on  $B_1^m$ . Indeed, letting  $\sigma_{\text{gap}} \stackrel{\text{def}}{=} \min_{j=1, \dots, m} |\lambda_j| > 0$ , then

$$|U(\theta)_j| = \left| \sum_{|\alpha| > 0} \frac{(c_j)_\alpha \theta^\alpha}{\alpha \cdot \lambda} \right| \leq \frac{1}{\sigma_{\text{gap}}} \left| \sum_{|\alpha| > 0} (c_j)_\alpha \theta^\alpha \right|.$$

holds for  $j = 1, \dots, n$ , uniformly in  $B_1^m$ .  $\square$



This proposition provides a fundamental feature of blow-up times. For compactifications and time-scale desingularizations discussed in the beginning of the present section, the function  $S$  is given below.

(4.1):  $S(s(\tau), x(\tau)) = s(\tau)^k$  and  $s(\tau) = P_1(e^{\Lambda\tau}\theta)$ .

(4.4) with  $k/2c \in \mathbb{N}$ :  $S(x(\tau)) = (1 - p(x(\tau))^{2c})^{k/2c} = (1 - \sum_{i=1}^n x_i(\tau)^{2\beta_i})^{k/2c}$  and  $x(\tau) = P(e^{\Lambda\tau}\theta)$ .

(4.5):  $S(x(\tau)) = (1 - \frac{2c-1}{2c}(1 - p(x(\tau))^{2c})) (1 - p(x(\tau))^{2c})^k$  and  $x(\tau) = P(e^{\Lambda\tau}\theta)$ .

Using these functions with the parameterization  $P$ , the function  $U(\theta)$  with the above choice equals to  $t_{\max} = t_{\max}(\theta)$  under corresponding compactifications and time-scale desingularizations. Note that the function  $S$  corresponds to the time-scale transformation factor. Different choice of time-scale desingularizations provides different  $S$  and, consequently, different determination of  $U(\theta) = t_{\max}(\theta)$ .

The inverse  $T^{-1}$  of compactifications *away from the horizon* can be described by analytic functions since it is defined by the  $n$ -tuples of composite functions of radicals and rational functions whose singularities in the sense of the loss of regularity and convergence of infinite series are located at infinity. The analytic dependence of  $t_{\max}$  on bounded initial data for (2.1) is therefore inherited by restricting our attention to stable manifolds of equilibria at infinity near blow-up.

**Theorem 4.6** (Analyticity of blow-up times). *Let  $t_{\max}$  be given by either the directional, the Poincaré-type with  $k/2c \in \mathbb{N}$  or the parabolic-type compactification, given by (4.1), (4.4) and (4.5), respectively. Let  $W_{\text{loc}}^s(p_*; g)$  be a local stable manifold for the desingularized vector field  $g$  given by the parameterization  $P$  satisfying all requirements presented in Proposition 4.5. Let  $y_0 \in \mathbb{R}^n$  be a point such that the solution  $y(t)$  to (2.1) with  $y(0) = y_0$  is mapped into the solution trajectory  $(T(y))(\tau)$  included in  $W_{\text{loc}}^s(p_*; g)$  through  $T$  and the time-scale desingularization. Then the blow-up time  $t_{\max}$  is real analytic at  $y_0$  in  $\text{int}_{T^{-1}(\mathcal{D})}T^{-1}(W_{\text{loc}}^s(p_*; g))$ , where  $\mathcal{D}$  is defined by (2.3) for directional compactifications and (2.6) for Poincaré- and parabolic-type compactifications, respectively. Moreover,  $t_{\max} = t_{\max}(y_0)$  converges to 0 as  $y_0$  goes to infinity along the solution  $y(t)$ .*

*Proof.* Let  $y_0 \in \text{int}_{T^{-1}(\mathcal{D})}T^{-1}(W_{\text{loc}}^s(p_*; g))$  be arbitrary. Then there is a unique point  $\theta_0 \in B_1^m$  such that  $y_0 = T^{-1}(P(\theta_0))$ . We shall write  $\theta_0 = P^{-1}(T(y_0))$ , where the expression of  $P^{-1}$  reflects the one-to-one property of  $P$  on  $B_1^m$ . Since  $T$  is analytic in the domain of definition (Remark 2.7), then so is  $P^{-1} \circ T$  in  $\text{int}_{T^{-1}(\mathcal{D})}T^{-1}(W_{\text{loc}}^s(p_*; g))$ <sup>16</sup>. Then the blow-up time  $t_{\max} = t_{\max}(y_0)$  at  $y_0$  is written by

$$t_{\max} = t_{\max}(\theta_0) = \int_0^\infty S \circ P(e^{\Lambda\tau}(P^{-1}(T(y_0))))d\tau \equiv t_{\max}(y_0).$$

The integrand is analytic in  $\text{int}_{T^{-1}(\mathcal{D})}T^{-1}(W_{\text{loc}}^s(p_*; g))$ , according to the same argument as the proof of Proposition 4.5. Therefore  $t_{\max} = t_{\max}(y_0)$  is analytic at  $y_0 \in \text{int}_{T^{-1}(\mathcal{D})}T^{-1}(W_{\text{loc}}^s(p_*; g))$ .

Our assumption for the solution  $y(t)$  implies that the property of  $y(t)$  going to infinity as  $t \rightarrow t_{\max}$  corresponds to  $(T(y))(\tau) \rightarrow p_*$  as  $\tau \rightarrow \infty$ . Moreover, for any  $y_0 \in \text{int}_{T^{-1}(\mathcal{D})}T^{-1}(W_{\text{loc}}^s(p_*; g))$ , we can choose a point  $\tilde{y}_0 \in \mathbb{R}^n$  such that  $T(\tilde{y}_0) \in W_{\text{loc}}^s(p_*; g)$  and that  $y_0 = y(t) = y(t; \tilde{y}_0)$  for some  $t > 0$ , where  $t$  is uniquely determined by  $\tilde{y}_0$ . The last assertion is equivalent to  $T(y_0) = (T(\tilde{y}_0))(\bar{\tau})$  for  $\bar{\tau} > 0$  uniquely determined by  $t$  and the time-scale desingularization. Fix the point  $\tilde{y}_0$ . By

<sup>16</sup>Analyticity of  $P^{-1}$  follows from that of  $P$  by assumption, linear isomorphism property of  $DP$  and the inverse function theorem for analytic functions. See e.g. [17] for the latter argument.

means of decomposition of  $t_{\max}$  in the same way as (4.2), the blow-up time  $t_{\max}$  at  $\tilde{y}_0$  is expressed by

$$t_{\max}(\tilde{y}_0) = \int_0^{\bar{\tau}} h(\tau) d\tau + \int_{\bar{\tau}}^{\infty} h(\tau) d\tau$$

with the corresponding choice of the integrand  $h(\tau) \equiv S \circ P(e^{\Lambda\tau}(P^{-1}(T(y_0))))$ . Notice that the second term in the right-hand side is the contribution of  $y_0$  to the determination of  $t_{\max}$ . As a result, we have

$$t_{\max}(y_0) = \int_{\bar{\tau}}^{\infty} h(\tau) d\tau.$$

As mentioned, the convergence of  $T(y_0)$  to  $p_*$  corresponds to  $\bar{\tau} \rightarrow \infty$ . Since  $h$  is analytic in  $B_1^m$ , the integral  $t_{\max}(y_0)$  goes to 0 as  $\bar{\tau} \rightarrow \infty$ . This implies the final statement in the theorem.  $\square$

Theorem 4.6 indicates that  $t_{\max}$  depends analytically on initial points on  $T^{-1}(W_{\text{loc}}^s(p_*; g))$ , provided that the non-resonance condition holds for eigenvalues of  $Dg(p_*)$ . Furthermore, a computer-assisted proof for the existence of  $P$  as discussed in Section 3 provides the *explicit* region where the analyticity of  $t_{\max}$  as a function of initial points of trajectories is guaranteed. Extending  $W_{\text{loc}}^s(p_*; g)$  through the flow and using the smooth dependence of the flow on initial points, we can extend  $t_{\max}$  as a smooth function of the initial conditions whose smoothness depends on that for the flow, as long as  $W_{\text{loc}}^s(p_*; g)$  is smoothly continued. In particular,  $t_{\max}$  can be analytically continued if the vector field  $g$  is analytic. Note that the analyticity, or even continuity of  $t_{\max}$  is not guaranteed *as a function of  $y$  in  $\mathbb{R}^n$*  since the expression of  $t_{\max}$  as an analytic function only makes sense on  $W_{\text{loc}}^s(p_*)$ . The different choice of  $p_*$  induce a different expression of  $P$ , and hence of  $t_{\max}$ .

Finally we shall derive a detailed implementation of  $t_{\max}$  for directional compactifications, namely the estimate of the integral  $\int_{\bar{\tau}}^{\infty} s(\tau)^k d\tau$  given in (4.2). The corresponding calculations of  $t_{\max}$  for Poincaré-type with  $k/2c \in \mathbb{N}$  and parabolic-type compactifications are achieved in the same manner. Let  $p_* \in \mathcal{E}$  be a hyperbolic equilibrium for a desingularized vector field. Assume that the parameterization method around  $p_*$  works and the local stable manifold  $W_{\text{loc}}^s(p_*)$  is obtained through the ( $m$ -dimensional) stable polydisk  $B_1^m$  and the parameterization  $P$ . For simplicity, stable eigenvalues  $\{\lambda_i\}_{i=1}^m$  of the linearized matrix of the desingularized vector field at  $p_*$  are assumed to be simple and real. In particular,  $\lambda_i < 0$  for  $i = 1, \dots, m$ . Recalling (3.3), write

$$\Lambda = \begin{pmatrix} \lambda_1 & & \\ & \ddots & \\ & & \lambda_m \end{pmatrix}.$$

Then the solution  $(s(\tau), \hat{x}(\tau)) \in W_{\text{loc}}^s(p_*)$  is written by

$$(s(\tau), \hat{x}(\tau)) = P(e^{\Lambda\tau}\theta) \text{ with } s(\tau) = P_1(e^{\Lambda\tau}\theta), \quad \theta = (\theta_1, \dots, \theta_m) \in B_1^m,$$

where

$$P(\theta) = \sum_{|\alpha| \geq 0} a_\alpha \theta^\alpha \equiv \begin{pmatrix} P_1(\theta) \\ \vdots \\ P_n(\theta) \end{pmatrix} \in \mathbb{R}^n, \quad \theta = \begin{pmatrix} \theta_1 \\ \vdots \\ \theta_m \end{pmatrix} \in \mathbb{R}^m, \quad a_\alpha = \begin{pmatrix} (a_1)_\alpha \\ \vdots \\ (a_n)_\alpha \end{pmatrix} \in \mathbb{R}^n, \quad (4.7)$$

is the parameterization of  $W_{\text{loc}}^s(p_*)$ . The rightmost integral in (4.2) can be calculated as follows, once we obtain a concrete form of  $P$ :

$$\begin{aligned} \int_{\tilde{\tau}}^{\infty} s(\tau)^k d\tau &= \int_{\tilde{\tau}}^{\infty} \left( P_1 \left( e^{\Lambda(\tau-\tilde{\tau})}\theta \right) \right)^k d\tau \equiv \int_0^{\infty} \left( P_1 \left( e^{\Lambda\tilde{\tau}}\theta \right) \right)^k d\tilde{\tau} \\ &= \int_0^{\infty} \left( \sum_{|\alpha| \geq 0} (a_1)_{\alpha} \left( e^{\Lambda\tilde{\tau}}\theta \right)^{\alpha} \right)^k d\tilde{\tau} \\ &= \int_0^{\infty} \left( \sum_{|\alpha| \geq 0} (a_1)_{\alpha} e^{(\alpha \cdot \lambda)\tilde{\tau}} \theta^{\alpha} \right)^k d\tilde{\tau}. \end{aligned}$$

Denote the *Cauchy product over multi-indices* by

$$(a * b)_{\alpha} = \sum_{\beta + \gamma = \alpha} a_{\beta} b_{\gamma}, \quad a_{\beta}, b_{\gamma} \in \mathbb{R} \quad \text{for} \quad \alpha, \beta, \gamma \in \mathbb{Z}_{\geq 0}^m, \quad (4.8)$$

and given  $k \in \mathbb{N}$  denote

$$(a^k)_{\alpha} = \overbrace{(a * \dots * a)}^{k \text{ times}}_{\alpha}.$$

Here we observe that  $(a_1)_{\mathbf{0}} = 0$ , since  $P(0) = p_*$  is the equilibrium for the desingularized vector field (2.10) and  $P_1(0) = 0$  from our choice of compactifications. Using the previous notation and the above fact, the above integral is formally written as follows:

$$\begin{aligned} \int_{\tilde{\tau}}^{\infty} s(\tau)^k d\tau &= \int_0^{\infty} \left\{ \sum_{|\alpha| \geq 0} (a_1^k)_{\alpha} e^{(\alpha \cdot \lambda)\tilde{\tau}} \theta^{\alpha} \right\} d\tilde{\tau} \\ &= \sum_{|\alpha| \geq 0} (a_1^k)_{\alpha} \theta^{\alpha} \left( \int_0^{\infty} e^{(\alpha \cdot \lambda)\tilde{\tau}} d\tilde{\tau} \right) \\ &= \sum_{|\alpha| > 0} (a_1^k)_{\alpha} \theta^{\alpha} \left( \int_0^{\infty} e^{(\alpha \cdot \lambda)\tilde{\tau}} d\tilde{\tau} \right) \\ &= - \sum_{|\alpha| > 0} (a_1^k)_{\alpha} \frac{\theta^{\alpha}}{\alpha \cdot \lambda}. \end{aligned} \quad (4.9)$$

In particular, the denominator  $\alpha \cdot \lambda$  is strictly negative for all possible  $\alpha$ , and the analyticity of  $P$  implies that the above infinite sum is convergent uniformly in  $B_1^m$ .

The final formula (4.9) implies that we can calculate the rigorous value of  $t_{\max}$  near blow-up, once we obtain the parameterization of the local stable manifold  $W_{\text{loc}}^s(p_*)$  and fix the point  $\theta \in B^m$ , namely  $P(\theta) \in W_{\text{loc}}^s(p_*)$ . As seen below, the similar expressions of  $t_{\max}$  to (4.9) can be obtained for Poincaré-type and parabolic-type compactifications.

**Remark 4.7** (Special case). *If  $n_s = 1$ , the explicit expression (4.9) admits the simpler form:*

$$(a * b)_n = \sum_{j \geq 0} a_j b_{n-j}, \quad a = (a_j)_{j \geq 0}, b = (b_j)_{j \geq 0}.$$

Indeed,  $\alpha$  becomes a single index  $l$  and

$$t_{\max} = \sum_{|\alpha|>0} (a_1^k)_\alpha \theta^\alpha \left( \int_0^\infty e^{(\alpha \cdot \lambda) \bar{\tau}} d\bar{\tau} \right) = -\frac{1}{\lambda} \sum_{l=k}^\infty (a_1^k)_l \frac{\theta^l}{l},$$

where we have used the fact that  $(a_1)_0 = 0$  and that the Cauchy product  $(a_1^k)_l = \overbrace{(a_1 * \dots * a_1)}^{k \text{ times}}_l$ , with  $l < k$  contains at least one  $(a_1)_0$ .

**Remark 4.8** (Integrands and smoothness of  $t_{\max}$ ). *The concrete procedure to compute the integral (4.9) or its upper bound depends on problems, namely the choice of compactifications and time-scale desingularizations.*

- Our first example (Section 5) applies a directional compactification, while the time-scale desingularization has the different form from (2.9) so that the resulting desingularized vector field is polynomial. Instead,  $t_{\max}$  requires integrations of rational-type functions. Nevertheless, the essence of the above argument, namely the absence of constant terms in the integrand of  $t_{\max}$ , can be applied to verifying that  $t_{\max} < \infty$ . Analyticity of integrand follows from that for both the numerator and the denominator with additional boundedness property of the denominator. Detailed derivation of  $t_{\max}$  or its upper bound is shown in subsequent sections.
- In the case of Poincaré-type compactifications, analyticity of  $t_{\max}$  is not guaranteed when  $k/2c \notin \mathbb{N}$ , since the function  $h(x) = x^{k/2c}$  is not analytic at  $x = 0$ . This failure comes from the “mismatch” of properties of vector fields in the sense that the order  $k + 1$  and the type  $\alpha$ , consequently the natural number  $c$ , determining an appropriate Poincaré-type compactifications are determined by the asymptotic quasi-homogeneity of vector fields. We then need further estimates for calculating  $t_{\max}$  in such a case. The difficulty originated from this issue can be overcome by choosing the parabolic-type compactifications.

**Remark 4.9** (Lyapunov functions versus parameterizations for expressing  $t_{\max}$ ). *Estimates of  $t_{\max}$  by means of Lyapunov functions (e.g. [48, 49, 57]) only provide upper bounds of  $t_{\max}$ , since they do not trace concrete trajectories on stable manifolds, but values of functionals on trajectories, implying that smoothness arguments for  $t_{\max}$  as a function of initial points cannot be derived. Instead, simple inequalities by means of Lyapunov functions provide upper bounds of  $t_{\max}$  even in the case of Poincaré-type compactifications with  $k/2c \notin \mathbb{N}$ , as demonstrated in [57]. Moreover, non-resonance condition (A3) is not required for estimations.*

On the other hand, we can trace trajectories on stable manifolds by means of parameterizations, indicating that  $t_{\max}$  is “exactly” calculated through the integration of given functions depending on solution trajectories. In particular, we can explicitly discuss properties of  $t_{\max}$  as a functions of initial points. In compensation for these precise information, however, we have to take care of analytic information of dynamical systems to ensure smoothness or analyticity of functions of interests, such as non-resonance condition (A3) for analyticity of  $P$  providing the conjugacy to linearizations, matching of integers  $k$  and  $c$  for Poincaré-type compactifications mentioned in Remark 4.8.

## 5 Example 1

In what follows, we show several applications of our proposed methodology not only to show its applicability but also to reveal several remarkable features of saddle-type blow-up solutions. The first problem is concerned with saddle-type blow-up solutions for the following system:

$$\begin{cases} \beta' = vB_1(\beta) - c\beta - c_1, \\ v' = v^2B_2(\beta) - cv - c_2, \end{cases} \quad ' = \frac{d}{d\zeta}, \quad (5.1)$$

where

$$B_1(\beta) = \frac{(\beta - \rho_1)(\beta - \rho_2)}{\beta}, \quad B_2(\beta) = \frac{\beta^2 - \rho_1\rho_2}{2\beta^2}$$

and  $\rho_2 > \rho_1$  are positive constants. Moreover,

$$c = \frac{v_R B_1(\beta_R) - v_L B_1(\beta_L)}{\beta_R - \beta_L} \quad (5.2)$$

and  $(c_1, c_2) = (c_{1L}, c_{2L})$  with

$$\begin{cases} c_{1L} = v_L B_1(\beta_L) - c\beta_L, \\ c_{2L} = v_L^2 B_2(\beta_L) - cv_L. \end{cases} \quad (5.3)$$

Points  $(\beta_L, v_L)$  and  $(\beta_R, v_R)$  are given in advance.

**Remark 5.1.** *The system (5.1) stems from the Riemann problem of the following system of conservation laws describing the (simplified) two-phase, one-dimensional incompressible flow [38]:*

$$\beta_t + (vB_1(\beta))_x = 0, \quad v_t + (v^2B_2(\beta))_x = 0 \quad (5.4)$$

with

$$(\beta(x, 0), v(x, 0)) = \begin{cases} U_L \equiv (\beta_L, v_L) & x < 0, \\ U_R \equiv (\beta_R, v_R) & x > 0. \end{cases} \quad (5.5)$$

Observe that  $B_1(\beta) < 0$  for  $\beta \in (\rho_1, \rho_2)$  and  $B_1(\beta) > 0$  for  $0 < \beta < \rho_1, \beta > \rho_2$ . Details are stated in [38].

The system (5.1) is the reduced problem of (5.4) satisfying viscosity profile criterion, namely the traveling wave problem with respect to the frame coordinate  $\zeta = x - ct$  with the boundary condition

$$\lim_{\zeta \rightarrow -\infty} (\beta(\zeta), v(\zeta)) = (\beta_L, v_L), \quad \lim_{\zeta \rightarrow +\infty} (\beta(\zeta), v(\zeta)) = (\beta_R, v_R),$$

where  $c$  is the speed of traveling waves. Saddle-type blow-up solutions for (5.1) are considered as components of singular shock wave solutions<sup>17</sup> to (5.4).

We choose the directional compactification (2.2) of type (0, 1) :  $(\beta, v) \mapsto (x_1, s) = (\beta, v^{-1})$  (cf. [38, 45]). Direct calculations yield the following desingularized vector field on  $\{r \geq 0\} \times \{\rho_1 \leq \beta \leq \rho_2\}$ :

$$\begin{cases} \frac{dx_1}{d\tau} = B_1(x_1) - cx_1s - c_1s, \\ \frac{ds}{d\tau} = -s \{B_2(x_1) - cs - c_2s^2\}, \end{cases} \quad (5.6)$$

<sup>17</sup>To make the correspondence precisely, the extended fast-slow system setting is required. Detail is shown in [38].

where  $\tau$  is the desingularized time-scale given by  $d\tau = s^{-1}dt$ . Obviously,  $(x_1, s) = (\rho_1, 0) \equiv p_1$  and  $(\rho_2, 0) \equiv p_2$  are equilibria of (5.6) on the horizon  $\mathcal{E} = \{s = 0\}$  and the vector field on  $\mathcal{E} \setminus \{p_1, p_2\}$  is monotone on each component.

On the other hand, the vector field (5.6) is *rational*. In order to nicely apply the parameterization method, we introduce *further* time-scale transformation as follows:

$$\frac{d\tau}{d\eta} = x_1^{-2}.$$

Then the resulting vector field is

$$\begin{cases} \frac{dx_1}{d\eta} = x_1(x_1 - \rho_1)(x_1 - \rho_2) - cx_1^3s - c_1x_1^2s, \\ \frac{ds}{d\eta} = -s \left\{ \frac{1}{2}(x_1^2 - \rho_1\rho_2) - x_1^2(cs + c_2s^2) \right\}. \end{cases} \quad (5.7)$$

Note that typical solutions of (5.6) are considered within the region  $\{\rho_1 \leq x_1 \leq \rho_2\}$  and  $\rho_1 > 0$ . Therefore the new vector field (5.7) is intrinsically the time-reparameterized vector field of (5.6) and hence these vector fields provide topologically the same information as each other.

The horizon is  $\{s = 0\}$  and equilibria on the horizon is  $(x_1, s) = (\rho_1, 0), (\rho_2, 0)$ . Looking at (5.7) only,  $(x_1, s) = (0, 0)$  can be also a stationary point, but it is not appropriate from our requirement.

**Remark 5.2** (Technical details). *When we solve the problem (5.7) in practice, we need to fix several parameters. In the present case,*

- *First, we fix  $x_L \equiv (x_{1,L}, s_L) = (1.9, 0.25)$  as a sample data. Then, following the directional compactification  $(x_1, s) = (\beta, v^{-1})$ , we obtain  $(\beta_L, v_L) = (1.9, 4)$ . Next, we fix  $x_R \equiv (x_{1,R}, s_R) = (1.5, 0.2)$  similarly. Then we obtain  $(\beta_R, v_R) = (1.5, 5)$ . Independently, we need to fix  $(\rho_1, \rho_2)$ . In the present case, we fix  $(\rho_1, \rho_2) = (1, 2)$ .*
- *Following standard arguments of systems of conservation laws, compute  $B_1(\beta), B_2(\beta)$  and  $c$  given above for  $(\beta, v) = (\beta_L, v_L), (\beta_R, v_R)$ .*

In the present study, we compute the stable manifold of the saddle equilibrium on the horizon  $(x_1, s) = (2, 0)$  for (5.7) in  $\{s \geq 0\}$  with parameters shown in Remark 5.2.

**Remark 5.3** (Continuation of the stable manifold and the total blow-up time). *Once we validate the local stable manifold  $W_{loc}^s(p_2)$  of the saddle (say  $(x_1, s) = (2, 0) \equiv p_2$ ) for (5.7), the continuation of  $W_{loc}^s(p_2)$  is realized by integrating (5.7) with the initial point located at  $W_{loc}^s(p_2)$  in backward time. Assume that  $p_0 \in W_{loc}^s(p_2)$ , which correspond to  $\theta$  through the parameterization  $P$ , for some  $\theta$ . Namely,  $P(\theta) = p_0$ . Then the blow-up time of the blow-up solution for (5.1) corresponding to global trajectory for (5.7) with the initial data given by (5.14) stated below. Let the corresponding value be  $t_{\max, loc}$ . Second we assume that (5.7) is integrated through  $p_0$  in backward time from  $-\eta = 0$  to  $-\eta = -\eta_0$ . Namely, assume that we have obtained a solution trajectory  $\{(x_1(-\eta), s(-\eta)) \mid -\eta \in [-\eta_0, 0]\}$  with  $(x_1(0), s(0)) = p_0$ . Then the corresponding passing time in the original time scale is*

$$t_{-\eta_0} = \int_0^{-\eta_0} \frac{s(-\eta)}{x_1(-\eta)^2} d(-\eta) = \int_0^{\eta_0} \frac{s(\eta)}{x_1(\eta)^2} d\eta.$$

Let  $p_{-\eta_0} := (x_1(-\eta_0), s(-\eta_0))$  for the backward solution trajectory  $\{(x_1(-\eta), s(-\eta)) \mid -\eta \in [-\eta_0, 0]\}$  with  $(x_1(0), s(0)) = p_0$ . Then the total blow-up time of the solution for (5.1) with the initial data  $T_d^{-1}(p_{-\eta_0})$  is

$$t_{\max, \text{loc}} + t_{-\eta_0}.$$

### 5.1 A local one-dimensional stable manifold of $p_2$ in (5.7)

Consider the system of desingularized ODEs

$$\dot{x} = g(x) = \begin{pmatrix} g_1(x_1, x_2) \\ g_2(x_1, x_2) \end{pmatrix} \stackrel{\text{def}}{=} \begin{pmatrix} x_1^3 - (\rho_1 + \rho_2)x_1^2 + \rho_1\rho_2x_1 - cx_1^3x_2 - c_1x_1^2x_2 \\ -\frac{1}{2}x_1^2x_2 + \frac{1}{2}\rho_1\rho_2x_2 + cx_1^2x_2^2 + c_2x_1^2x_2^3 \end{pmatrix} \quad (5.8)$$

Furthermore, at  $x^{(2)} \stackrel{\text{def}}{=} (\rho_2, 0)$

$$Dg(x^{(2)}) = \begin{pmatrix} \rho_2(\rho_2 - \rho_1) & -\rho_2^2(c\rho_2 + c_1) \\ 0 & -\frac{\rho_2}{2}(\rho_2 - \rho_1) \end{pmatrix}.$$

We focus on the one-dimensional stable manifold of the steady state  $x^{(2)}$  with stable eigenvalue  $\lambda \stackrel{\text{def}}{=} -\frac{\rho_2}{2}(\rho_2 - \rho_1) < 0$  and corresponding stable eigenvector

$$v \stackrel{\text{def}}{=} \begin{pmatrix} -\rho_2^2(c\rho_2 + c_1) \\ -\frac{3\rho_2}{2}(\rho_2 - \rho_1) \end{pmatrix}.$$

Our goal is to produce an analytic function  $P: (-\nu, \nu) \rightarrow \mathbb{R}^2$  that parameterizes  $W_{\text{loc}}^s(x^{(2)})$ . The Taylor series representation has the form

$$P(\theta) = \sum_{n=0}^{\infty} a_n \theta^n \quad \text{where } a_n = \begin{pmatrix} (a_1)_n \\ (a_2)_n \end{pmatrix}.$$

By Lemma 3.2  $P$  will represent the stable manifold if

$$P(0) = \begin{pmatrix} \rho_2 \\ 0 \end{pmatrix}, \quad DP(0) = v = \begin{pmatrix} -\rho_2^2(c\rho_2 + c_1) \\ -\frac{3\rho_2}{2}(\rho_2 - \rho_1) \end{pmatrix}, \quad \text{and} \quad \lambda \theta \frac{\partial P}{\partial \theta}(\theta) = g(P(\theta)).$$

From this we can immediately conclude that

$$\begin{pmatrix} (a_1)_0 \\ (a_1)_0 \end{pmatrix} = \begin{pmatrix} \rho_2 \\ 0 \end{pmatrix}, \quad \begin{pmatrix} (a_1)_1 \\ (a_2)_1 \end{pmatrix} = \begin{pmatrix} -\rho_2^2(c\rho_2 + c_1) \\ -\frac{3\rho_2}{2}(\rho_2 - \rho_1) \end{pmatrix}, \quad \text{and} \quad \lambda \sum_{n=0}^{\infty} n a_n \theta^n = g \left( \sum_{n=0}^{\infty} a_n \theta^n \right), \quad (5.9)$$

where

$$g \left( \sum_{n=0}^{\infty} a_n \theta^n \right) = \sum_{n=0}^{\infty} \begin{pmatrix} (a_1^3)_n - (\rho_1 + \rho_2)(a_1^2)_n + \rho_1\rho_2(a_1)_n - c(a_1^3 a_2)_n - c_1(a_1^2 a_2)_n \\ -\frac{1}{2}(a_1^2 a_2)_n + \frac{1}{2}\rho_1\rho_2(a_2)_n + c(a_1^2 a_2^2)_n + c_2(a_1^2 a_2^3)_n \end{pmatrix} \theta^n.$$

Let

$$\ell^1 \stackrel{\text{def}}{=} \left\{ b = (b_n)_{n \geq 2} : \|b\|_1 \stackrel{\text{def}}{=} \sum_{n \geq 2} |b_n| < \infty \right\}.$$

For  $j = 1, 2$ , denote  $a_j = ((a_j)_n)_{n \geq 2}$ , and  $a = (a_1, a_2)$ . Define  $F = (F_1, F_2): (\ell^1)^2 \rightarrow (\ell^1)^2$  by

$$(F_1(a))_n \stackrel{\text{def}}{=} \lambda n (a_1)_n - ((a_1^3)_n - (\rho_1 + \rho_2)(a_1^2)_n + \rho_1 \rho_2 (a_1)_n - c(a_1^3 a_2)_n - c_1(a_1^2 a_2)_n) \quad (5.10)$$

$$(F_2(a))_n \stackrel{\text{def}}{=} \lambda n (a_2)_n - \left( -\frac{1}{2}(a_1^2 a_2)_n + \frac{1}{2}\rho_1 \rho_2 (a_2)_n + c(a_1^2 a_2^2) + c_2(a_1^2 a_2^3) \right) \quad (5.11)$$

for  $n \geq 2$ , and observe that if there exists  $\tilde{a} \in (\ell^1)^2$  such that  $F(\tilde{a}) = 0$ , then we have obtained the desired parameterization.

### 5.1.1 A computer-assisted proof

Fixing  $N = 300$ , we computed the bounds  $Y_0, Z_0, Z_1$  and  $Z_2$  as presented in Sections 3.1, 3.2, 3.3 and 3.4, respectively. Then, we applied Theorem 3.5 to prove existence of  $\tilde{a} \in B_r(\bar{a})$  such that  $F_1(\tilde{a}) = F_2(\tilde{a}) = 0$  with  $F_1$  and  $F_2$  given in (5.10) and (5.11), respectively. More explicitly, we got that  $\|\tilde{a} - \bar{a}\|_X \leq r = 4.2 \times 10^{-13}$ .

The Taylor series representation of the parameterization of the local stable manifold has the form

$$P(\theta) = \sum_{n=0}^{\infty} \tilde{a}_n \theta^n \quad \text{where } \tilde{a}_n = \begin{pmatrix} (\tilde{a}_1)_n \\ (\tilde{a}_2)_n \end{pmatrix}$$

and denote by

$$P^{(N)}(\theta) = \sum_{n=0}^N \bar{a}_n \theta^n \quad \text{where } \bar{a}_n = \begin{pmatrix} (\bar{a}_1)_n \\ (\bar{a}_2)_n \end{pmatrix}$$

the numerical approximation of the local stable manifold. Then,

$$\begin{aligned} \|P - P^{(N)}\|_{\infty} &= \sup_{\theta \in (-\nu, \nu)} \|P(\theta) - P^{(N)}(\theta)\|_{\infty} \\ &= \sup_{\theta \in (-\nu, \nu)} \max(|P_1(\theta) - P_1^{(N)}(\theta)|, |P_2(\theta) - P_2^{(N)}(\theta)|) \\ &\leq \sup_{\theta \in (-\nu, \nu)} \max\left(\sum_{n=0}^{\infty} |(\tilde{a}_1)_n - (\bar{a}_1)_n| |\theta|^n, \sum_{n=0}^{\infty} |(\tilde{a}_2)_n - (\bar{a}_2)_n| |\theta|^n\right) \\ &\leq \max\left(\sum_{n=0}^{\infty} |(\tilde{a}_1)_n - (\bar{a}_1)_n| \nu^n, \sum_{n=0}^{\infty} |(\tilde{a}_2)_n - (\bar{a}_2)_n| \nu^n\right) \\ &= \max(\|\tilde{a}_1 - \bar{a}_1\|_{\nu}, \|\tilde{a}_2 - \bar{a}_2\|_{\nu}) \\ &= \|\tilde{a} - \bar{a}\|_X \leq r = 4.2 \times 10^{-13}. \end{aligned}$$

### 5.1.2 Computing the blow-up time

Given a point  $(x_1(0), s(0)) \in W_{loc}^s(p_2)$  (with  $p_2 = (2, 0)$ ), the blow-up time is given by

$$t_{\max} = \int_0^{\infty} \frac{s(\eta)}{x_1(\eta)^2} d\eta. \quad (5.12)$$



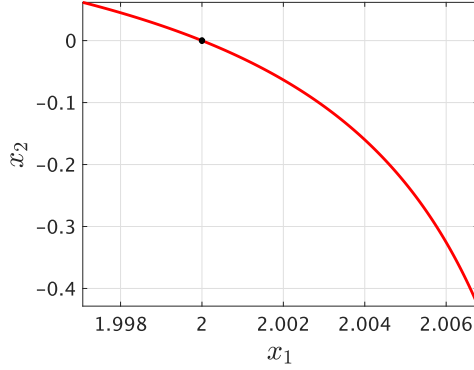


Figure 3: The rigorously computed stable manifold with rigorous error bound  $\|P - P^{(N)}\|_\infty \leq r = 4.2 \times 10^{-13}$ .

Given that  $(x_1(0), s(0)) = (P_1(\theta), P_2(\theta))$  for a given  $\theta \in (-\nu, \nu)$ , we get from (3.4) that  $\varphi(t, P(\theta)) = P(e^{\lambda t}\theta)$  for all  $t \geq 0$ . Hence, the solution  $(x_1(t), s(t))$  with initial condition  $(x_1(0), s(0)) = (P_1(\theta), P_2(\theta))$  is given by  $(x_1(t), s(t)) = P(e^{\lambda t}\theta)$ .

Rescaling the time interval  $\eta \in [0, \infty]$  to  $u \in [\theta, 0]$  leads (via the change of coordinates  $u = e^{\lambda\eta}\theta$ ) to

$$t_{\max} = \int_0^\infty \frac{s(\eta)}{x_1(\eta)^2} d\eta = \int_0^\infty \frac{P_2(e^{\lambda\eta}\theta)}{[P_1(e^{\lambda\eta}\theta)]^2} d\eta = \int_\theta^0 \frac{1}{\lambda u} \frac{P_2(u)}{[P_1(u)]^2} du. \quad (5.13)$$

Now, note that

$$P_2(u) = \sum_{n \geq 0} (\tilde{a}_2)_n u^n = \sum_{n \geq 1} (\tilde{a}_2)_n u^n$$

since  $(\tilde{a}_2)_0 = (p_2)_2 = 0$ . Denote

$$Q(u) \stackrel{\text{def}}{=} \frac{P_2(u)}{u} = \frac{1}{u} \sum_{n \geq 1} (\tilde{a}_2)_n u^n = \sum_{n \geq 0} (\tilde{a}_2)_{n+1} u^n = \sum_{n \geq 0} \tilde{q}_n u^n$$

where  $\tilde{q}_n \stackrel{\text{def}}{=} (\tilde{a}_2)_{n+1}$  for  $n \geq 0$ . Hence, equation (5.13) becomes

$$t_{\max} = \frac{1}{\lambda} \int_\theta^0 \frac{Q(u)}{[P_1(u)]^2} du.$$

Assume now that we have (again using rigorous numerics) obtained

$$R(u) \stackrel{\text{def}}{=} \frac{Q(u)}{[P_1(u)]^2} = \sum_{n \geq 0} r_n u^n$$

with rigorous error bounds. Using that information,

$$t_{\max} = \frac{1}{\lambda} \int_\theta^0 \sum_{n \geq 0} r_n u^n du = \frac{1}{\lambda} \sum_{n \geq 0} r_n \int_\theta^0 u^n du = -\frac{1}{\lambda} \sum_{n \geq 0} \frac{r_n}{n+1} \theta^{n+1}, \quad (5.14)$$

which is in essence computable (that is we can provide a numerical approximation together with rigorous error bounds). In the Figure 4 below, we present a rigorous numerical computation (with rigorous bounds) of the value of  $t_{\max}$  as a function of  $\theta$ , that is as a function of the initial condition  $P(\theta)$  on  $W_{loc}^s(p_2)$ . The rigorous error bound is obtained by computing rigorously the Taylor coefficients of  $r_n$  in the expansion (5.14). We present how to do that next.

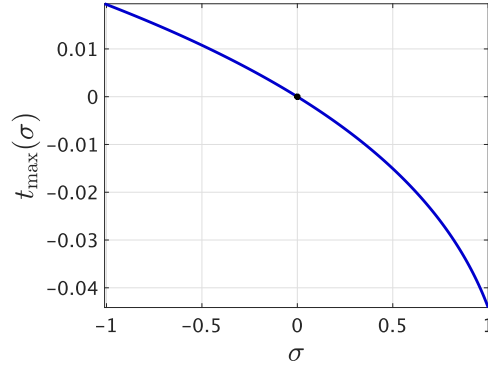


Figure 4: The numerical values of  $t_{\max}$  according to formula (5.14).

### 5.1.3 Rigorous computation of the coefficients $r_n$

Given  $\tilde{a} = (\tilde{a}_1, \tilde{a}_2)$  with  $\|\tilde{a} - \bar{a}\|_X \leq r = 4.2 \times 10^{-13}$  the power series coefficients of  $P_i(u) = \sum_{n \geq 0} (\tilde{a}_i)_n u^n$ . The goal in this section is to compute rigorously the coefficients  $r_n$  of  $R(u) = \sum_{n \geq 0} r_n u^n$  such that  $[P_1(u)]^2 R(u) = Q(u)$ . This amounts to solve the Taylor coefficients equation

$$\psi(r) \stackrel{\text{def}}{=} \tilde{a}_1^2 r - \tilde{q} = 0. \quad (5.15)$$

Using Newton's method, assume that we computed  $\bar{r}$  such that  $\psi(\bar{r}) \approx 0$ . Denote by  $D\psi^{(N)}(\bar{r})$  the Jacobian of  $\psi^{(N)}$  at  $\bar{r}$ . The next step is to construct the linear operator  $A^\dagger$  (an approximate derivative of the derivative  $D\psi(\bar{r})$ ), and the linear operator  $A$  (an approximate inverse of  $D\psi(\bar{r})$ ). Let  $A^\dagger$  be defined as

$$(A^\dagger h)_n = \begin{cases} (D\psi^{(N)}(\bar{r})h^{(N)})_n & \text{for } 0 \leq n \leq N, \\ (\tilde{a}_1^2)_0 & \text{for } n > N, \end{cases}$$

Consider now a matrix  $A^{(N)} \in M_{N+1}(\mathbb{R})$  computed so that  $A^{(N)} \approx D\psi^{(N)}(\bar{r})^{-1}$ . This allows defining the linear operator  $A$  whose action on an element  $h \in \ell_\nu^1$

$$(Ah)_n = \begin{cases} (A^{(N)}h^{(N)})_n & \text{for } 0 \leq n \leq N \\ \frac{1}{(\tilde{a}_1^2)_0} h_n & \text{for } n > N. \end{cases}$$

Having obtained an approximate solution  $\bar{r}$  and the linear operators  $A^\dagger$  and  $A$ , the next step is to construct the bounds  $Y_0$ ,  $Z_0$ ,  $Z_1$  and  $Z_2(r)$  satisfying (3.14), (3.15), (3.16) and (3.17), respectively.

Note that since problem (5.15) is linear, then  $Z_2 = 0$ .

**The bound  $Y_0$ .** We look for a bound such that  $\|A\psi(\bar{r})\|_\nu \leq Y_0$ . Expand

$$\psi(\bar{r}) = \tilde{a}_1^2 \bar{r} - \tilde{q} = (\bar{a}_1 + \delta_1)^2 \bar{r} - (\bar{q} + \delta_q) = \bar{\psi}(\bar{r}) + \psi^\delta(\bar{r}),$$

where

$$\bar{\psi}(\bar{r}) \stackrel{\text{def}}{=} \bar{a}_1^2 \bar{r} - \bar{q} \quad \text{and} \quad \psi^\delta(\bar{r}) \stackrel{\text{def}}{=} 2\delta_1 \bar{a}_1 \bar{r} + \delta_1^2 \bar{r} - \delta_q$$

and  $\delta_1 \stackrel{\text{def}}{=} \tilde{a}_1 - \bar{a}_1$  and  $\delta_q \stackrel{\text{def}}{=} \tilde{q} - \bar{q}$ . Hence, we can compute  $Y_0$  such that

$$\begin{aligned} \|A\psi(\bar{r})\|_\nu &\leq \|A\bar{\psi}(\bar{r})\|_\nu + \|A\|_{B(\ell_\nu^1)} \|\psi^\delta(\bar{r})\|_\nu \\ &\leq \|A\bar{\psi}(\bar{r})\|_\nu + \|A\|_{B(\ell_\nu^1)} \left( 2\|\bar{a}_1\|_\nu \|\bar{r}\|_\nu + \|\bar{r}\|_\nu r_0 + \frac{1}{\nu} \right) r_0 \leq Y_0, \end{aligned}$$

where we used that

$$\|\delta_q\|_\nu = \sum_{n \geq 0} |(\tilde{a}_2)_{n+1} - (\bar{a}_2)_{n+1}| \nu^n = \frac{1}{\nu} \sum_{n \geq 0} |(\tilde{a}_2)_{n+1} - (\bar{a}_2)_{n+1}| \nu^{n+1} \leq \frac{1}{\nu} \|\tilde{a}_2 - \bar{a}_2\|_\nu \leq \frac{r_0}{\nu}.$$

**The bound  $Z_0$ .** It is the same computation as the one presented in Section 3.2.

**The bound  $Z_1$ .** Given  $h \in \ell_\nu^1$ , denote

$$z \stackrel{\text{def}}{=} D\psi(\bar{r})h - A^\dagger h$$

which is given component wise by

$$z_n = \begin{cases} ((\tilde{a}_1^2 - \bar{a}_1^2)h)_n = (2\delta_1 \bar{a}_1 h + \delta_1^2 h)_n & \text{for } 0 \leq n \leq N, \\ (\tilde{a}_1^2 h)_n - (\bar{a}_1^2)_0 h_n = (2(\delta_1)_0 (\bar{a}_1)_0 + (\delta_1)_0^2) h_n + \sum_{k=1}^n (\tilde{a}_1^2)_k h_{n-k} & \text{for } n > N. \end{cases}$$

Define  $\beta_k = (\tilde{a}_1^2)_k$  for  $k > 0$  and  $\beta_0 = 0$ . Hence,

$$\begin{aligned} \|Az\|_\nu &\leq \|A\|_{B(\ell_\nu^1)} \|2\delta_1 \bar{a}_1 h + \delta_1^2 h\|_\nu + \frac{1}{(\bar{a}_1^2)_0} \sum_{n \geq N+1} |(\beta * h)_n| \nu^n \\ &\leq \|A\|_{B(\ell_\nu^1)} (2r_0 \|\bar{a}_1\|_\nu + r_0^2) + \frac{1}{(\bar{a}_1^2)_0} \|\beta\|_\nu, \end{aligned}$$

where

$$\|\beta\|_\nu = \sum_{n \geq 1} |(\tilde{a}_1^2)_n| \nu^n \leq \sum_{n=1}^{2N+2} |(\tilde{a}_1^2)_n| \nu^n + 2\|\bar{a}_1\|_\nu r_0 + r_0^2.$$

We therefore set

$$Z_1 \stackrel{\text{def}}{=} \|A\|_{B(\ell_\nu^1)} (2r_0 \|\bar{a}_1\|_\nu + r_0^2) + \frac{1}{(\bar{a}_1^2)_0} \left( \sum_{n=1}^{2N+2} |(\tilde{a}_1^2)_n| \nu^n + 2\|\bar{a}_1\|_\nu r_0 + r_0^2 \right).$$

Assume that using the radii polynomial approach of Theorem 3.5, we prove the existence  $\tilde{r} \in B_{r_{\min}}(\bar{r})$  such that  $\psi(\tilde{r}) = 0$ . Hence, given  $\theta \in (-\nu, \nu)$ ,  $t_{\max}$  given in (5.14) can be controlled

$$\begin{aligned} t_{\max} &= -\frac{1}{\lambda} \sum_{n \geq 0} \frac{\tilde{r}_n}{n+1} \theta^{n+1} \\ &\in -\frac{1}{\lambda} \sum_{n=0}^N \frac{\tilde{r}_n}{n+1} \theta^{n+1} + \frac{1}{|\lambda|} \sum_{n \geq 0} \frac{|\tilde{r}_n - \bar{r}_n|}{n+1} |\theta|^{n+1} [-1, 1] \\ &\in -\frac{1}{\lambda} \sum_{n=0}^N \frac{\tilde{r}_n}{n+1} \theta^{n+1} + \frac{r_{\min}}{|\lambda|} [-1, 1], \end{aligned}$$

which can be evaluated rigorously with interval arithmetic.

**Remark 5.4.** *The above estimate directly shows the analyticity of  $t_{\max}$  on  $\theta$ , which is implicitly guaranteed by analyticity of the parameterization  $P$  and the uniform boundedness of the denominator  $x_1(\eta) = P_1(u)$  away from 0 on  $W_{loc}^s(p_2)$ . See Figure 3 about the latter fact.*

## 5.2 Extension of the stable manifold of $p_2$ in (5.7) and blow-up time validations

Once we validate the local stable manifold of a saddle equilibrium, we can extend the manifold integrating (5.7) in the backward time direction, which is achieved by standard rigorous integrator of ODEs. Recall that we rewrite the system of differential equations (5.7) as in (5.8), that is

$$\dot{x} = g(x) = \begin{pmatrix} g_1(x_1, x_2) \\ g_2(x_1, x_2) \end{pmatrix} \stackrel{\text{def}}{=} \begin{pmatrix} x_1^3 - (\rho_1 + \rho_2)x_1^2 + \rho_1\rho_2x_1 - cx_1^3x_2 - c_1x_1^2x_2 \\ -\frac{1}{2}x_1^2x_2 + \frac{1}{2}\rho_1\rho_2x_2 + cx_1^2x_2^2 + c_2x_1^2x_2^3 \end{pmatrix},$$

where  $\cdot = \frac{d}{d\eta}$ ,  $x_2 \equiv s$ ,  $(\rho_1, \rho_2) = (1, 2)$ ,  $(\beta_R, v_R) = (1.5, 5)$ ,  $(\beta_L, v_L) = (1.9, 4)$  with the constant  $c$  in (5.2) and  $(c_1, c_2) = (c_{1L}, c_{2L})$  satisfying

$$\begin{cases} c_{1L} = v_L B_1(\beta_L) - c\beta_L, \\ c_{2L} = v_L^2 B_2(\beta_L) - cv_L. \end{cases}$$

We integrate (5.7) backward in time. Taking  $\xi \stackrel{\text{def}}{=} -\eta$ , we integrate

$$\begin{cases} \frac{dx_1}{d\xi} = -(x_1^3 - (\rho_1 + \rho_2)x_1^2 + \rho_1\rho_2x_1 - cx_1^3x_2 - c_1x_1^2x_2), \\ \frac{dx_2}{d\xi} = -\left(-\frac{1}{2}x_1^2x_2 + \frac{1}{2}\rho_1\rho_2x_2 + cx_1^2x_2^2 + c_2x_1^2x_2^3\right). \end{cases} \quad (5.16)$$

from 0 to  $\xi_0$  with the initial point  $(x_1(0), x_2(0)) = p_0 = P(\theta)|_{\theta=-1}$ , which is on the local stable manifold  $W_{loc}^s(p_2)$ . The rigorous integrator we have used is mentioned in Remark 4.1. Furthermore, we rigorously compute the passing time in the original time scale using the following formula:

$$t_{\xi_0} = \int_0^{\xi_0} \frac{x_2(\xi)}{x_1(\xi)^2} d\xi,$$

where  $x_1(\xi)$  and  $x_2(\xi)$  denote the solution of (5.16).

In the present example, (5.7) is integrated with the initial point at the boundary of locally validated stable manifold, which is the boundary of the red curve in Figure 3 with  $x_2 > 0$ , in the backward time direction and compute an enclosure of the evolution time in the original time-scale:

$$t_{-\eta} = \int_0^{-\eta} \frac{x_2(\tilde{\eta})}{x_1(\tilde{\eta})^2} d\tilde{\eta}.$$

The blow-up time of the corresponding blow-up solution with the initial point  $T_d^{-1}(x_1(\eta), x_2(\eta))$  is then enclosed by the sum of enclosures of  $t_{\max}$  and  $t_{-\eta}$ . Figure 5 draws the blow-up time  $t_{\max}$  of blow-up solutions as a function of initial points on  $T_d^{-1}(W^s(p_2))$ . Note that the point in the figure where the corresponding blow-up time tends to infinity is the source equilibrium for (5.7), which corresponds to the bounded source for (5.1). Rigorous enclosures of  $t_{\max}$  on several sample points are shown in Table 1. Finally, we can reconstruct the true blow-up profile of the validated saddle-type blow-up solution through the directional compactification  $T_d$ , which is drawn in Figure 6. Note that this profile cannot be computed in the direct way since small perturbations of initial points violate the profile<sup>18</sup>.

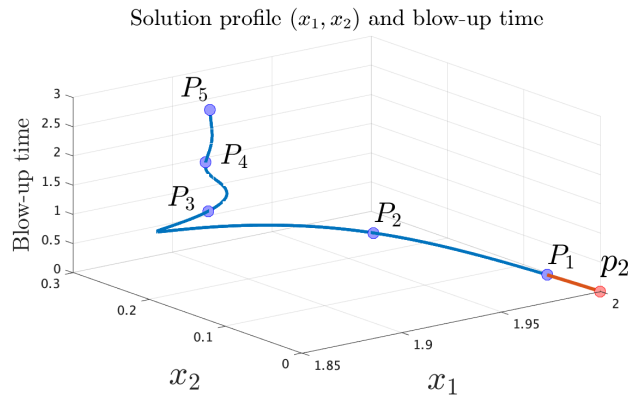


Figure 5: The extended stable manifold  $W^s(p_2)$  for (5.7) and corresponding blow-up times

The blue curve is the validated stable manifold  $W^s(p_2)$ . Numbers near points along the curve correspond to those shown in Table 1 where the rigorous enclosures of blow-up times are shown.

**Remark 5.5.** *The integrand of  $t_{\max}$  has a different form from typical integrands shown in Section 2. Indeed, the integrand of (5.12) is a rational function consisting of two analytic functions. Nevertheless, the function  $x_1(\eta)$  determining the denominator attains the value around 2 with sufficiently small error bounds so that the function  $1/x_1(\eta)^2$  is analytic at  $x_1(0)$ , which is justified through the parameterization  $P$ , provided the trajectory  $\{x_1(\eta), s(\eta)\}_{\eta \in [0, \infty)}$  is located on the interior of  $W_{loc}^s(p_2)$ . In particular, Proposition 4.5 and Theorem 4.6 can be still applied to showing*

<sup>18</sup>As far as we have calculated (in non-rigorous sense), solutions of (5.7) through points *near* validated solutions (in Figure 5) go to the direction so that the  $x_1$ -component goes to  $+\infty$  directly, or rounding the bounded source (near  $P_5$  in Figure 5).

Points (label)	$x_1$	$x_2$	Blow-up time
$P_1$	1.99704842870 $_{221}^{362}$	0.06209042154 $_{03}^{164}$	0.01945344745 $_{624}^{758}$
$P_2$	1.971379977171 $_{031}^{454}$	0.22265490227 $_{37387}^{46532}$	0.1821531459 $_{776968}^{806739}$
$P_3$	1.895702934910 $_{105}^{671}$	0.24142735005 $_{28752}^{30887}$	1.00170345745 $_{2293}^{7477}$
$P_4$	1.89771158641 $_{7872}^{819}$	0.250316449049 $_{6631}^{8725}$	1.78231786657 $_{067}^{7252}$
$P_5$	1.899856004192 $_{361}^{656}$	0.25017265254 $_{49681}^{51455}$	2.6651422937 $_{42664}^{50833}$

Table 1: Blow-up time enclosures for (5.1)

“Points (label)” correspond to points drawn in Figure 5. “Blow-up time” is the validated enclosure of blow-up time for (5.1) through the preimage of points under  $T_d$ .

that  $t_{\max}$  (5.12) depends analytically on initial data. Note that arguments in Section 5.1.3 directly confirm the analyticity of  $t_{\max}$ .

## 6 Example 2: application to higher-dimensional systems

The second example is the following (artificial) system in  $\mathbb{R}^3$ :

$$\begin{cases} y'_1 = y_1(y_1^2 - 1), \\ y'_2 = y_1^2 y_2 + y_1^2 y_3, \\ y'_3 = y_1^2 y_3 + \delta^{-1} \{c y_1^2 y_3 - y_2(y_2 - a y_1)(y_1 - y_2) + w y_1^3\}. \end{cases} \quad (6.1)$$

The present system is asymptotically homogeneous of order 3, namely asymptotically quasi-homogeneous of type  $\alpha = (1, 1, 1)$ . We thus apply the Poincaré-type compactification<sup>19</sup> to obtain the associated desingularized vector field as written by (2.12)-(2.14). In the present case,  $k = 2, n = 3, \alpha_j = \beta_j = c = 1$  for  $j = 1, \dots, n$  and hence

$$\begin{cases} \tilde{f}_1(x) = x_1^3 - \left(1 - \sum_{i=1}^3 x_i^2\right) x_1, \\ \tilde{f}_2(x) = x_1^2 x_2 + x_1^2 x_3, \\ \tilde{f}_3(x) = x_1^2 x_3 + \delta^{-1} \{c x_1^2 x_3 - x_2(x_2 - a x_1)(x_1 - x_2) + w x_1^3\}, \end{cases} \quad (6.2)$$

derived by (2.13), is applied to determining (2.12). The concrete form is

$$\begin{aligned} \dot{x}_1 &= g_1(x) \stackrel{\text{def}}{=} \tilde{f}_1(x) - x_1 G(x) \\ \dot{x}_2 &= g_2(x) \stackrel{\text{def}}{=} \tilde{f}_2(x) - x_2 G(x) \\ \dot{x}_3 &= g_3(x) \stackrel{\text{def}}{=} \tilde{f}_3(x) - x_3 G(x) \end{aligned} \quad (6.3)$$

<sup>19</sup>In the present demonstration, radicals in the Poincaré-type compactification do not prevent us from  $C^1$  studies of dynamical systems. In particular, the linear stability analysis of equilibria on the horizon makes sense. Indeed, the lower-order terms in (6.1) are chosen so that our methodology properly works, following discussions in [45].

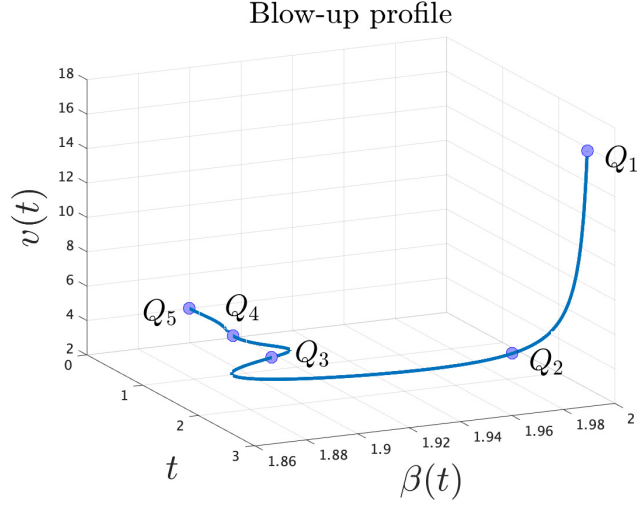


Figure 6: Blow-up profile corresponding to Figure 5

Each point  $Q_i$  ( $i = 1, \dots, 5$ ) corresponds to the preimage of  $P_i$  in Figure 5 under the directional compactification  $(x_1, x_2) = (\beta, v^{-1})$ . The initial time  $t = 0$  is set so that  $Q_5 = (\beta(0), v(0))$ .

where

$$\begin{aligned}
G(x) &\stackrel{\text{def}}{=} \sum_{j=1}^3 x_j \tilde{f}_j(x) \\
&= x_1 \left\{ x_1^3 - \left( 1 - \sum_{i=1}^3 x_i^2 \right) x_1 \right\} + x_2 \{ x_1^2 x_2 + x_1^2 x_3 \} \\
&\quad + x_3 [ x_1^2 x_3 + \delta^{-1} \{ c x_1^2 x_3 - x_2 (x_2 - a x_1) (x_1 - x_2) + w x_1^3 \} ] \\
&= x_1^2 \{ -1 + 2x_1^2 + x_1 x_2 + 2x_2^2 + \delta^{-1} w x_1 x_3 + (2 + \delta^{-1} c) x_3^2 \} - \delta^{-1} x_2 x_3 (x_2 - a x_1) (x_1 - x_2).
\end{aligned}$$

The direct calculation of the Jacobian matrix of (6.3) is quite lengthy. Assuming that the Jacobian matrix of  $\tilde{f}$  with respect to  $x$  is calculated, the Jacobian matrix of  $g$  with respect to  $x$  is calculated as follows:

$$\frac{\partial g_i}{\partial x_j} = \frac{\partial \tilde{f}_i}{\partial x_j} - \delta_{ij} \left( \sum_{k=1}^3 x_k \tilde{f}_k(x) \right) - x_i \sum_{k=1}^3 \left\{ \delta_{jk} \tilde{f}_k(x) + x_k \frac{\partial \tilde{f}_k}{\partial x_j} \right\},$$

where  $\delta_{ij}$  is the Kronecker's delta. In the present case, the Jacobian matrix of  $\tilde{f}$  is

$$J\tilde{f} = \begin{pmatrix} 3x_1^2 - \left(1 - \sum_{i=1}^3 x_i^2\right) + 2x_1^2 & 2x_1x_2 & 2x_1x_3 \\ 2x_1(x_2 + x_3) & x_1^2 & x_1^2 \\ \tilde{f}_{31} & \tilde{f}_{32} & \tilde{f}_{33} \end{pmatrix},$$

$$\begin{aligned} \tilde{f}_{31} &= 2x_1x_3 + \delta^{-1} \{2cx_1x_3 + ax_2(x_1 - x_2) - x_2(x_2 - ax_1) + 3wx_1^2\}, \\ \tilde{f}_{32} &= \delta^{-1} \{-(x_2 - ax_1)(x_1 - x_2) - x_2(x_1 - x_2) + x_2(x_2 - ax_1)\}, \\ \tilde{f}_{33} &= (1 + \delta^{-1}c)x_1^2. \end{aligned}$$

We observe that there are (at least) three equilibria on the horizon  $\{p(x)^2 \equiv \sum_{i=1}^3 x_i^2 = 1\}$ , one of which, denoted by  $p_0$ , has a one-dimensional stable manifold and two of which, denoted by  $p_1$  and  $p_2$ , have two-dimensional stable manifolds. In the present study we fix the following parameters:

$$(a, c, \delta, w) = (0.3, 0.7, 9.0, 0.02).$$

We have computed the concrete position and associated eigenvalues, which are approximately given as follows:

$$\begin{aligned} p_0 &\approx (0.9333789, 0.3588924, 0), \\ \lambda_1(p_0) &\approx -1.74239248, \quad \lambda_2(p_0) \approx 0.033880 + 0.1430256i, \quad \lambda_3(p_0) = \overline{\lambda_2(p_0)}, \\ p_1 &\approx (0.7180928, 0.6959473, 0), \\ \lambda_1(p_1) &\approx -0.11437086, \quad \lambda_2(p_1) = 0.1544775, \quad \lambda_3(p_1) \approx -1.0313145, \\ p_2 &\approx (0.9985628, -0.0535924, 0), \\ \lambda_1(p_2) &\approx -1.994255, \quad \lambda_2(p_2) \approx -0.1870901, \quad \lambda_3(p_2) \approx 0.26464449. \end{aligned}$$

On the other hand, (6.2) possesses a source in a bounded region, namely  $\{\sum_{i=1}^3 x_i^2 < 1\}$ , which is

$$p_b \approx (0.7071051816183367, 0.001504037399468, -0.001504037399468).$$

The parameterization method applied to three equilibria on the horizon;  $p_0$ ,  $p_1$  and  $p_2$ , for (6.3) provides local stable manifolds with rigorous error enclosures. Distributions of these local stable manifolds are drawn in Figure 9.

## 6.1 Blow-up time computation

Since the compactification is homogeneous (namely  $\alpha = (1, \dots, 1)$  for defining compactifications) and  $k = 2$  in the present example, the maximal existence time  $t_{\max}$  is

$$t_{\max} = \int_0^\infty \kappa(x(\tau))^{-k} d\tau = \int_0^\infty (1 - \|x\|^2) d\tau, \quad (6.4)$$

according to (4.4). Let  $P$  be a parameterization around  $x_* \in \mathcal{E}$  whose image of  $B^{n_s}$  determines the local stable manifold  $W_{loc}^s(x_*)$  of  $x_*$  such that  $P(0) = x_*$ .  $P$  is assumed to have a polynomial



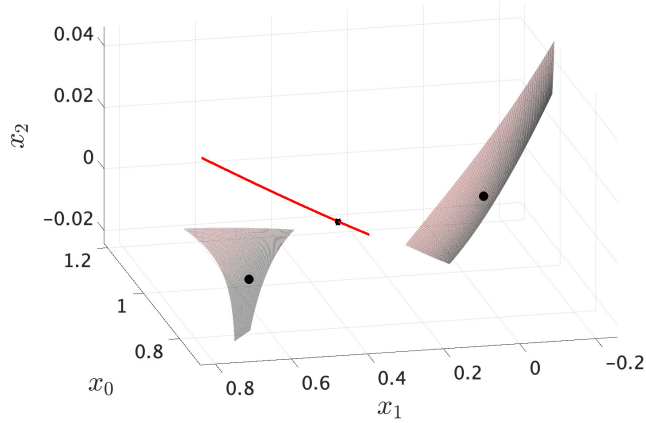


Figure 7: The rigorously computed local stable manifolds for hyperbolic equilibria for (6.3). The  $C^0$  rigorous error bound for the manifold around  $p_1$  (left) is  $\|P - P^{(N)}\|_\infty \leq r = 8.2 \times 10^{-9}$  with  $N = 50$ , while it is  $\|P - P^{(N)}\|_\infty \leq r = 9.8 \times 10^{-10}$  with  $N = 60$  for the manifold around  $p_2$  (right) and  $\|P - P^{(N)}\|_\infty \leq r = 9.8 \times 10^{-13}$  with  $N = 160$  for the manifold around  $p_0$  (center). The black dots are equilibria on the horizon; denoting  $p_1$ ,  $p_0$  and  $p_2$  from the left to the right.

expression (cf. (4.7))

$$P(\theta) = \sum_{|\alpha| \geq 0} a_\alpha \theta^\alpha, \quad \theta = \begin{pmatrix} \theta_1 \\ \vdots \\ \theta_{n_s} \end{pmatrix} \in \mathbb{R}^{n_s}, \quad a_\alpha = \begin{pmatrix} (a_1)_\alpha \\ \vdots \\ (a_n)_\alpha \end{pmatrix} \in \mathbb{R}^n$$

satisfying  $a_0 = x_*$ .  $\alpha = (\alpha_1, \dots, \alpha_{n_s}) \in \mathbb{Z}_{\geq 0}^{n_s}$  denotes the multi-index and  $\theta^\alpha = \theta_1^{\alpha_1} \dots \theta_{n_s}^{\alpha_{n_s}}$ . Assuming that the solution trajectory  $x(\tau)$  is on  $W_{loc}^s(x_*)$ , the parameterization argument indicates that

$$x(\tau) = P(Q^{-1}e^{\Lambda\tau}Q\theta_0), \quad \Lambda = \text{diag}(\lambda_1, \dots, \lambda_{n_s}) \quad \text{with} \quad \text{Re } \lambda_i < 0.$$

For a while, we further assume that  $Q = I$ ,  $\lambda_i \in \mathbb{R}$  for  $i = 1, \dots, n_s$  and  $k = 2$ . Then

$$P(\theta) = \sum_{|\alpha| \geq 0} a_\alpha \theta(\tau)^\alpha, \quad \theta(\tau) = \begin{pmatrix} e^{\lambda_1 \tau} (\theta_1)_0 \\ \vdots \\ e^{\lambda_{n_s} \tau} (\theta_{n_s})_0 \end{pmatrix}, \quad \theta_0 = \begin{pmatrix} (\theta_1)_0 \\ \vdots \\ (\theta_{n_s})_0 \end{pmatrix}, \quad a_\alpha \equiv ((a_1)_\alpha, \dots, (a_n)_\alpha) \in \mathbb{R}^n$$

and

$$\begin{aligned}
t_{\max} &= \int_0^\infty \left\{ 1 - \sum_{i=1}^n \left( \sum_{|\alpha| \geq 0} (a_i)_\alpha \theta(\tau)^\alpha \right)^2 \right\} d\tau \\
&= \int_0^\infty \left\{ 1 - \sum_{i=1}^n \left( \sum_{|\beta| \geq 0} \sum_{|\gamma| \geq 0} (a_i)_\beta (a_i)_\gamma e^{(\sum_{j=1}^m (\beta_j + \gamma_j) \lambda_j) \tau} \theta_0^{\beta + \gamma} \right) \right\} d\tau \\
&= \int_0^\infty \left\{ 1 - \sum_{i=1}^n \sum_{|\alpha| \geq 0} (a_i * a_i)_\alpha e^{(\alpha \cdot \lambda) \tau} \theta_0^\alpha \right\} d\tau,
\end{aligned}$$

where  $(a * b)_\alpha$  denotes the discrete convolution over the multi-index  $\alpha \in \mathbb{Z}_{\geq 0}^{n_s}$  given in (4.8) and  $\theta_0^\alpha = ((\theta_1)_0)^{\alpha_1} \dots ((\theta_{n_s})_0)^{\alpha_{n_s}}$ . Here we use the fact

$$\sum_{i=1}^n \sum_{|\alpha| \geq 0} (a_i * a_i)_\alpha e^{(\alpha \cdot \lambda) \tau} \theta_0^\alpha = \sum_{i=1}^n ((a_i)_0)^2 = \|x_*\|^2 = 1$$

since  $P(0) = x_*$  and  $x_* \in \mathcal{E} = \{\|x\| = 1\}$  as mentioned in Remark 4.3. Thus we have

$$\begin{aligned}
\int_0^\infty \left\{ 1 - \sum_{i=1}^n \sum_{|\alpha| \geq 0} (a_i * a_i)_\alpha e^{(\alpha \cdot \lambda) \tau} \theta_0^\alpha \right\} d\tau &= - \int_0^\infty \sum_{|\alpha| > 0} \sum_{i=1}^n (a_i * a_i)_\alpha e^{(\alpha \cdot \lambda) \tau} \theta_0^\alpha d\tau \\
&= - \sum_{|\alpha| > 0} \left( \sum_{i=1}^n (a_i * a_i)_\alpha \right) \frac{\theta_0^\alpha}{\alpha \cdot \lambda},
\end{aligned}$$

where the denominator is strictly negative for all possible  $\alpha$  and the analyticity of  $P$  ensures the convergence of the above series. Finally, we have the following expression of  $t_{\max}$ :

$$t_{\max} = - \sum_{|\alpha| > 0} \left( \sum_{i=1}^n (a_i * a_i)_\alpha \right) \frac{\theta_0^\alpha}{\alpha \cdot \lambda}. \quad (6.5)$$

Remark that the above expression makes sense only if

$$\|P(\theta_0)\|^2 = \sum_{i=1}^n \left( \sum_{|\alpha| \geq 0} (a_i)_\alpha \theta(\tau)^\alpha \right)^2 = 1 + \sum_{|\alpha| > 0} \left( \sum_{i=1}^n (a_i * a_i)_\alpha \right) \theta(\tau)^\alpha < 1$$

by definition of the Poincaré compactification. With an explicit expression or enclosure of  $P(\theta)$ , the quantity (6.5) or its enclosure is rigorously calculated for each  $\theta_0 \in B^{n_s}$ . The above procedure is applied with  $n = 3$  and  $n_s = 1$  or  $2$  in the present problem.

If  $n_s = 1$ , the expression (6.5) can be simplified by considering the single index  $l \geq 1$  instead of the multi-index  $\alpha$  to obtain

$$t_{\max} = -\frac{1}{\lambda} \sum_{l \geq 1} \left\{ \sum_{i=1}^n (a_i * a_i)_l \right\} \frac{\theta_0^l}{l}.$$

In practice the computation of the Taylor coefficients  $a_1, \dots, a_n$  comes from a successful application of the Newton-Kantorovich type theorem (Theorem 3.5) applied to  $F : X \rightarrow X'$  given in (3.9). More precisely, denote by  $\bar{a}_1, \dots, \bar{a}_n$  the numerical approximations (of order  $N$ ) and  $r_0 > 0$  such that the true coefficients satisfy

$$\|a - \bar{a}\|_X = \max_{j=1, \dots, n} \|a_j - \bar{a}_j\|_1 \leq r_0.$$

Denote  $b = a - \bar{a}$  and note that

$$\begin{aligned} t_{\max} &= - \sum_{|\alpha| > 0} \left( \sum_{i=1}^n (a_i * a_i)_\alpha \right) \frac{\theta_0^\alpha}{\alpha \cdot \lambda} \\ &= - \sum_{|\alpha|=0}^{2N} \left( \sum_{i=1}^n (\bar{a}_i * \bar{a}_i)_\alpha \right) \frac{\theta_0^\alpha}{\alpha \cdot \lambda} - 2 \sum_{|\alpha| > 0} \left( \sum_{i=1}^n (\bar{a}_i * b_i)_\alpha \right) \frac{\theta_0^\alpha}{\alpha \cdot \lambda} \\ &\quad - \sum_{|\alpha| > 0} \left( \sum_{i=1}^n (b_i * b_i)_\alpha \right) \frac{\theta_0^\alpha}{\alpha \cdot \lambda}. \end{aligned}$$

Denote, the spectral gap of the stable eigenvalues by

$$\sigma_{\text{gap}} \stackrel{\text{def}}{=} \min_{j=1, \dots, n_s} |\lambda_j| > 0$$

and note that  $\sigma_{\text{gap}} = \min_{|\alpha| > 0} |\alpha \cdot \lambda|$ . Hence, for all  $\theta_0 \in B_1^{n_s}$ ,

$$\begin{aligned} \left| 2 \sum_{|\alpha| > 0} \left( \sum_{i=1}^n (\bar{a}_i * b_i)_\alpha \right) \frac{\theta_0^\alpha}{\alpha \cdot \lambda} \right| &= \left| 2 \sum_{i=1}^n \left( \sum_{|\alpha| > 0} (\bar{a}_i * b_i)_\alpha \frac{\theta_0^\alpha}{\alpha \cdot \lambda} \right) \right| \\ &\leq \frac{2}{\sigma_{\text{gap}}} \sum_{i=1}^n \sum_{|\alpha| > 0} |(\bar{a}_i * b_i)_\alpha| \\ &= \frac{2}{\sigma_{\text{gap}}} \sum_{i=1}^n \|\bar{a}_i * b_i\|_1 \\ &\leq \left( \frac{2}{\sigma_{\text{gap}}} \sum_{i=1}^n \|\bar{a}_i\|_1 \right) r_0. \end{aligned}$$

Similarly, we can show that

$$\left| - \sum_{|\alpha| > 0} \left( \sum_{i=1}^n (b_i * b_i)_\alpha \right) \frac{\theta_0^\alpha}{\alpha \cdot \lambda} \right| \leq \frac{nr_0^2}{\sigma_{\text{gap}}}.$$

Denoting

$$\tilde{\delta} \stackrel{\text{def}}{=} \left( \frac{2}{\sigma_{\text{gap}}} \sum_{i=1}^n \|\bar{a}_i\|_1 \right) r_0 + \frac{nr_0^2}{\sigma_{\text{gap}}},$$

then a rigorous enclosure of  $t_{\max}$  is given by the computable formula

$$t_{\max} \in - \sum_{|\alpha|=0}^{2N} \left( \sum_{i=1}^n (\bar{a}_i * \bar{a}_i)_\alpha \right) \frac{\theta_0^\alpha}{\alpha \cdot \lambda} + [-\tilde{\delta}, \tilde{\delta}].$$

## 6.2 Distribution of $t_{\max}$ near blow-up

In the present example, saddle equilibria  $p_1$  and  $p_2$  on the horizon both have 2-dimensional stable manifolds. Once the parameterization method is applied to validating these invariant manifolds, the blow-up time  $t_{\max}$  defined by (6.4) is obtained as a function of the parameter  $\theta$  determining local stable manifolds. In particular, we can validate distributions of  $t_{\max}$  on local stable manifolds.

Figure 8 draws the distributions of  $t_{\max}$ . Since the vector field (6.3) itself can be defined outside  $\bar{D}$ , namely in  $\{\|x\| > 1\}$  also,  $t_{\max}$  can attain negative values. Nevertheless, from the viewpoint that (6.3) is obtained from (6.1) through the compactification, only the positive values make sense as the blow-up time of solutions to (6.1). Now we pay attention to the following facts, which follow from fundamental arguments of compactifications (cf. [45]):

- The horizon  $\mathcal{E}$  is a codimension one invariant submanifold of  $\mathbb{R}^3$ .
- The integrand determining  $t_{\max}$  (e.g. (6.4)) is identically zero on  $\mathcal{E}$ .

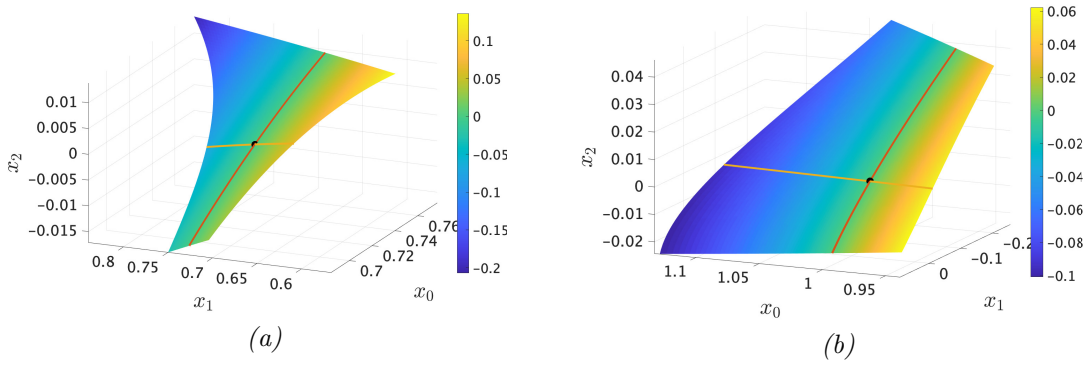


Figure 8: Distribution of  $t_{\max}$  in (6.4). (a) Distribution of  $t_{\max}$  around  $p_1$ . (b) Distribution of  $t_{\max}$  around  $p_2$ . Surfaces are validated local stable manifolds of equilibria (black dots). Only positive values of  $t_{\max}$  make sense as blow-up times of blow-up solutions for (6.1). In both figures, yellow curves and red curves denote  $P(\{\theta_2 = 0\})$  and  $P(\{\theta_1 = 0\})$ , respectively. The red curves are located in the horizon  $\mathcal{E}$ . According to eigendirections at equilibria, asymptotic behavior of trajectories on these manifolds are essentially governed by dynamics on  $P(\{\theta_1 = 0\})$ . On the other hand, dynamics in the directions do little contributions to  $t_{\max}$ .

Results in Figure 8 indeed reflect the above nature. For example, one-dimensional submanifold of two-dimensional stable manifolds of  $p_1$  and  $p_2$  are located on the horizon where  $t_{\max}$  is identically zero. Our computations further indicate that the region  $\{t_{\max} > 0\}$  is included in  $\{\|x\| < 1\}$ . Looking at the region  $\{t_{\max} > 0\}$ , like the previous example in Figure 4, we can discuss the distribution of blow-up times.

From our present observations, we have an interesting result about the distribution of blow-up times. In the present example, eigenvalues determining stable submanifolds on the horizon have smaller moduli than the transverse direction. In other words, *the leading (stable) eigendirections are directed tangent to the horizon (red curves in Figure 8) in both manifolds*. Asymptotic behavior of trajectories around equilibria is therefore essentially determined by the exponential decay behavior in the direction parallel to the horizon. On the other hand, level sets of  $t_{\max}$  are distributed so that

they are foliated parallel to the horizon, equivalently the level set  $t_{\max} = 0$ , in both cases. These observations may look strange from the viewpoint of the asymptotic behavior around (hyperbolic) equilibria. Indeed, dynamics around hyperbolic equilibria of interest are essentially governed by leading eigendirection, implying that the behavior along the leading eigendirection should mainly contribute to estimate  $t_{\max}$ . However, the integrand in (6.4) is almost zero near the horizon. More precisely, according to the proof of the blow-up criterion theorem (Theorem 2.12 whose proof is found in [45]), the integrand as a function of  $\tau$  decays exponentially fast near the horizon<sup>20</sup>. Therefore asymptotic behavior of solution trajectories near the horizon does little contributions to  $t_{\max}$ . As a consequence, *blow-up time is essentially foliated parallel to the horizon, no matter where the leading eigendirection is distributed*. This is a reason why the level set of  $t_{\max}$  is distributed parallel to the horizon.

### 6.3 Extension of blow-up trajectories

As demonstrated in Section 5, we can extend local stable manifolds globally by rigorous integration of (6.3) in backward time direction. In the present case, we have a (bounded) source equilibrium  $p_b$  and we have succeeded in validating connecting orbits between three equilibria on the horizon and  $p_b$ . The validated *global* stable manifolds are drawn in Figure 9. These stable manifolds separate the asymptotic behavior of solution trajectories outside the manifolds, although we omit the detailed description of phase portraits since it is hard to clearly visualize.

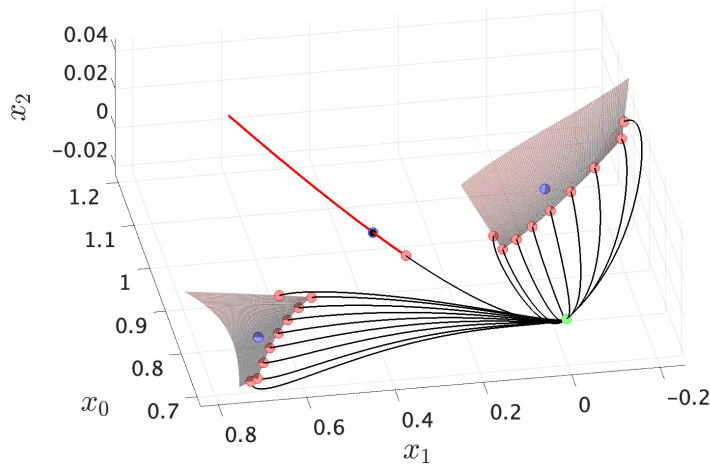


Figure 9: The rigorously computed trajectories on global stable manifolds for hyperbolic equilibria for (6.3). Local stable manifolds colored by pink and red are validated by the parameterization method, Figure 7. The green dot denotes the (bounded) source equilibrium  $p_b$ .

<sup>20</sup>Hyperbolicity of equilibria is used for the proof, implying that the dynamical property of equilibria, and potentially general invariant sets, plays a key role in determining the distribution of  $t_{\max}$  around 0.

## 7 Example 3: blow-up separatrix

The final example is

$$\begin{cases} u' = u^2 - v, \\ v' = \frac{1}{3}u^3 - u. \end{cases} \quad (7.1)$$

The present vector field originally comes from the Keyfitz-Kranser model [40] demonstrating a non-trivial example of system of conservation laws including *singular shock waves*. See [40] or references therein for details. A brief introduction of the model is also shown in [49]. Our purpose here is to validate blow-up solutions for (7.1) as well as bounded heteroclinic connections among bounded equilibria towards the global phase portrait. The present study unravels a significant characteristic of saddle-type blow-up solutions, which shall be called a *blow-up separatrix*.

Firstly, a direct calculation yields the following.

**Lemma 7.1.** *The vector field (7.1) is asymptotically quasi-homogeneous of type (1, 2) and order 2.*

Note that (7.1) is *not quasi-homogeneous*. On the other hand, the system (7.1) possesses the symmetry

$$(t, u, v) \mapsto (-t, -u, v). \quad (7.2)$$

Namely, if  $(u(t), v(t))$  is a solution to (7.1), then so is  $(-u(-t), v(-t))$ . This property is used to understand the global phase portrait of (7.1) including infinity.

To study the dynamics at infinity, we introduce the quasi-parabolic compactification of type (1, 2) given by

$$u = \frac{x_1}{1 - p(x)^4}, \quad v = \frac{x_2}{(1 - p(x)^4)^2}, \quad p(x)^4 = x_1^4 + x_2^2.$$

Then the corresponding desingularized vector field  $g$  is given by the following:

$$\begin{cases} \dot{x}_1 = g_1(x) \stackrel{\text{def}}{=} (x_1^2 - x_2)H_1(x) - x_1H_2(x) \\ \dot{x}_2 = g_2(x) \stackrel{\text{def}}{=} \left\{ \frac{1}{3}x_1^3 - (1 - p(x)^4)^2x_1 \right\} H_1(x) - 2x_2H_2(x), \end{cases} \quad (7.3)$$

where  $\dot{\phantom{x}} = \frac{d}{d\tau}$  and

$$H_1(x) = \frac{1}{4} \{1 + 3p(x)^4\}, \quad H_2(x) = x_1^3(x_1^2 - x_2) + \frac{x_2}{2} \left\{ \frac{1}{3}x_1^3 - (1 - p(x)^4)^2x_1 \right\}.$$

Fortunately, we know that *all equilibria (including the origin) are hyperbolic* and hence we do not need additional desingularization. Detailed information of our targeting equilibria are the following:

- The origin  $p_0 = (x_1, x_2) = (0, 0)$ , which is **saddle**.
- A bounded equilibrium  $p_b^+ = (x_1, x_2) \approx (0.7328506362011802, 0.5370700549804747)$ , which is **source**.
- A bounded equilibrium  $p_b^- = (x_1, x_2) \approx (-0.7328506362011802, 0.5370700549804747)$ , which is **sink**.

- Equilibrium on the horizon  $p_{\infty,s}^{\pm} = (x_1, x_2) \approx (\pm 0.8861081289780320, 0.6192579489210105)$ , which are **saddle**.
- Equilibria on the horizon  $p_{\infty}^{\pm} = (x_1, x_2) \approx (\pm 0.989136995894977, 0.206758557005180)$ . The point  $p_{\infty}^+$  is **sink**, while  $p_{\infty}^-$  is **source**.

A sample numerical computation indicate that there is a chain of global trajectories connecting  $p_0$  and  $p_b$ , and  $p_b$  and  $p_{\infty,s}$ , respectively. The numerically computed global phase portrait including infinity is shown in Figure 10. The figure indicates that the whole phase space is separated into two subdomains by a heteroclinic chain among equilibria, including those on the horizon.

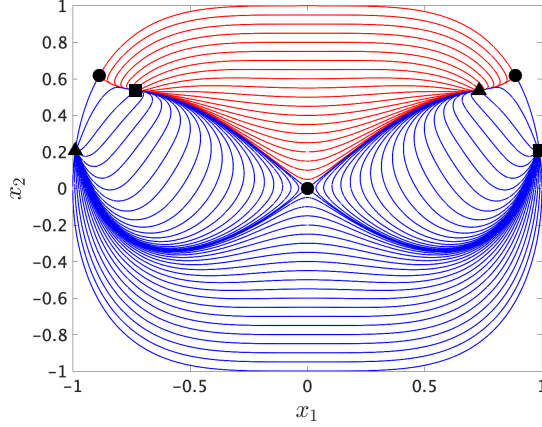


Figure 10: A global phase portrait of (7.3) through rough numerical simulations. Black squares, circles and triangles denote sink, saddle and source equilibria, respectively. Note that all objects here are obtained by (non-rigorous) numerical integration of (7.3). The flow direction is partially shown in Figure 14 below. The boundary of the collection of curves (quasi-sphere-like shape) is the horizon  $\mathcal{E}$ . All trajectories through points on the red region correspond to time-global solutions for (7.1), while those through points on the blue region correspond to blow-up solutions for (7.1) in either positive or negative time direction. These two regions are separated by the chain of connecting orbits, some of which correspond to saddle-type blow-up solutions.

**Remark 7.2.** Here we have chosen the parabolic-type compactification in the present argument for the following reasons. First, our objective here is the global phase portrait for (7.1), which is insufficient to study only one local chart, namely directional compactifications. The change of coordinates by numerics (both in rigorous and non-rigorous sense) requires unnecessary and difficult tasks. Second, Poincaré-type compactifications are inappropriate to study (7.1) including dynamics at infinity, since (7.1) is asymptotically quasi-homogeneous only in the asymptotic sense, and the application to Poincaré-type compactifications to such a system cause the loss of regularity of the desingularized vector field at infinity, as mentioned in Remark 2.8.

One of our main goals here is to construct the chain, mainly connecting orbits among  $\{p_{\infty,s}^+, p_b^+, p_0\}$ . Like in the previous examples, the local stable manifold  $W_{loc}^s(p_{\infty,s}^+)$  of the saddle  $p_{\infty,s}^+$  on the horizon can be validated by the parameterization method. Validated local stable manifolds of  $p_{\infty,s}^+$  as

well as  $p_0$  are shown in Figure 11. These are validated through the parameterization method in the same way as Sections 5 and 6. We omit the detailed implementation of the method applied to the present problem since the basic idea is identical, while we need lengthy calculations of terms we should enclose.

We then extend the manifold inside  $\mathcal{D} \equiv \{p(x) < 1\}$  by the rigorous integration of (7.3). According to numerical simulations (Figure 10),  $W^s(p_{\infty,s}^+)$  is connected to the source  $p_b^+$ . Since  $p_b^+$  is a source equilibrium, rigorous integration of (7.3) in backward time direction provide the computer-assisted validation of the connecting orbit from  $p_{\infty,s}^+$  to  $p_b^+$  in a standard way using the techniques introduced in e.g. [48]. In particular, a *time-global* trajectory connecting equilibria can be validated. On the other hand, we have another bounded equilibrium; the origin  $p_0$ . Eigenvalue validation indicates that  $p_0$  is a saddle, and the global trajectory connecting the source  $p_b^+$  and the origin  $p_0$  is also validated by extending the local stable manifold  $W_{loc}^s(p_0)$  of  $p_0$  via the parameterization and the rigorous integration of (7.3) in backward time direction. By symmetry, we obtain the chain of connecting orbits among the points  $\{p_{\infty,s}^\pm, p_b^\pm, p_0\}$ . Note that all these points are validated with rigorous errors through the parameterization method. Also note that the connecting orbit between  $p_{\infty,s}^\pm$  exists through the fact that the horizon  $\mathcal{E}$  is invariant and there are no equilibria between them (cf. [45]).

As a consequence, an invariant closed curve consisting of connecting orbits among equilibria  $\{p_{\infty,s}^\pm, p_b^\pm, p_0\}$  is constructed, as indicated in Figure 10, with computer-assisted proof. The well-known Jordan's Closed Curve Theorem indicates that the invariant closed curve decomposes the phase space  $\overline{\mathcal{D}}$  into two regions. In the sequel we study the nature of solutions through points on these separated regions from the viewpoint of blow-up behavior.

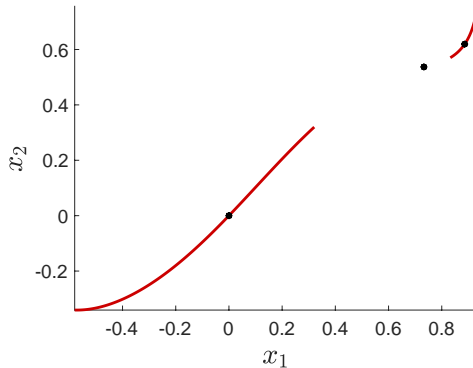


Figure 11: Local stable manifolds  $W_{loc}^s(p_{\infty,s}^+)$  and  $W_{loc}^s(p_0)$  for (7.3). Black dots are equilibria  $p_0, p_b^+$  and  $p_{\infty,s}^+$  from the left, respectively. Red curves are validated local stable manifolds with rigorous error bounds  $\|P - P^{(N)}\|_\infty \leq r = 5.171 \times 10^{-14}$  for  $p_0$  and  $\|P - P^{(N)}\|_\infty \leq r = 1.381 \times 10^{-10}$  for  $p_{\infty,s}^+$ , respectively. In both validations, the approximation order  $N$  is chosen as  $N = 100$ . Since  $p_b^+$  is source, it does not admit a non-trivial stable manifold.



## 7.1 Blow-up time computation

The maximal existence time of the solution  $(y_1(t), y_2(t))$  for the original vector field is given as follows (see (4.5) and [48]):

$$t_{\max} = \int_0^\infty \frac{1}{4} \{1 + 3(x_1(\tau)^4 + x_2(\tau)^2)\} (1 - x_1(\tau)^4 - x_2(\tau)^2) d\tau.$$

Let  $x_* = (x_{*,1}, x_{*,2}) \in \mathcal{E}$  be a saddle equilibrium. Note that  $x_{*,1}^4 + x_{*,2}^2 = 1$  by definition of the present parabolic-type compactification.

As in the previous case, let  $P$  be a parameterization whose image of  $B^{n_s}$  determines the local stable manifold of  $x_*$  such that  $P(0) = x_*$ .  $P$  is assumed to have a power series expression (4.7) satisfying  $a_0 = x_*$ .

Assume that the trajectory  $\{(x_1(\tau), x_2(\tau))\}$  is included in  $W^s(x_*)$  for the desingularized vector field.

In the present case,  $n = 2$ , and we consider only the case  $n_s = 1$ . Calculations below are slightly simplified by introducing  $u = e^{\lambda\tau}\theta_0$ , where  $\lambda$  be the stable eigenvalue at  $x_*$ . Indeed, we have

$$x(\tau) = P(e^{\lambda\tau}\theta_0) = P(u) = \sum_{j \geq 0} a_j u^j \in \mathbb{R}^2, \quad u \in \mathbb{R}, \quad a_j \equiv ((a_1)_j, (a_2)_j)^T \in \mathbb{R}^2.$$

Letting  $a_i = \{(a_i)_j\}_{j \geq 0}$  for  $i = 1, 2$ , we have

$$\begin{aligned} t_{\max} &= \int_{\theta_0}^0 \frac{1}{4} (1 + 3(P_1^4(u) + P_2^2(u))) (1 - P_1^4(u) - P_2^2(u)) \frac{du}{\lambda u} \\ &= - \int_0^{\theta_0} \frac{1}{4} \left( 1 + 3 \sum_{j \geq 0} ((a_1^4)_j + (a_2^2)_j) u^j \right) \left( 1 - \sum_{j \geq 0} ((a_1^4)_j + (a_2^2)_j) u^j \right) \frac{du}{\lambda u}. \end{aligned}$$

Using that

$$P_1^4(u) + P_2^2(u) = \sum_{j \geq 0} ((a_1^4)_j + (a_2^2)_j) u^j = 1 + \sum_{j \geq 1} ((a_1^4)_j + (a_2^2)_j) u^j,$$

we have the following exact formula for  $t_{\max}$ :

$$\begin{aligned} t_{\max} &= \int_0^{\theta_0} \left( 1 + \frac{3}{4} \sum_{j \geq 1} ((a_1^4)_j + (a_2^2)_j) u^j \right) \left( \sum_{j \geq 1} ((a_1^4)_j + (a_2^2)_j) u^j \right) \frac{du}{\lambda u} \\ &= \int_0^{\theta_0} \left( \sum_{j \geq 1} ((a_1^4)_j + (a_2^2)_j) u^{j-1} + \frac{3}{4} \sum_{j \geq 2} ((a_2^4)_j + 2(a_1^4 * a_2^2)_j + (a_1^8)_j) u^{j-1} \right) \frac{du}{\lambda} \\ &= \frac{1}{\lambda} \left( \sum_{j \geq 1} ((a_1^4)_j + (a_2^2)_j) \frac{\theta_0^j}{j} + \frac{3}{4} \sum_{j \geq 2} ((a_2^4)_j + 2(a_1^4 * a_2^2)_j + (a_1^8)_j) \frac{\theta_0^j}{j} \right). \end{aligned} \quad (7.4)$$

## 7.2 Blow-up separatrix

In what follows, we discuss a characteristic nature of systems involving saddle-type blow-up solutions. From Figure 10, we numerically observe that the compactified phase space is separated into two domains, one of which consists of points whose trajectories tend to the origin as  $\tau \rightarrow \pm\infty$ , while another consists of points whose trajectories tend to equilibria on the horizon as either  $\tau \rightarrow -\infty$  or  $\tau \rightarrow +\infty$ . Namely, the latter set corresponds to the collection of initial points whose solution trajectories blow up in finite times in the original coordinate. A significant importance of this observation is that these two domains are divided by a sequence of solution trajectories *including blow-up solutions*, the invariant curve validated in the beginning of the present section. We shall denote the invariant curve  $C_{sep}$ , which is illustrated in Figure 14 below. In particular, saddle-type blow-up solutions themselves or bounded time-global trajectories connecting blow-up solutions can locally divide initial points into the above two classes. We shall call the invariant curve *including trajectories corresponding to blow-up solutions* separating the whole domain a **blow-up separatrix**. Since blow-up solutions generated by sink equilibria on the horizon are stable under perturbations of initial points<sup>21</sup>, the saddle structure of equilibria, possibly also general hyperbolic invariant sets, on the horizon plays a key role in the above nature.

The above separation of initial points indicates that blow-up times are *not* continuous with respect to initial data. In particular, the saddle-type blow-up solutions can violate the continuous dependence of the maximal existence time of solutions on initial data. Our next study here is the more precise investigation of continuous dependence of the maximal existence time on initial data. To state our problem more concretely, consider a line segment  $\ell$  which is transverse to the blow-up separatrix  $C_{sep}$ . See Figure 12. In the present case, the segment  $\ell$  is chosen so that  $C_{sep}$  and  $\ell$  are orthogonal to each other at the boundary  $p_{0,s}$  of  $W_{loc}^s(p_{\infty,s}^+)$  validated by the parameterization method (cf. Figure 11). The boundary  $p_{0,s}$  of  $W_{loc}^s(p_{\infty,s}^+)$  in  $\mathcal{D}$  is then uniquely determined as the intersection  $C_{sep} \cap \ell \equiv \{p_{0,s}\}$ .

Our problem here is then stated as follows, where colors mentioned below correspond to those in Figures 10 and 12.

**Problem 7.3.** *Does the blow-up time vary continuously on  $\ell$ ? If not, study whether  $t_{\max}$  is discontinuous only in each side of  $C_{sep}$  on  $\ell$ , or discontinuous in both sides of  $C_{sep}$ .*

This problem reveals a qualitative nature of saddle-type blow-up solutions as a component of blow-up separatrix. To study the above problem, the following steps are operated.

1. Set a line segment  $\ell$  transverse to the blow-up separatrix  $C_{sep}$ .
2. Compute the blow-up time of the solution through  $\{p_{0,s}\} \equiv C_{sep} \cap \ell$ .
3. Choose several points on  $\ell$  in the blue region, shown in Figure 12, and validate blow-up times through these points.
4. Plot all validated blow-up times and study the distribution.
5. If the distribution provides continuous dependence on initial data, study the details. If not, we have a new message for nature of blow-up solutions, namely the existence of “discontinuity” of blow-up solutions in an appropriate sense.

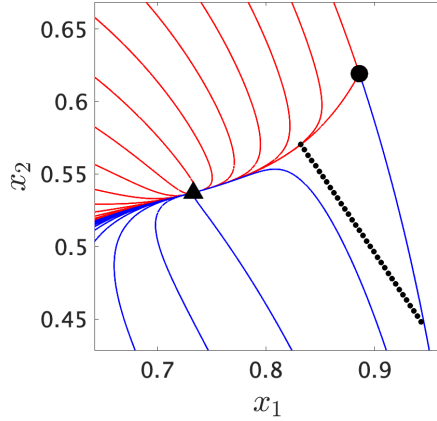


Figure 12: Zoom-in of Figure 10: choice of the segment  $\ell$ . The black ball is the saddle  $p_{\infty,s}^+$ , while the black triangle is the source  $p_b^+$ . The red curve connecting  $p_{\infty,s}^+$  and  $p_b^+$  is a component of the blow-up separatrix  $C_{sep}$ . Recall that trajectories through points in the red region correspond to time-global solutions for (7.1), while trajectories through points in the blue region correspond to blow-up solutions for (7.1). A line  $\ell$  transverse to  $C_{sep}$  in the present study is the collection of small black balls.

The point  $p_{0,s}$  decomposes the line segment  $\ell$  into two pieces, denoted by  $\ell_l$  and  $\ell_r$  consisting of points on  $\ell$  on the left and the right side of  $p_{0,s}$ , respectively. Our validations, rigorous integrations of (7.3) in forward time direction, show that all sample points on  $\ell_r$  converge to  $p_{\infty}^+$  as  $\tau \rightarrow \infty$ , which correspond to a family of (sink-type) blow-up solutions. Their validated blow-up times as well as the blow-up time of the solution on the separatrix are shown in Figure 13 with their rigorous error bounds. Looking at Figure 13, the corresponding blow-up times increase as sectional points become close to  $W^s(p_{\infty,s})$ , while the blow-up time of the solution on the separatrix significantly increases. On the other hand, all points on  $\ell_l$  converge to the sink equilibrium  $p_b^-$ . Since the preimage of  $p_b^-$  under the compactification is bounded, the corresponding solution in the original time-scale exists for all  $t \geq 0$ . This fact is easily confirmed by showing that  $t_{\max} = \infty$ . These observations show that  $t_{\max}$  is discontinuous as a function of points on  $\ell$  at  $p_{0,s}$  from  $\ell_l$ .

Next we discuss the continuity of  $t_{\max}$  at  $p_{0,s}$  on  $\{p_{0,s}\} \cup \ell_r$ . Our validations show that

$$t_{\max}(p_{0,s}) \in 3.109637008_{391221}^{441572},$$

which is much higher than  $t_{\max}$  on typical points on  $\ell_r$  according to Figure 13. However,  $t_{\max} = t_{\max}(p)$  drastically increases as  $p \in \ell_r$  approaches to  $p_{0,s}$ . At the point  $p \in \ell_r$  with  $|p_{0,s} - p| = 1.0 \times 10^{-13}$ , validation of blow-up solutions did not succeed. As long as we have validated, we cannot conclude the discontinuity of  $t_{\max}$  at  $p_{0,s}$  in both sides. Nevertheless, we can still conclude that  $t_{\max}$  behaves in a singular manner around  $p_{0,s}$  where the trajectory approaches to different invariant sets.

**Remark 7.4.** *Rigorous enclosures of  $t_{\max}$  off  $W^s(p_{\infty,s})$ , in particular  $t_{\max}$  for sink-type blow-up*

<sup>21</sup>Under time reversal transformation, the same conclusion holds true for source equilibria.

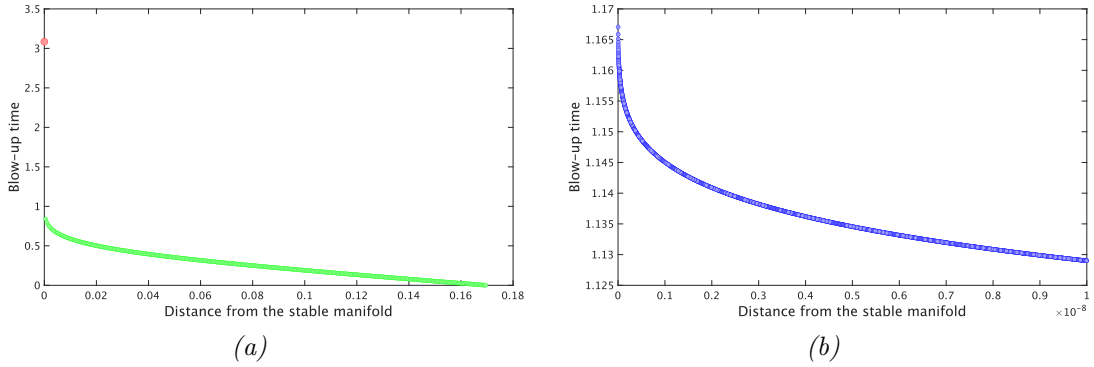


Figure 13: Blow-up times of solutions with initial points on  $\ell$

We have totally chosen 10,000 points on  $\ell_r$  for validating  $t_{\max}$ .

(a) Relationship of points on  $\ell_r$  and the blow-up times of solutions through those points. Horizontal: distance from  $p_{0,s}$  on  $\ell$ . Vertical: blow-up time  $t_{\max}$  of the corresponding solution. The value 0 on the horizontal axis corresponds to  $p_{0,s}$ . The blow-up time  $t_{\max} = t_{\max}(p)$  looks discontinuous at  $p = p_{0,s}$ . The red point denotes  $t_{\max}(p_{0,s})$ , while green points denote  $t_{\max} = t_{\max}(p)$  at  $p \in \ell \setminus \{p_{0,s}\}$ . All plotted blow-up times here expect  $t_{\max}(p_{0,s})$  have rigorous error bounds less than  $3.7235 \times 10^{-5}$ , while the rigorous error bound of  $t_{\max}(p_{0,s})$  is  $2.5175 \times 10^{-11}$ .

(b) Zoom-in of the graph (a) for points within the distance  $\leq 1.0 \times 10^{-8}$  from  $p_{0,s}$ . All plotted blow-up times here expect  $t_{\max}(p_{0,s})$  have rigorous error bounds less than  $1.8288 \times 10^{-2}$ . As  $p \in \ell_r$  approaches to  $p_{0,s}$ ,  $t_{\max}$  significantly increases. In the present study we do not have validations for  $t_{\max}$  associated with points  $p \in \ell_r$  within the distance  $\leq 1.0 \times 10^{-13}$ .

solutions, are validated by local Lyapunov functions and rigorous integrations of (7.3), which are exactly machineries applied in [49]. The difference of orders of (the worst) rigorous error bounds of  $t_{\max}$  on and off  $W^s(p_{\infty,s})$  shown in Figure 13 comes from the that of the methodology for validating rigorous bounds of  $t_{\max}$ . Nevertheless, there is no significant influence on the qualitative tendency of  $t_{\max}$  in the present study.

**Remark 7.5** (Behavior of  $t_{\max}$ : a numerical experiment). *We have numerically calculated the behavior of  $t_{\max}$  as a function of distance to the stable manifold in Figure 13-(b). Let  $x$  be the distance of a point  $p$  from  $p_{0,s}$  in  $\ell_r$  and  $t_{\max}(x)$  be the corresponding blow-up time. As far as we have calculated, we could not match  $t_{\max}(x)$  by functions of the form  $x^a$ ,  $e^{ax}$ ,  $c(\ln x)^a$ , and  $Cx^a(\ln x)^b$  for constants  $a, b, c$ . It is needless to say that this asymptotic form can be different for smaller  $x$  and a different choice of  $\ell$ .*

Now we move to another problem stated below.

**Problem 7.6.** *Does the blow-up behavior depend on norms of initial points ?*

In arguments of blow-up criteria, norms or values of several functionals of initial points are typically concerned for determining whether or not the corresponding solutions blow up. In many cases, there are mathematical arguments showing that initial points whose norms or associated functionals are sufficiently large induce finite-time blow-up. On the other hand, there are also several mathematical results of blow-up behavior which do not mention the magnitude of initial data. The aim of the present issue here is to reveal a qualitative characterization of blow-up separatrix  $C_{sep}$ , which partially gives an answer to the above question.

To this end, we choose two pairs of initial points. One pair is located close to  $p_{\infty,s}^+$ , while another pair is located close to the origin. In both pairs, two initial points are located at the opposite side to each other across  $C_{sep}$ . More precisely, the former pair is chosen close to  $(x_1, x_2) = (0.83, 0.53)$ , while the latter pair is chosen close to  $(x_1, x_2) = (0.32, 0.32)$ . The corresponding points *in the original coordinate* are approximately

$$(u, v) = (3.39444993, 4.69501202) \quad \text{and} \quad (u, v) = (0.36072017, 0.40662201), \quad (7.5)$$

respectively. The same methodology we have shown is applied to validating time-global trajectories for (7.3) through each point, showing that the fate of trajectories are completely separated for both pair of initial points. More precisely, initial points in one side of  $C_{sep}$  induce time-global solutions, while those in another side of  $C_{sep}$  induce blow-up solutions. See Figures 14 and 15. The important point here is that the above behavior can be validated *even near the origin*, like the second case in (7.5). The same tendency can be observed at initial points arbitrarily close to the origin as long as the blow-up separatrix includes the origin, and hence we can conclude that *the magnitude of initial points does not always play roles in characterizing the blow-up behavior in the presence of the blow-up separatrix in the above sense*.

**Remark 7.7.** *Since the connecting orbit between the origin and the source  $p_b^+$  is away from the horizon, the maximal existence time of the corresponding solution is infinity in both direction, showing that  $t_{\max}$  near the origin is discontinuous at most on one side of the orbit.*

We end this section summarizing several features of blow-up separatrix we have validated.

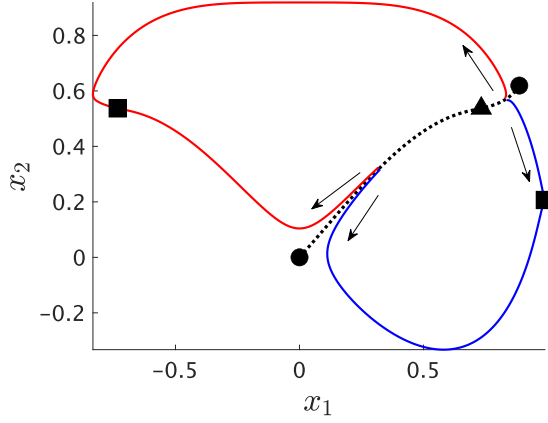


Figure 14: Blow-up separatrix

A nature of blow-up separatrix  $C_{sep}$ , the collection of dotted curves, is drawn. Red curves correspond to time-global solutions for (7.1), while blue curves correspond to blow-up solutions for (7.1). Colors correspond to Figure 10. Initial points are indeed separated by  $C_{sep}$ , no matter how large they are. See also Figure 15.

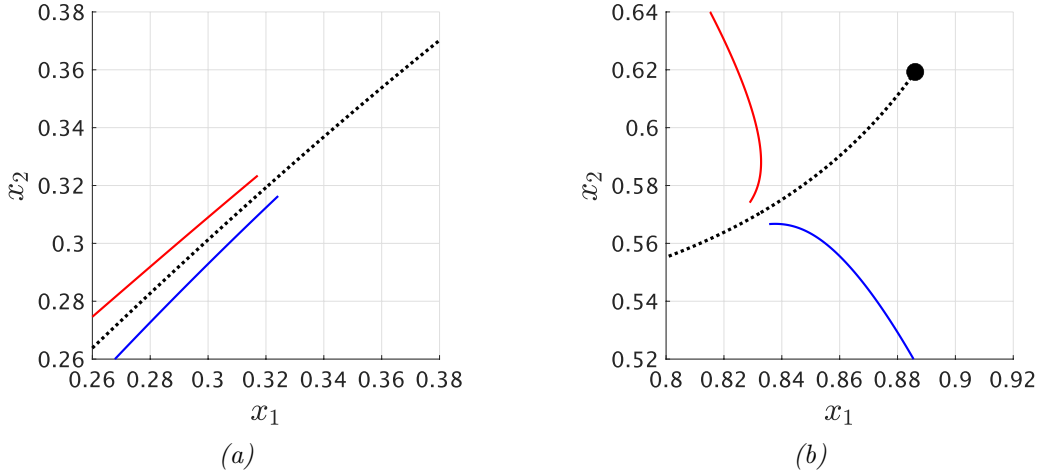


Figure 15: Zoom-in of initial points in Figure 14

Endpoints of colored curves in (a) denote initial points of the time-global solution (red) and the blow-up solution (blue) going to the direction towards the origin, respectively, while those in (b) denote initial points of the time-global solution (red) and the blow-up solution (blue) going to the direction towards the saddle  $p_{\infty,s}^+$ , respectively.

- The blow-up time  $t_{\max}$  varies in a singular manner near the separatrix;
- Arbitrarily small open neighborhoods of the separatrix include points inducing both time-global solutions and finite-time blow-up, no matter how large initial points are.

As a consequence, saddle-type blow-up solutions can play key roles in characterizing the global dynamics possessing both time-global solutions and finite-time blow-up independent of the magnitude of initial points.

## Concluding remarks

In this paper, we have shown several characteristics of blow-up solutions for autonomous ODEs which are unstable under perturbations of initial points with the computer-assisted proofs of their existence and analytic characterization of blow-up times. The essence of our methodology for characterizing blow-up nature presented in this paper consists of the following:

- compactifications of the phase space and time-scale desingularizations of vector fields,
- parameterization of (un)stable manifolds of invariant sets on the horizon, and
- extension of invariant manifolds by rigorous integrations of differential equations.

All these methodologies can be applied to various dynamical systems under quite mild assumptions. Comparing with preceding works involving rigorous numerics of blow-up solutions where the above essence are partially included, the difference of the present argument from those are summarized as follows.

- In [48, 49, 57], rigorous numerics for (sink-type) blow-up solutions for ODEs are reported. The difference of the present study from those is the application of the parameterization method. By using the parameterization method, we can validate invariant manifolds no matter how unstable the invariant sets (on the horizon) are, which enables us to validate saddle-type blow-up solutions in the similar way to sink-type ones. Moreover, parameterization of invariant manifolds provides the exact and explicit formula of the blow-up time as a function of initial points. The formula is also applied to various dynamical systems and will provide analytic arguments of blow-up times.
- In [16], rigorous numerics of blow-up profiles for fourth-order ODEs of the form (1.3) are reported. Treatments of the problem rely on assuming the ansatz of blow-up profiles, namely a priori asymptotic form of blow-up solutions and reduce the original problem to the existence of a bounded time-periodic solution for the auxiliary equation. Moreover, the standard Floquet theory provides its hyperbolicity and stability. In practical problems addressed in [16], validated solutions are proved to be unstable. An estimate of blow-up times is also addressed, while only an explicit lower bound is provided. In the present study, on the other hand, blow-up solutions are directly addressed without any assumptions of concrete profiles, which can be provided by applications of compactifications and time-scale desingularizations. Moreover, both upper and lower bounds of blow-up times are obtained from general formulas of blow-up times obtained directly by time-scale desingularizations. It should be noted that *no assumptions of blow-up phenomena for any solutions are used* for the present validations.

The sharp estimation of the parameterization of invariant manifolds provides sharp estimates of blow-up times.

In any cases, *computer-assisted proofs* or *rigorous numerics* possess a potential to analyse concrete quantitative and qualitative of solution families for various dynamical systems, even for blow-up problems.

We leave several comments about the link to blow-up behavior arising in the suspension bridge problem. As noted in Section 1.2, it is proved in [16] with the computer assistance that there is an unstable hyperbolic periodic orbit  $\Gamma = \{w(t)\}$  expressing an asymptotic behavior of blow-up behavior for (1.3) with specific  $k$  and  $f$ . It is then conjectured in [16] that, for the appropriately transformed dynamics from the problem of the form (1.3), *the boundary of the basin of attraction of the origin coincides with  $W^s(\Gamma)$* . A consequence of the conjecture is the existence of a three dimensional manifold which “separates” the phase space and for which solutions with initial conditions taken on one side of the manifold blow-up in finite time while on the other side, solutions converge to the origin. In the present paper, we have focused on unstable, in particular saddle-type, blow-up solutions which can extract the above nature. We have revealed here that unstable blow-up solutions, even with the simpler asymptotic behavior than [16], can separate the phase space so that initial points on one side determine time-global solutions, while those on the other side induce blow-up solutions. Our examples show that trajectories inducing the above separation are not always saddle-type blow-up solutions or their stable manifold itself, but bounded global trajectories connecting saddle-type blow-up solutions. We have called the collection of global trajectories connecting saddle-type (unstable) blow-up solutions *the blow-up separatrix*. The global nature of the blow-up separatrix can be explained through connecting orbits for dynamical systems through compactifications and time-scale desingularizations. We believe that the separatrix can characterize the “boundary” of the basin of attraction mentioned in [16].

Note that the above separatrix is characterized only for stationary blow-up (Theorem 2.12) so far. On the other hand, a computer-assisted proof of the existence of (un)stable manifolds of hyperbolic *periodic orbits* is already established in e.g. [13], and the treatment of blow-up solutions involving periodic orbits at infinity is also established in [45, 46], namely the same machinery as shown in Section 2 can be applied. Going back to the suspension bridge problem, combination of preceding works with the arguments in the present paper can contribute to unravel the nature of blow-up behavior in (1.3) only with a few mild assumptions.

## Acknowledgements

JPL was supported by an NSERC Discovery Grant. KM was partially supported by Program for Promoting the reform of national universities (Kyushu University), Ministry of Education, Culture, Sports, Science and Technology (MEXT), Japan, World Premier International Research Center Initiative (WPI), MEXT, Japan, and JSPS Grant-in-Aid for Young Scientists (B) (No. JP17K14235). AT was partially supported by JSPS KAKENHI Grant Numbers JP18K13453, JP20H01820.



## References

- [1] K. Anada, T. Ishiwata, and T. Ushijima. A numerical method of estimating blow-up rates for nonlinear evolution equations by using rescaling algorithm. *Japan Journal of Industrial and Applied Mathematics*, pages 1–15, 2017.
- [2] G. Arioli and F. Gazzola. A new mathematical explanation of what triggered the catastrophic torsional mode of the Tacoma Narrows Bridge. *Applied Mathematical Modelling*, 39(2):901–912, 2015.
- [3] B. Barker, J.D. Mireles-James, and J. Morgan. Parameterization method for unstable manifolds of standing waves on the line. *SIAM J. Appl. Dyn. Syst.*, 19(3):1758–1797, 2020.
- [4] E. Berchio, A. Ferrero, F. Gazzola, and P. Karageorgis. Qualitative behavior of global solutions to some nonlinear fourth order differential equations. *Journal of Differential Equations*, 251(10):2696–2727, 2011.
- [5] M. Berger and R.V. Kohn. A rescaling algorithm for the numerical calculation of blowing-up solutions. *Communications on pure and applied mathematics*, 41(6):841–863, 1988.
- [6] M. Berz and K. Makino. Verified integration of ODEs and flows using differential algebraic methods on high-order Taylor models. *Reliable Computing*, 4(4):361–369, 1998.
- [7] D. Bonheure and L. Sanchez. Heteroclinic orbits for some classes of second and fourth order differential equations. In *Handbook of differential equations: ordinary differential equations*, volume 3, pages 103–202. Elsevier, 2006.
- [8] M. Breden, J-P. Lessard, and J.D. Mireles James. Computation of maximal local (un) stable manifold patches by the parameterization method. *Indagationes Mathematicae*, 27(1):340–367, 2016.
- [9] F. Bünger. A Taylor model toolbox for solving ODEs implemented in MATLAB/INTLAB. *Journal of Computational and Applied Mathematics*, 368:112511, 2020.
- [10] X. Cabré, E. Fontich, and R. de la Llave. The parameterization method for invariant manifolds. I. Manifolds associated to non-resonant subspaces. *Indiana Univ. Math. J.*, 52(2):283–328, 2003.
- [11] X. Cabré, E. Fontich, and R. de la Llave. The parameterization method for invariant manifolds. II. Regularity with respect to parameters. *Indiana Univ. Math. J.*, 52(2):329–360, 2003.
- [12] X. Cabré, E. Fontich, and R. de la Llave. The parameterization method for invariant manifolds. III. Overview and applications. *J. Differential Equations*, 218(2):444–515, 2005.
- [13] R. Castelli, J.-P. Lessard, and J.D. Mireles-James. Parameterization of invariant manifolds for periodic orbits (II): A posteriori analysis and computer assisted error bounds. *Journal of Dynamics and Differential Equations*, 30(4):1525–1581, 2018.
- [14] C.-H. Cho. Numerical detection of blow-up: a new sufficient condition for blow-up. *Japan Journal of Industrial and Applied Mathematics*, 33(1):81–98, 2016.

- [15] C.-H. Cho, S. Hamada, and H. Okamoto. On the finite difference approximation for a parabolic blow-up problem. *Japan Journal of Industrial and Applied Mathematics*, 24(2):131–160, 2007.
- [16] L. D’Ambrosio, J.-P. Lessard, and A. Pugliese. Blow-up profile for solutions of a fourth order nonlinear equation. *Nonlinear Analysis: Theory, Methods & Applications*, 121:280–335, 2015.
- [17] J. Dieudonné. *Foundations of modern analysis*. Academic Press, New York, 1960.
- [18] F. Dumortier. Techniques in the theory of local bifurcations: Blow-up, normal forms, nilpotent bifurcations, singular perturbations. In *Bifurcations and Periodic Orbits of Vector Fields*, pages 19–73. Springer, 1993.
- [19] F. Dumortier. Compactification and desingularization of spaces of polynomial Liénard equations. *Journal of Differential Equations*, 224(2):296–313, 2006.
- [20] F. Dumortier and C. Herssens. Polynomial Liénard equations near infinity. *Journal of differential equations*, 153(1):1–29, 1999.
- [21] F. Dumortier, J. Llibre, and J.C. Artés. *Qualitative theory of planar differential systems*. Springer, 2006.
- [22] U. Elias and H. Gingold. Critical points at infinity and blow up of solutions of autonomous polynomial differential systems via compactification. *Journal of mathematical analysis and applications*, 318(1):305–322, 2006.
- [23] M. Fila and H. Matano. Blow-up in nonlinear heat equations from the dynamical systems point of view. *Handbook of dynamical systems*, 2:723–758, 2002.
- [24] H. Fujita. On the nonlinear equations  $\Delta u + e^u = 0$  and  $\partial v / \partial t = \Delta v + e^v$ . *Bulletin of the American Mathematical Society*, 75(1):132–135, 1969.
- [25] V.A. Galaktionov and J.-L. Vázquez. The problem of blow-up in nonlinear parabolic equations. *Discrete & Continuous Dynamical Systems-A*, 8(2):399, 2002.
- [26] F. Gazzola and R. Pavani. Blow up oscillating solutions to some nonlinear fourth order differential equations. *Nonlinear Analysis: Theory, Methods & Applications*, 74(17):6696–6711, 2011.
- [27] F. Gazzola and R. Pavani. Wide oscillation finite time blow up for solutions to nonlinear fourth order differential equations. *Archive for Rational Mechanics and Analysis*, 207(2):717–752, 2013.
- [28] H. Gingold. Approximation of unbounded functions via compactification. *Journal of Approximation Theory*, 131(2):284–305, 2004.
- [29] A. Giraldo, B. Krauskopf, and H.M. Osinga. Computing connecting orbits to infinity associated with a homoclinic flip bifurcation. *J. Comput. Dyn.*, 7(2):489–510, 2020.
- [30] J. L. Gonzalez and J. D. Mireles James. High-order parameterization of stable/unstable manifolds for long periodic orbits of maps. *SIAM J. Appl. Dyn. Syst.*, 16(3):1748–1795, 2017.

- [31] J. Hell. Conley index at infinity. *Ph.D. Thesis in Freie Universität Berlin*, 2010.
- [32] M.A. Herrero and J.J.L. Velázquez. A blow-up mechanism for a chemotaxis model. *Annali della Scuola Normale Superiore di Pisa-Classe di Scienze*, 24(4):633–683, 1997.
- [33] T.-H. Hsu. Viscous singular shock profiles for a system of conservation laws modeling two-phase flow. *Journal of Differential Equations*, 261(4):2300–2333, 2016.
- [34] G.W. Hunt, H.M. Bolt, and J.M.T. Thompson. Structural localization phenomena and the dynamical phase-space analogy. *Proceedings of the Royal Society of London. A. Mathematical and Physical Sciences*, 425(1869):245–267, 1989.
- [35] F. Immler. A verified ODE solver and the Lorenz attractor. *Journal of Automated Reasoning*, 61(1):73–111, 2018.
- [36] M. Kashiwagi. kv - C++ Numerical Verification Libraries. <http://verifiedby.me/kv/>.
- [37] M. Kashiwagi and S. Oishi. Numerical validation for ordinary differential equations — iterative method by power series arithmetic. *Proc. 1994 Symposium on Nonlinear theorem and its Applications (NOLTA '94 Symposium, 1994.10.7)*, pages 243–246, 1994.
- [38] B.L. Keyfitz, R. Sanders, and M. Sever. Lack of hyperbolicity in the two-fluid model for two-phase incompressible flow. *DISCRETE AND CONTINUOUS DYNAMICAL SYSTEMS SERIES B*, 3(4):541–564, 2003.
- [39] H. Kokubu and R. Roussarie. Existence of a singularly degenerate heteroclinic cycle in the Lorenz system and its dynamical consequences: Part I. *Journal of Dynamics and Differential Equations*, 16(2):513–557, 2004.
- [40] H.C. Kranzer and B.L. Keyfitz. A strictly hyperbolic system of conservation laws admitting singular shocks. In *Nonlinear evolution equations that change type*, pages 107–125. Springer, 1990.
- [41] A.C. Lazer and P.J. McKenna. Large-amplitude periodic oscillations in suspension bridges: some new connections with nonlinear analysis. *Siam Review*, 32(4):537–578, 1990.
- [42] J.-P. Lessard, K. Matsue, and A. Takayasu. Codes of “A geometric characterization of unstable blow-up solutions with computer-assisted proof”. <https://github.com/taklab-org/GC-ubs-CAP>.
- [43] J.-P. Lessard and C. Reinhardt. Rigorous Numerics for Nonlinear Differential Equations Using Chebyshev Series. *SIAM J. Numer. Anal.*, 52(1):1–22, 2014.
- [44] R. J. Lohner. Enclosing the solutions of ordinary initial and boundary value problems. In E. Kaucher, U. Kulisch, and Ch. Ullrich, editors, *Computer Arithmetic, Scientific Computation and Programming Languages*, pages 255–286,. B.G.Teubner, 1987.
- [45] K. Matsue. On blow-up solutions of differential equations with Poincaré-type compactifications. *SIAM Journal on Applied Dynamical Systems*, 17(3):2249–2248, 2018.

- [46] K. Matsue. Geometric treatments and a common mechanism in finite-time singularities for autonomous ODEs. *Journal of Differential Equations*, 267(12):7313–7368, 2019.
- [47] K. Matsue, T. Hiwaki, and N. Yamamoto. On the construction of Lyapunov functions with computer assistance. *Journal of Computational and Applied Mathematics*, 319:385–412, 2017.
- [48] K. Matsue and A. Takayasu. Numerical validation of blow-up solutions with quasi-homogeneous compactifications. *Numerische Mathematik*, 145:605–654, 2020.
- [49] K. Matsue and A. Takayasu. Rigorous numerics of blow-up solutions for ODEs with exponential nonlinearity. *Journal of Computational and Applied Mathematics*, 374:112607, 2020.
- [50] J. D. Mireles James. Validated numerics for equilibria of analytic vector fields: invariant manifolds and connecting orbits. In *Rigorous numerics in dynamics*, volume 74 of *Proc. Sympos. Appl. Math.*, pages 27–80. Amer. Math. Soc., Providence, RI, 2018.
- [51] N. Mizoguchi. Type II blowup in a doubly parabolic Keller-Segel system in two dimensions. *Journal of Functional Analysis*, 271(11):3323–3347, 2016.
- [52] L.A. Peletier and W.C. Troy. *Spatial patterns: higher order models in physics and mechanics*, volume 45. Springer Science & Business Media, 2012.
- [53] S.M. Rump and M. Kashiwagi. Implementation and improvements of affine arithmetic. *Nonlinear Theory and Its Applications, IEICE*, 6(3):341–359, 2015.
- [54] D.G. Schaeffer, S. Schechter, and M. Shearer. Nonstrictly hyperbolic conservation laws with a parabolic line. *Journal of differential equations*, 103(1):94–126, 1993.
- [55] S. Schechter. Existence of Dafermos profiles for singular shocks. *Journal of Differential Equations*, 205(1):185–210, 2004.
- [56] M. Sever. *Distribution solutions of nonlinear systems of conservation laws*. American Mathematical Soc., 2007.
- [57] A. Takayasu, K. Matsue, T. Sasaki, K. Tanaka, M. Mizuguchi, and S. Oishi. Numerical validation of blow-up solutions for ordinary differential equations. *Journal of Computational and Applied Mathematics*, 314:10–29, 2017.
- [58] W. Tucker. A rigorous ode solver and smale’s 14th problem. *Foundations of Computational Mathematics*, 2(1):53–117, 2002.
- [59] J.B. van den Berg, J.D. Mireles-James, J.-P. Lessard, and K. Mischaikow. Rigorous numerics for symmetric connecting orbits: even homoclinics of the Gray-Scott equation. *SIAM J. Math. Anal.*, 43(4):1557–1594, 2011.
- [60] M. Winkler. Finite-time blow-up in the higher-dimensional parabolic-parabolic Keller-Segel system. *Journal de Mathématiques Pures et Appliquées*, 100(5):748–767, 2013.
- [61] P. Zgliczynski.  $C^1$  Lohner Algorithm. *Foundations of Computational Mathematics*, 2(4):429–465, 2002.

- [62] P. Zgliczyński. Covering relations, cone conditions and the stable manifold theorem. *J. Differential Equations*, 246(5):1774–1819, 2009.
- [63] G. Zhou and N. Saito. Finite volume methods for a Keller-Segel system: discrete energy, error estimates and numerical blow-up analysis. *Numerische Mathematik*, 135(1):265–311, 2017.